HOKKAIDO UNIVERSITY

Title	Studies on the Minerals from the Manganese Deposit of the Kaso Mine, Japan
Author(s)	Yosimura, Toyohumi
Citation	Journal of the Faculty of Science, Hokkaido Imperial University. Ser. 4, Geology and mineralogy, 4(3-4), 313-451
Issue Date	1939-02
Doc URL	http://hdl.handle.net/2115/35803
Type	bulletin (article)
File Information	4(3-4)_313-452.pdf

Instructions for use

Hokkaido University Collection of Scholarly and Academic Papers : HUSCAP

STUDIES ON THE MINERALS FROM THE MANGANESE DEPOSIT OF THE KASO MINE, JAPAN

By

Toyohumi YOSIMURA

With 19 Plates and 13 Text-figures

Contribution from the Department of Geology and Mineralogy, Faculty of Science, Hokkaidō Imperial University, No. 212.

CONTENTS

CHAPTER I
INTRODUCTION

The Kaso mine is situated about 25 kilometers to the west of the city of Utunomiya, Totigi Prefecture, and consists of workings on a large vein-formed manganese deposit. Numerous minerals, most of them being manganiferous, were found by the author and some of them were already described in articles[1] written in Japanese.

This report presents the results of studies on the mineralogy of the Kaso deposit, including the description of "kasoite", which the author proposes as the name for a new barium mineral of the feldspar group after the mine where it has been found.

Part A
Geology and Ore deposit

CHAPTER II
GEOLOGY

For the broader geologic features of the districts and the surrounding region the reader is referred to the geologic map Sheet[2]

(1) T. Yosimura: Journ. Geol. Soc. Japan, 82–90, (1935).
„ : „ „ **43** 129–143, (1936).
„ : „ „ **43** 877–910, (1936).
„ : „ „ **45** 91–204, (1938).

(2) Scale 1:200,000; published by the Imperial Geological Survey of Japan in (1889).

"NIKKÔ" surveyed by T. NASA and the explanatory text thereof by the same author.

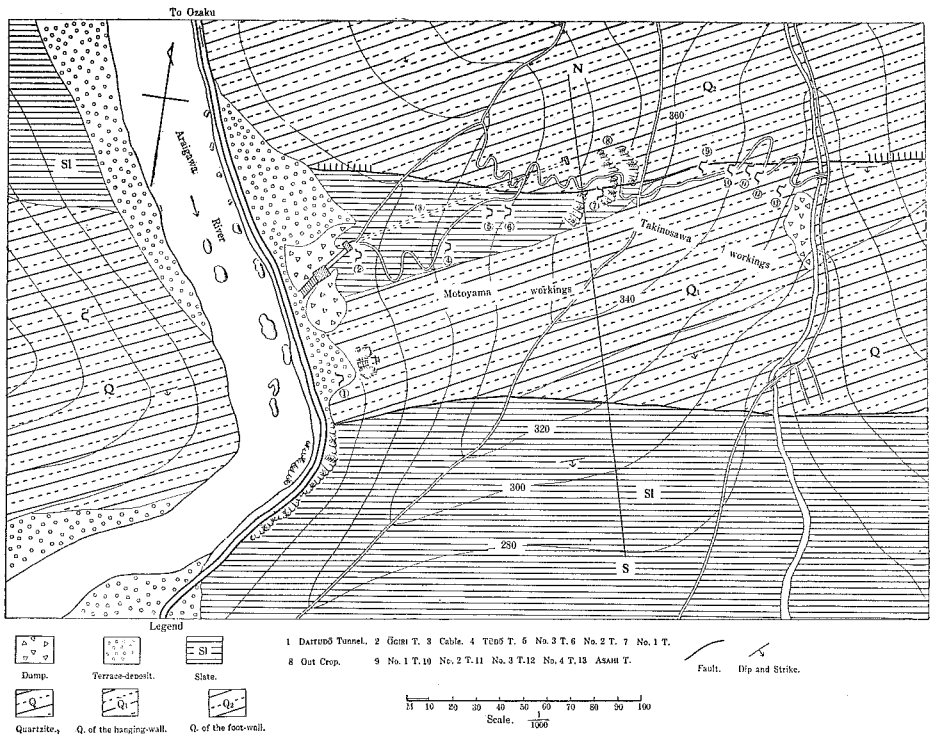

Fig. 1. Geologic map of the Kaso mine.

In Figure 1 is shown the geologic map of the vicinity of the Kaso mine as surveyed by the author. The Palaeozoic formation of the area is composed of alternations of quartzite and slate, generally striking 40 degrees east of north with dips 60 to 80 degrees to southeast. A shear zone, running from east to west in the district, passes through the mine and two distinct faults are mapped in Figure 1.

The manganese ore has been deposited along the northern one of these two faults. On the same shear zone there are several other manganese mines, such as the ŌASI, the SIRANÉ, the OZAKU and the YORIGURI mines, and small unworkable outcrops of manganese ore are very numerous in the vicinity.

Igneous rocks of basic composition, mostly represented by metadiabases, occur frequently as dikes in the Palaeozoic formation.

The country rocks together with the metadiabase dikes have been intruded by a batholith of porphyritic granite which is found widespread in the northern part of the district. Chert and slate have been changed to quartzite and hornfels, and the manganese deposits themselves have also been metamorphosed by this igneous intrusion.

CHAPTER III

PETROGRAPHY

(a) Sedimentary rocks.
- (1) Siliceous rocks.
  - Chert
  - Quartzite
- (2) Argillosiliceous rocks.
  - Black quartzite
  - Siliceous slate
  - Sandstone
- (3) Argillaceous rocks.
  - Slate
  - Radiolarian slate

(b) Metamorphic rocks.
- (1) Metamorphosed siliceous rocks.
  - Quartzite
- (2) Metamorphosed argillosiliceous rocks.
  - Quartz-garnet-biotite-hornfels
  - Quartz-biotite-cordierite-hornfels
- (3) Metamorphosed argillaceous rocks.
  - Slate with quartz-spot
  - Slate with quartz-biotite-spot
  - Slate with cordierite-spot
  - Biotite-hornfels
  - Garnet-biotite-hornfels

(c) Igneous rocks.
- (1) Contact-metamorphosed diabase.
- (2) Metadiabase.
- (3) *"Kuroboku"*.
- (4) Schistose metadiabase.
- (5) Scapolite salite aplite.
- (6) Hornblendite.
  - Relationships of igneous rocks.

(a) Sedimentary rocks.

Sedimentary rocks of the Kaso mine are found to be rarely free from the effects of igneous intrusion. Almost all siliceous rocks are seen traversed by numerous quartz veinlets, most of which are genetically related to the ascending solution emanating from the magma. Not a few of these primary quartz veins contain minute lath-shaped crystals of albite. Argillaceous rocks are more or less phyllitic. Some of them break into octahedral pieces on fracture (Pl. XXXVI (I), Fig. 1).

The Radiolarian slate is a dark grey phyllitic rock with weak silky lustre. Under the microscope it shows ring-shaped skeletons of *Radiolaria* (cf. Pl. XXXVII (II), Fig. 4).

It may be worthy of note that skeletal remains of *Radiolaria* were found in such argillaceous sediments. The results of the chemical analysis of this rock made by the author are remarkable for low lime and high potash content (Table 1). Only a trace of manganese was detected in this rock. It is, therefore, evident that the manganese found abundantly in garnet-hornfelses which have been obviously derived from the Radiolarian slate has been introduced from the ascending mineralizing solution during or before the contact-metamorphism.

TABLE 1. Chemical composition of Radiolarian slate.

	wt. %
SiO_2	69.90
TiO_2	0.28
Al_2O_3	12.94
Fe_2O_3	—
FeO	5.30
MnO	—
CaO	0.62
MgO	2.60
BaO	—
Na_2O	0.21
K_2O	6.08
H_2O^+	1.46
H_2O^-	0.18
P_2O_5	0.31
S	1.07
$O = \frac{1}{2}S$	−0.27
Total	100.68

(b) Metamorphic rocks.

Only a few remarks will be made on the metamorphic rocks enumerated above. It is an interesting fact that quartz-biotite-spots and cordierite-spots are found closely associated in a quartz-biotite-cordierite-hornfels, and the former is related evidently to an earlier mineralization than the latter. During such successive metamorphisms the biotite alters at first into green chlorite and then the latter disappears giving place to a cordierite porphyroblast (cf. Pl. LIII (XVIII), Fig. 1).

The distribution of various metamorphosed rocks indicates no regular relationship to that of the dikes of igneous rocks. Such low-grade metamorphism might have been affected either by physical deformations due to the dislocation of strata or thermal rearrangement of molecules due to the intrusion of igneous bodies.

(c) Igneous rocks.

Metadiabases occur as dikes striking east to west in the same faulted zone that carries the manganese deposit of the Kaso mine.

A stock of quartz porphyry which is exposed near the Ozaku mine, situated about 3 kilometers to the west of the Kaso mine, with several offsets of related acidic rocks which are seen penetrating through the Paleozoic formation, has had considerable metamorphic effects upon these diabasic dikes and some of the manganese veins simultaneously. These diabasic rocks, therefore, seem to be contemporaneous with the manganese deposit and, moreover, an intimate genetical relationship is assumed between them. They can be subdivided and arranged after the order of intrusion as follows:

1) Contact-metamorphosed diabase.
2) Metadiabase.
3) *Kuroboku.*
4) Schistose metadiabase.
5) Scapolite salite aplite.
6) Hornblendite.

Of these six intrusives, four rock-types, (1) to (4), are found as independent dikes, while the other two occur as narrow veins about 2 cm in thickness penetrating the larger metadiabase dikes.

The quartz-porphyry mentioned above and the porphyritic granite in the northern part of the district seem to have little genetical relation to the manganese deposit. They have merely modified the

mineral assemblages of the manganese deposits found in the vicinity as a result of contact-metamorphism occasioned by their intrusion.

Some genetical relationships may possibly be assumed between the acidic igneous rocks and the introduction of so large an amount of various quartz veins in the last stage of mineralization. There are, however, no decisive data available for the explanation of such relations.

(1) Contact-metamorphosed diabase.

This rock occurs as dikes traversing the Palaeozoic formation. These dikes have distinct jointings developed perpendicular to their walls. Megascopically the rock is brownish-grey with dark green spots and looks like a hornfels. Under the microscope it is seen to consist of actinolitic hornblende, contact-biotite and plagioclase (cf. Pl. LI (XVI), Fig. 4).

The results of chemical analysis of this rock are given in Table 2, I. They show the original composition of the diabases most correctly, because the bulk composition usually remains nearly unchanged by a simple thermal metamorphism.

(2) Metadiabase.

Metadiabase occurs as dikes one of which 20 m wide and hundreds of meters long is exposed in the vicinity of the Kaso mine. They are usually intruded along the bedding plane of the Palaeozoic formation, but, sometimes, they lie across the strata. The main portion of the dike consists of porphyritic metadiabase containing large phenocrysts of common hornblende.

Phenocrysts of basic plagioclase are seen extremely albitized, and their interspaces are filled with chloritic or serpentinic material. Iron-ore is a conspicuous feature of the rock, occurring as shapeless grains or stout skeletal growths indicative of ilmenite (cf. Pl. XXXVI (I), Fig. 5). Apatite crystals are also found abundantly. Analysis of this rock yielded the results given in Table 2, II.

(3) *Kuroboku.*

Penetrating the porphyritic main portion there are developed numerous veins of nonporphyritic dark green metadiabase, which, under the microscope, consists dominantly of green actinolitic hornblende.

The narrow offsets of these metadiabase dikes are usually made up wholly of such green hornblende. A platy piece of such compact aphanitic rock clangs like a metal blade when struck a sharp blow. Such specimens are called "*Kuroboku*" and collected for amusement. The chemical composition of this rock given in Table 2, III, is notable for its high titania and iron content. *Kuroboku* has apparently been derived from metadiabases as an ultimate product of an advanced autometamorphism. The abundance of titania and iron may be one of the characteristic features of such metamorphics.

(4) Schistose metadiabase.

This rock shows distinct schistosity and consists almost exclusively of much lighter-coloured hornblende than that found in *Kuroboku*. It may, consequently, be better to term it amphibole-schist. It occurs in the above mentioned fault zone and some specimens have been collected in the dump of the Kaso mine. The results of an analysis of this rock are given in Table 2, IV.

(5) Scapolite salite aplite.

Numerous leucocratic veins about 2 cm in thickness are seen to traverse the metadiabase dike. These veinlets consist mainly of quartz, calcite and albite, but sometimes a plenty of scapolite and green salite are found instead of quartz and calcite. Nearly monomineralic veinlets of scapolite are not uncommon. Interesting occurrences of heulandite after scapolite were observed occasionally. A detailed account of these two minerals will be presented in Chapters XVII, a and XVIII, b.

A leucocratic aplite which contained rather numerous crystals of scapolite was analysed by the author with the results given in Table 2, V. Fifty six-one hundredths percent of chlorine determined by the silverchloride method may be taken as one of the positive data in support of a scapolite constituent.

(6) Hornblendite.

Veinlets consisting exclusively of actinolitic green hornblende occur frequently penetrating every member of igneous origin described above. Only a slight admixture of quartz can be observed under the microscope.

Analysis of this rock yielded the results given in Table 2, VI. Mineralogical properties of this green hornblende will be described in detail in Chapter XV, b.

Relationships of igneous rocks.

Six specimens each representative of the six basic igneous rocks described above were analysed by the author with the following results (Table 2, I–VI).

Their normative constituents and their Niggli's values calculated on the basis of the figures given in this Table are presented in the succeeding Tables 3 and 4.

TABLE 2. Chemical composition of basic igneous rocks from the Kaso mine.

	I.	II.	III.	IV.	V.	VI.
d	2.84	2.76	3.17	3.05	3.06	3.11
SiO_2	53.10	46.32	34.35	37.22	45.38	48.37
TiO_2	0.80	2.45	4.23	2.37	1.36	0.15
Al_2O_3	17.94	14.87	14.18	12.90	9.35	6.75
Fe_2O_3	0.22	0.40	6.20	3.92	0.56	1.91
FeO	8.03	9.38	16.40	14.67	9.51	13.75
MnO	0.27	0.09	0.05	0.10	0.42	0.20
CaO	8.27	9.49	9.68	10.44	19.87	12.84
MgO	6.88	5.73	7.20	13.25	9.06	14.62
Na_2O	1.38	2.38	1.83	0.20	0.93	tr
K_2O	2.20	1.20	1.35	0.31	0.84	tr
H_2O^+	1.58	4.70	2.64	3 95	2.70	2.38
H_2O^-	0.12	0.17	0.10	0.16	0.12	0.18
P_2O_5	0.27	2.22	1.68	1.00	0.90	0.19
Others	—	—	—	—	0.38(1)	—
	101.06	99.40	99.89	100.49	101.38	101.34

I. Contact-metamorphosed diabase.
II. Porphyritic metadiabase.
III. *Kuroboku*, the autometamorphosed metadiabase.
IV. Schistose metadiabase.
V. Scapolite salite aplite.
VI. Hornblendite.

(1) (0.56% Cl)—(0.18% equivalent oxygen).

TABLE 3. Norms.

	I.		II.		III.		IV.		V.		VI.	
Ab	11.6	61.4	21.4	56.8	15.7	50.2	1.8	38.6	7.8	31.7	tr	18.3
An	36.9		27.9		26.7		35.0		18.9		18.3	
Or	12.9		7.5		7.8		1.8		5.0		tr	
Fs	13.7	32.4	13.8	31.9	18.4	41.3	17.0	57.2	14.8	68.8	23.5	79.5
Rh	0.5		0.1		0.1		0.2		0.7		0.4	
Wo	1.1		2.7		4.2		5.7		30.9		18.7	
En	17.1		15.3		18.6		34.3		22.4		36.9	
Q	3.7	6.2	0.5	11.3	(−13.0)		(−9.0)		(−5.7)		(−1.6)	
Ilm	1.6		5.0		8.3	21.5	4.8	13.2	2.6	5.2	0.3	3.8
Mt	0.2		0.4		9.2		5.9		0.6		2.8	
Ap	0.7		5.4		4.0		2.5		2.0		0.7	

TABLE 4. Niggli's values.

	I.	II.	III.	IV.	V.	VI.
al	27	23	17	14	11	8
fm	44	43	58	65	44	67
c	22	26	20	20	42	25
alk	7	8	5	1	3	0
si	135	123	69	69	91	97

	II′.	IV′.	VI′.
al	23.5	15	7
fm	40.5	60	62
c	31.5	20	29
alk	4.5	5	2
si	100.0	80	95

II′. Niggli's value of "Pyroxenit-hornblendit-gabbro."
IV′. ,, "Hornblendit."
VI′. ,, "Pyroxenit."

II′, IV′, VI′. After U. Grubenmann & P. Niggli: Gesteinsmetamorphose, S. 40, (1924).

The analyses are arranged from I to VI after the sequence of mineralization. It is noteworthy that the silica does not increase uniformly, but has a minimum value at No. III, quite contrary to the usual behavior in case of the crystallization from the magmatic melt. On the other hand the alumina decreases steadily. So the variation diagram was drawn taking "al" of the Niggli's value as the abscissa (Fig. 2).

The remarkable increase in the total sum of the ferromagnesian minerals (normative), the decrease in that of the feldspathic minerals

(normative), and the minimum value of SiO_2 and the maximum value of $TiO_2 + P_2O_5$ at No. III (analysis of *Kuroboku*); all these peculiarities are probably due to the autometamorphic nature of this evolution of igneous rocks. Similar variation diagram would be expected in connection with the propylitisation of effusive igneous rocks which has also been explained as a result of autometamorphism.

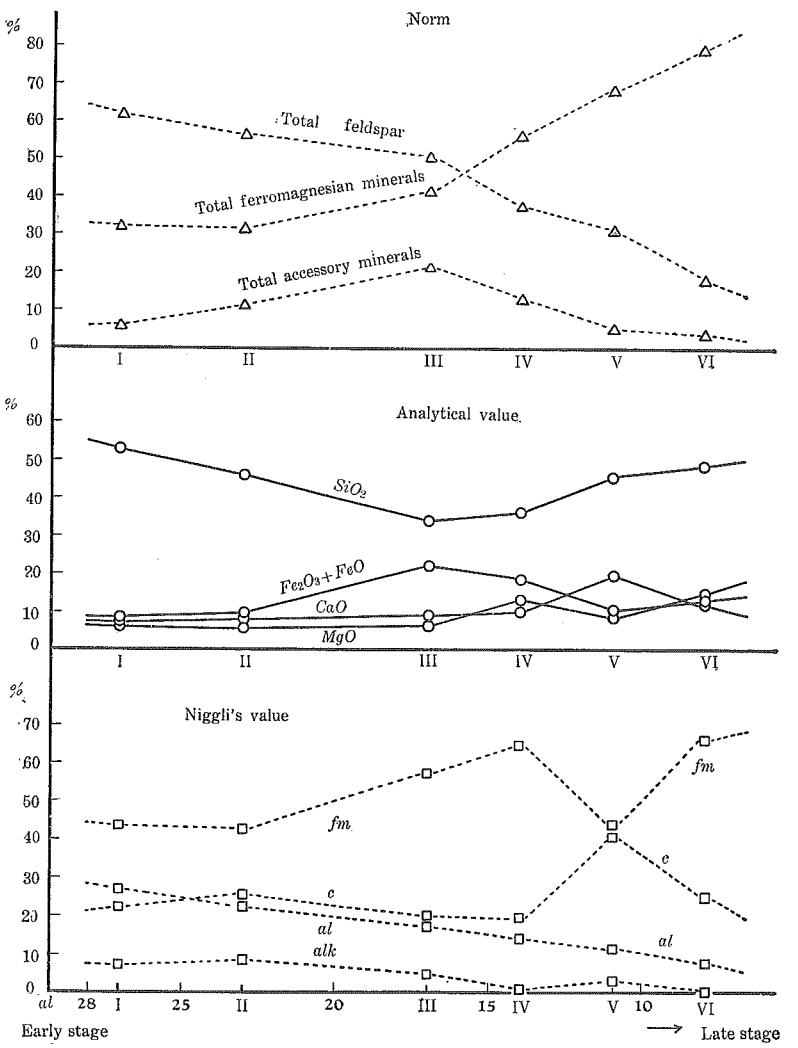

Fig. 2. Diagrams illustrating the variations of the chemical compositions of the basic igneous rocks.

Irregularities seen at No. V in the curves of fm and c of the Niggli's value (Fig. 2) will be smoothed if the sum of fm + c is graphed instead of treating each of them separately. In amphiboles and pyroxenes FeO, MgO and CaO can be substituted for each other to a large extent, so it may be more reasonable not to treat them separately in making a variation diagram.

CHAPTER IV
ORE DEPOSIT

The ore deposit of the Kaso mine is contained in a complicated rhodonite vein which has been deposited along a fault plane between quartzite and slate (cf. Fig. 1, p. 317, the geologic map and Fig. 3

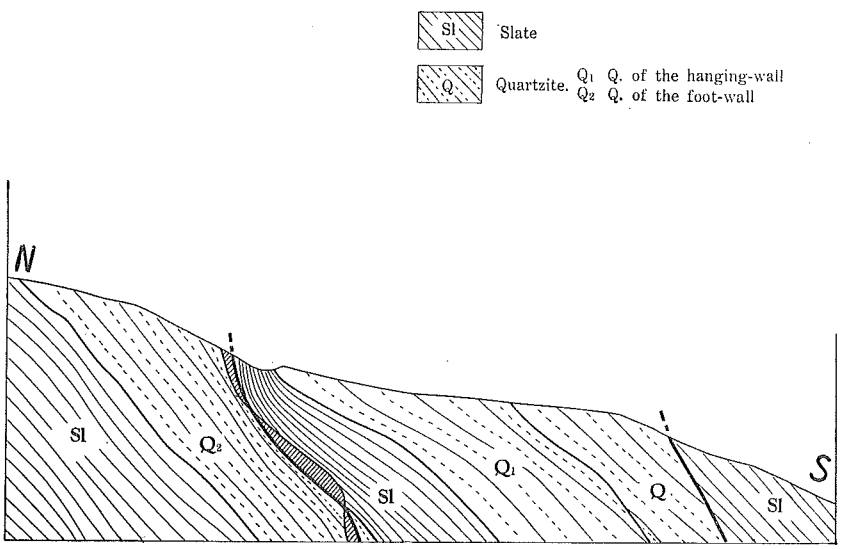

Fig. 3. Cross section of the Kaso mine. The line of section is shown in Fig. 1.

the profile). Minerals of the deposit fall into three groups each related to a different stage of mineralization. Thus the mineralization of the Kaso mine is divided into three stages, A, B and C, after the sequence of deposition.

The products of the first stage, stage A, are found as xenoliths enclosed in the main ore body, and are characterized by the abundance of Ca, Fe (Mn), and Na.

The products of the mineralization of the second stage, stage B, constitute the main part of the ore deposit. Rhodonite, tephroite and rhodochrosite are the most important minerals produced in stage B. This mineralization is characterized by the abundance of Ba, Mn (Fe), K, and Na.

The last stage, stage C, is characterized by Si and Mg, (Mn), which have been embodied in various minerals such as quartz, ankerite, manganactinolite, mangantremolite, manganphlogopite, penwithite and soapstone. Before or during the mineralization of this last stage the fault-zone had again been disturbed resulting in numerous small faults or fissures developed in the previously deposited main ore body. These cracks or fissures might have repeatedly opened and been filled by veinlets consisting of the minerals mentioned above.

Minerals containing each of the elements characteristic of the three stages will be described in detail in the following chapters. It is evident that all these elements have been introduced from the magmatic emanations originating from the ascending igneous body. Magnesium, however, is the only element as to the origin of which much remains to be mentioned.

Some of the magnesia mineralized in stage C might have already been introduced in A or B stage by the assimilation of the wall rock, and have been inherited to the solutions of the last stage. But most of the magnesia is seemingly of primary origin. The primary introduction of magnesium is most evident in the formation of mangantremolite which is apparently a product of the alteration of rhodonite simply reacted upon by a solution related to the hornstone vein of C stage without cooperations of materials derived from the country rock.

In the following Table 5 the distribution of magnesium is shown arranged after the sequence of mineralization. The distribution is compared with associating alumina contents, because the alumina seems to be the most stable and immobile constituent during such mineralization.

The earlier and consequently more powerful mineralization of each stage has resulted in a rather regular vein-formed deposit consisting chiefly of various manganese silicate minerals, having sharp and nearly linear junctions with the wall rock, while the later mineralization has produced irregular-shaped ore bodies characteristic of metasomatic deposit.

TABLE 5. Distribution of magnesium in relation to alumina.

Stage.	Minerals.	MgO	Al_2O_3	MgO/Al_2O_3
Country rock	Slate	2.60	12 94	0.202
,,	Cordierite-hornfels	7.81	32.36	0.242
Wall rock altered in stage A	*Tetuban*	4.20	16.80	0.249
,, B	Siliceous *Azukiban*	2.12	19.80	0.107
,, B	Argillaceous *Azukiban*	5.80	13.51	0.429
,, C	*Kakusekiban*	2.03	11.00	0.185
Igneous rock	Contact-metamorphosed diabase	6.88	17.94	0.384
,,	Metadiabase	5.73	14.87	0.383
,,	*Kuroboku*	7.20	14.18	0.507
,,	Schistose metadiabase	13.25	12.90	1.028
,,	Scapolite-salite-aplite	9.06	9.35	0.968
,,	Green hornblende vein	14.62	6.75	2.170
Stage A	Manganhedenbergite	2.19	0.35	6.25
,, ,,	Green ironhornblende	5.25	8.00	0.66
Stage B	Green biotite	16.15	16.18	1.00
,, C	Manganactinolite	10.62	2.42	4.43
,, ,,	Mangantremolite	13.24	tr	∞
,, ,,	Manganphlogopite	17.58	15.17	1.17
,, ,,	Chlorite	12.91	12.97	1.00
,, ,,	Opaline penwithite	3.97	1.02	3.88
,, ,,	Brown penwithite	6.02	1.07	5.60
,, ,,	Black penwithite	5.68	0.82	6.92
,, ,,	Soapstone	24.58	0.18	136.8

Rhodochrosite masses which are mined as the principal ore have been deposited in irregular lense-shaped shoots, orientation of which are dependent upon the inclination of the fault plane and the folding of the strata of the mother rock. A sketch of the underground workings of the Kaso mine presented in Fig. 4 shows obviously the metasomatic character of the rhodochrosite deposit.

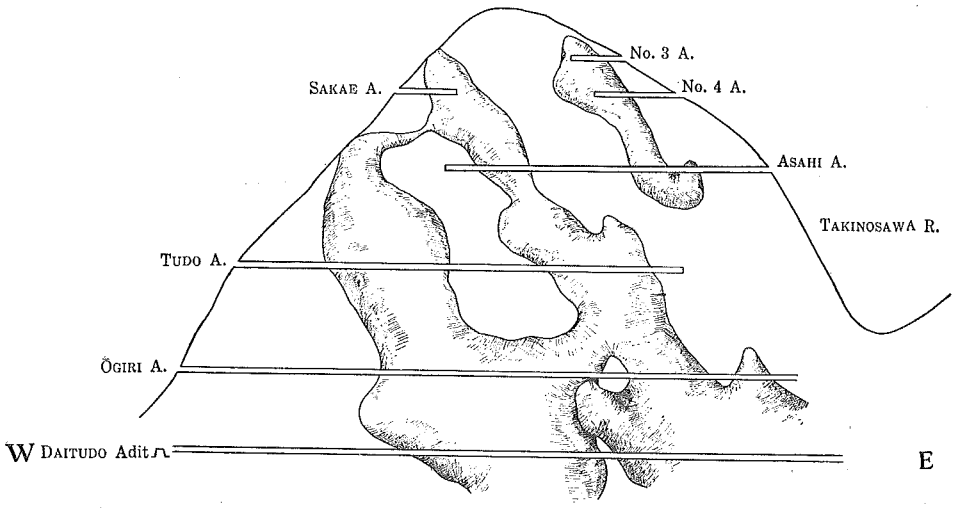

Fig. 4. Perspective of the underground workings of the Kaso mine viewed from the south.

CHAPTER V

MANGANESE ORES

Ores of the Kaso mine consist of the following three groups each characterized by its particular assemblage of minerals. The nomenclature of the ores is given after the usage at the Kaso mine. Most of the terms, furthermore, are applicable throughout Japan.

(a) *"Azuki"*-ore.[1]

Azuki-ore is a compact massive ore consisting of microscopically fine-grained rhodochrosite crystals. Colour pink, brown, chestnut-brown or black, variegated owing to the admixture of various impurities. It is sometimes ribboned.

Varieties of *Azuki*-ore.

(1) *Azuki*-ore proper.

Colour pink to pinkish-white, with no or very small amounts of impurities. Analysis is given in Table 6, No. 3.

(1) "AZUKI" means in Japanese "the red bean".

(2) Chocolate-brown *Azuki*-ore.

This is the ore of the highest grade among the *Azuki*-ores. The chocolate-brown colour is due to the admixture of the sesquioxide of manganese probably derived from altered manganosite or braunite, the unaltered remnants of which are found frequently in a thin slice of this ore. Manganese percentage often exceeds 50%.

(3) Greenish-grey *Azuki*-ore.

This ore contains an abundance of relict crystals of tephroite or knebelite. As the silica percentage is a little higher this ore is not ranked among the highest-grade ores, but the manganese percentage is generally remarkably high.

(4) Spotted *Azuki*-ore.

The spotted ore is usually a product of the metasomatic replacement of the black alabandite ore by the pink *Azuki*-ore proper.

(5) Bluish-grey *Azuki*-ore.

This is a hard compact ore rich in alleghanyite crystals. This ore looks like a kind of hornfels though considerably heavier. Analysis in Table 6, No. 2.

(6) Brown *Azuki*-ore.

This is a kind of rhodochrosite ore stained brown as a result of contamination of numerous minute patches of penwithite which are probably due to the degradation of alleghanyite crystals. Analysis in Table 6, No. 4.

(7) Ribboned *Azuki*-ore.

The ribboned structure is due to the leaf-by-leaf injection of a rhodochrositic solution in a more or less phyllitic wall rock or a fractured pre-existing ore. If the injection has taken place into the bluish-grey or chocolate-brown *Azuki*-ore, as is usually the case, the ribboned ore is, without fail, a high grade one. Such injection, nevertheless, has sometimes occurred into the phyllitic wall rock, for example, the *Azukiban*. The ribboned ore in this case is extremely inferior in quality though looking quite the same.

(8) Black *Azuki*-ore.

This is one kind of the principal rhodochrosite ores contaminated heavily with black pigmental substances (cf. Chap. XVIII, g). It is an interesting fact that the black *Azuki*-ore has been mineralized,

as a rule, later than the other *Azuki*-ores. On an example shown in Pl. LIII (XVIII), Fig. 2, it is seen that the brecciated light-coloured *Azuki*-ore proper is cemented by the black ore. Such black pigment seems to be the product of the end of B stage.

Some of the black ores have been deposited replacing the black graphitic fault-gouge frequently found in Paleozoic rocks. They are too high in silica and will not pay if worked. Analysis No. 5 in Table 6.

(b) *"Hie"*-ore.[1]

A greenish-grey dense ore with sporadic white spots of carbonate minerals is called *"Hie"*-ore (cf. Pl. XXXVIII (III), Fig. 3). The dominant mineral of this ore is the masive tephroite. Those mixed with a larger quantity of grey rhodochrosite are a high-grade ore, although the silica percentage is a little higher than that of the *Azuki*-ore. The chemical composition of this ore will probably be represented approximately by that of the brown *Azuki*-ore given in Table 6, No. 4.

TABLE 6. Analyses of ores.

	1.	2.	3.	4.	5.
d	3.38	3.66	3.58	3.40	3.29
FeO	7.26	3.01	1.40	0.77	1.73
MnO	43.18	52.28	54.14	52.22	28.22
CaO	3.10	1.98	3.77	1.54	8.45
MgO	2.50	3.19	1.46	3.12	6.00
CO_2	33.42	28.61	35.35	20.06	7.97
SiO_2	5.38	7.10	2.68	16.31	46.10
Al_2O_3	1.28	2.84	—	2.43	1.35
H_2O	1.62	0.25	0.12	2.21	0.21
Insoluble	2.67	0.16[2]	—	—	0.15[3]
	100.41	99.42	98.92	98.66	100.18

(1) The first carbonate ore. Reproduced from Table 23.
(2) Bluish-grey *Azuki*-ore (containing alleghanyite).
(3) *Azuki*-ore proper. Reprod. from Table 25.
(4) Brown *Azuki*-ore (hydrothermally altered ore derived from No. 2.).
(5) Black low-grade ore with abundant impurities.

(1) *"Hié"* means in Japanese "the seed of the panic-grass".
(2) TiO_2.
(3) $BaSO_4$.

(c) *"Kuro"*-ore.[1]

Black oxidized ores found on the outcrop or in the fissures traversing the main ore body are called *"Kuro"*-ore, which, however, has been worked almost to the last basketful in the past. These ores are evidently the oxidation product affected by the percolating water. Analysis of this ore will be mentioned with reference to pyrolusite (Chap. IX, g, Table 17).

CHAPTER VI

ALTERATION OF WALL ROCKS

The wall rocks of the Kaso deposit have been subjected to a series of successive alterations, which can be classified as follows.

1) Disseminations of manganese minerals accelerated by faulting and fracturing.
2) Impregnations of materials emanating from the ascending mineralizing solution.
3) Contact-metamorphism of the wall rocks which had already been altered to some extent by previous mineralizing solutions.

(i) Disseminations of ore minerals.

The ore body has often very irregular junctions with the wall rock, with lenses and veinlets of the ore frequently found isolated in the latter.

Such dissemination of ore minerals is very prominent in the fractured zone of the deposit, being itself an alteration of a physical nature, but it usually is accompanied by an intense alteration of a chemical nature as will be described below. An example of isolated fragments of a rhodonite veinlet is presented in Pl. LI (XVI), Fig. 2. A few pieces of the rhodonite mass torn off by a microscopic fault into its gouge-clay are seen gradually altered from their margin into clusters of mangantremolite crystals, which are characteristic of the alteration caused by the mineralizing solution of C stage.

(ii) Impregnations of emanating substances.

Volatile substances which had accompanied the manganese ore were expelled on the solidification of the ore and were impregnated

(1) *"Kuro"* means in Japanese "the black colour".

in the wall rock. Different suites of elements which were emanated in each stage of mineralization have resulted in different modes of alterations of the wall rock. The following four types of altered wall rocks were observed in the Kaso mine.

1) *Tetuban.*
2) *Azukiban.*
3) *Aburaban.*
4) *Kakusekiban.*

(a) *"Tetuban".*(1)

Mineralizing solution of stage A seems to have given off a plenty of Ca, Fe, Mn and Na. Impregnations of pyrrhotite and black pigments, accompanied by intrusions of albite veinlets, are frequently seen especially in the argillaceous wall rocks. Thus there occurs a heavy black rock, which the author would name *"Tetuban"*.

(b) *"Azukiban".*(2)

In stage B impregnations of kasoite, a new barium feldspar, and rhodochrosite accompanied by pigmental Fe-Ti-ore are seen more extensively, resulting in two kinds of altered wall rocks, the one "feldspathic *Azukiban"* and the other "carbonate *Azukiban"*.

The impregnation of feldspar and carbonate mineral which have been driven off from the ascending magmatic solution is an analogous mineralization with the formation of a spilite or an "adinole" slate. Similarly with the *Azukiban* two kinds of adinole are reported, viz., the "feldspathic adinole" and the "carbonate adinole".

"Azukiban" is a phyllitic rock, coloured reddish-violet owing to the impregnation of Fe-Ti-ore. The chemical composition of the *Azukiban* shows little difference from that of the Tetuban as will be compared in Table 7 below.

The analysis given in Table 7, No. 4 was made on a deep reddish-brown *Azukiban* picked up from a specimen traversed by a net-work of kasoite veins. It is, therefore, an example of feldspathic *Azukiban.* A remarkable introduction of Ti, Fe, Mn, and Ba is evident in the results of this analysis.

---

(1) *"Tetuban"* means in Japanese "a wall rock rich in iron".

(2) *"Azukiban"* means in Japanese "a wall rock coloured red like the red bean".

Desilication is also worthy of note. The dissemination of kasoite, which is itself strikingly unsaturated in silica, has resulted in a noticeable removal of SiO_2.

(c) *"Aburaban"*.[1]

Mineralizing solutions of stage C, especially those which have precipitated veinlets consisting of rhodochrosite and ankerite, give off emanations which change the wall rock into a chloritic rock. The product is, consequently, a dark green and greasy-feeling rock. The author would name it *"Aburaban"* after the usage of the miners.

(d) *"Kakusekiban"*.[2]

The mineralization of C stage, on the other hand, was accompanied by an intense silicification which has resulted in some remarkable alterations of the wall rock. Such siliceous altered rock would be called *"Kakusekiban"* (cf. Pl. XXXVIII (III), Fig. 5). Ferromagnesian mineral such as actinolite or biotite were transformed by this silicification into a corresponding amount of mangantremolite or green chlorite respectively.

(iii) Contact-metamorphism of altered wall rocks.

As already stated in the preceding chapters the deposition of the manganese ore in the Kaso mine had generally been accomplished before the intrusion of the granite took place in this district. The altered wall rocks, consequently, were intensely affected by this contact-metamorphism, except some younger rocks such as *Aburaban* and *Kakusekiban* which owe their origin to the mineralization of C stage.

The contact effect on *Azukiban* and *Tetuban* is represented chiefly by the garnetization of these rocks. Argillaceous rocks contaminated by manganese minerals are, as a general rule, most liable to be garnetized by a contact-metamorphism. Various black garnets were found in the metamorphosed *Tetuban* and red garnets in the metamorphosed *Azukiban* (Cf. Chap. XII).

Garnetized wall rocks as well as other contact-metamorphosed rocks are seen to have been affected by the alteration of the more

(1) *"Aburaban"* means in Japanese "a wall rock looking like grease".

(2) *"Kakusekiban"* means in Japanese "a wall rock which resembles hornstone".

advanced stage, because the garnetization is evidently prior to the C stage mineralization. The effects of *Aburaban*-formation are, consequently, also evident in a garnetized rock, the matrix of which has completely been changed into aggregates of crystal flakes of chlorite and serpentine, while the crystals of garnet themselves are seen remaining quite fresh and unmarred.

Chemical compositions of the altered wall rocks are compared in the following Table 7.

TABLE 7. Analyses of altered wall rocks.

	1.	2.	3.	4.	5.	6.
d	—	2.70	2.98	2.93	2.79	2.72
SiO_2	74.50	69.90	45.70	47.98	28.99	74.91
TiO_2	—	0.28	0.45	1.16	0.10	0.16
Al_2O_3	14.20	12.94	16.80	13.51	12.97	11.00
Fe_2O_3	4.45	—	6.42	2.23	8.97	0.90
FeO	0.30	5.30	6.38	8.22	17.85	3.70
MnO	—	tr	3.43	3.70	2.28	0.12
CaO	0.50	0.62	1.32	1.58	0.84	0.41
MgO	1.62	2.60	4.20	5.80	12.91	2.03
BaO	—	—	6.90	6.60	—	—
Na_2O	2.08	0.21	0.23	1.09	n.d	1.54
K_2O	0.94	6.08	5.60	5.46	n.d	2.60
H_2O^+	1.33	1.46	1.06	1.50	10.95	2.05
H_2O^-	—	0.18	0.16	0.11	3.35	0.06
P_2O_5	—	0.31	0.08	0.98	n.d	0.07
S	—	1.07	1.72	—	—	—
—O	—	—0.27	—0.42	—	—	—
	99.92	100.68	99.93	99.02	99.21	99.55

(1) Clayslate : Sōri, near the Kaso mine : T. Nasa : Expl. Text of Sheet "Nikko," (1889).
(2) Radiolarian slate : Kaso mine : Yosimura : In this article.
(3) *Tetuban* : ,, ,, ,,
(4) *Azukiban* : ,, ,, ,,
(5) *Aburaban* : ,, ,, ,,
(6) *Kakusekiban* : ,, ,, ,,

CHAPTER VII

PARAGENESIS OF MINERALS

As stated in the preceding chapter, the mineralization of the Kaso mine can be divided into three stages as follows;

Stage A ..... the stage when Ca, Fe (Mn) and Na emanated from the magmatic source.
Stage B ..... the stage when Ba, Mn (Fe), K, Na emanated.
Stage C ..... the stage when Mg, (Mn), K, Si emanated.

Each stage is divided further into three periods, each of which is characterized by a particular constituent mineral as follows;

1. Stage A
   - Period A_1 ..... Manganhedenbergite period.
   - Period A_2 ..... Knebelite period.
   - Period A_3 ..... First carbonate period.
2. Stage B
   - Period B_1 ..... Rhodonite period.
   - Period B_2 ..... Tephroite period.
   - Period B_3 ..... Main carbonate period.
3. Stage C
   - Period C_1 ..... Hornstone period.
   - Period C_2 ..... Pegmatitic quartz period.
   - Period C_3 ..... Rock-crystal period.

Each of these nine periods is not only characterized by a particular mineral but also by a definite range of the mineralizing temperature.

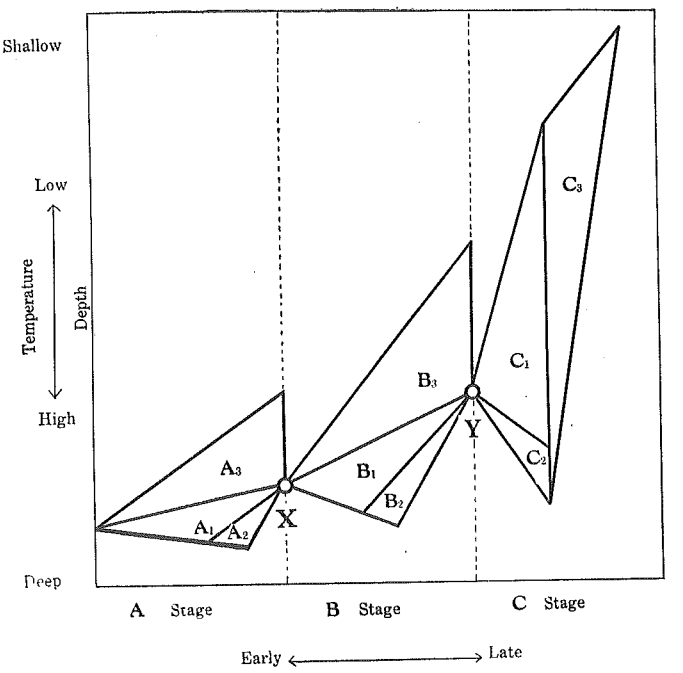

Fig. 5. Diagram showing time temperature (depth) relationships of the nine periods of mineralization of the Kaso deposit.

A schematic diagram as presented in Figure 5 was drawn to show these relationships with considerations of overlapping of mineralizations both in time and temperature.

Minerals found in the Kaso deposit are arranged in the following Tables 8–10 grouped under the heads of the above mentioned nine periods of mineralization.

TABLE 8. Minerals produced in Stage A .... the stage of introduction of Ca, Fe, (Mn), Na.

Period A_1; Manganhedenbergite period.	Manganhedenbergite, Albite, Bariumalbite, Green ironhornblende, Amber-yellow garnet, Pyrrhotite Calcite B
Period A_2; Knebelite period.	Ironknebelite—knebelite Picroknebelite Celsian
Period A_3; First carbonate period.	Fe-Mn-calcite—Fe-rhodochrosite. Manganiferous calcite Dannemorite Green phlogopite Marmatite
"*Tetuban*" a wall rock altered by the mineralizing solution of stage A.	Pyrrhotite Black substance Black garnet

TABLE 9. Minerals produced in Stage B .... the stage of introduction of Ba, Mn (Fe), Na and K.

Period B_1; Rhodonite period.	Ironrhodonite–blood-red-rhodonite—pink-rhodonite Kasoite Green biotite Bementite Wine-yellow garnet. Ca-rhodochrosite A Fe-Ti-ore Chalcopyrite

Period B_2; Tephroite period.	Manganknebelite–irontephroite–tephroite Mangancalcite B Mangancalcite C Zincblende Galena Alleghanyite Alabandite
Period B_3; Main carbonate period.	Rhodochrosite Manganosite Black substance Sericite
"*Azukiban*" a wall rock altered by the mineralizing solution of stage B.	Kasoite Hyalophane Fe-Ti-ore Red garnet Allanite

TABLE 10. Minerals produced in Stage C .... the stage of introduction of Mg, (Mn) K, Si.

Period C_1; Hornstone period.	Hornstone-quartz vein Cinnamon-yellow garnet Manganphlogopite Manganactinolite–mangantremolite Hyalophane–adularia Allanite Penwithite Ca-rhodochrosite B–mangancalcite A –ankerite Fe-Ti-ore
Period C_2; Pegmatitic quartz period.	Pegmatitic quartz Black penwithite Carmine-red rhodonite Tephroite Yellow garnet Hyalophane–alkali feldspar
Period C_3; Rock-crystal period.	Rock-crystal Pink rhodochrosite Mangancalcite D Pyrite Soapstone Pyrochroite Pyrolusite
"*Aburaban*"–a wall rock altered by the mineralizing carbonate-rich solution of C stage. "*Kakusekiban*"–a wall rock altered by the siliceous solution of C stage.	Quartz Chlorite Serpentine

The practical mineral assemblages found in the Kaso deposit are so diverse that it is impossible to enumerate all of them. The author, therefore, will list here as their representatives only the important assemblages in terms of actually observed masses or veins.

Stage A.

Period A_1: Manganhedenbergite period.

(1) Manganhedenbergite vein.

Manganhedenbergite A. Bariumalbite, Green ironhornblende, Calcite B, Pyrrhotite

(2) Manganhedenbergite mass.

Manganhedenbergite B, Amber-yellow garnet, Pyrrhotite, Calcite B.

(3) Albite vein.

Albite, Green ironhornblende, Epidote

Period A_2: Knebelite period.

(4) Ironknebelite vein.

(5) Picroknebelite vein.

Picroknebelite, Celsian, Mangancalcite

Period A_3: The first carbonate period.

(6) The first carbonate ore.

Fe-rhodochrosite, Marmatite

(7) Saccharoidal carbonate ore.

Manganiferous calcite, Knebelite, Dannemorite, Green phlogopite, Amber-yellow garnet

Stage B.

Period B_1: Rhodonite period.

(8) Ironrhodonite kasoite vein.

Ironrhodonite, Kasoite, Wine-yellow garnet, Green biotite

(9) Rhodonite kasoite vein.

Pink rhodonite, Wine-yellow garnet, Kasoite, Green biotite, Chalcopyrite, Pyrrhotite

(10) Rhodonite vein.

Pink rhodonite, Wine-yellow garnet, Bementite

(11) Rhodochrosite rhodonite vein.

Blood-red rhodonite, Ca-rhodochrosite A, Knebelite, irontephroite

(12) Quartz rhodochrosite rhodonite vein

Pink rhodonite, Ca-rhodochrosite A, Wine-yellow garnet, Quartz, Fe-Ti-ore, Allanite

(13) Quartz rhodonite vein.

Pink rhodonite, Ca-rhodochrosite A, Microcrystalline quartz

(14) Fibrous rhodonite vein.

Fibrous pink rhodonite, Hornstone quartz, Black substance, Hyalophane

Period B_2: Tephroite period.

(15) Blood-red rhodonite manganknebelite vein.

Blood-red rhodonite, Manganknebelite, Mangancalcite C, Fe-Ti-ore

(16) Tephroite vein.

Irontephroite, Tephroite, Mangancalcite C, Rhodochrosite, Wine-yellow garnet, Zincblende, Galena

(17) Contact-zone between the first carbonate ore and the rhodonite vein.

Ironknebelite, Mangancalcite B, Amber-yellow garnet, Marmatite

(18) Contact-zone between the *Azuki*-ore and a pink rhodonite vein.

Irontephroite, Mangancalcite B, Wine-yellow garnet, Alabandite

(19) Alleghanyite alabandite mass.

Alleghanyite, Rhodonite, Tephroite, Alabandite, Rhodochrosite

(20) Alabandite mass.

Alabandite, Rhodochrosite, Alleghanyite

Period B_3: The main carbonate period.

(21) *Azuki*-ore.

Rhodochrosite, Various pigmental impurities

(22) Bluish-grey *Azuki*-ore.

Rhodochrosite, Alleghanyite, Wine-yellow garnet

(23) Brown *Azuki*-ore.

Rhodochrosite, Penwithite after alleghanyite, Wine-yellow garnet

(24) Black *Azuki*-ore.

Rhodochrosite, Fibrous pink rhodonite, Manganosite, Black substance, Sericite

Stage C.

Period C_1: Hornstone period.

(25) Hornstone vein.

Hornstone quartz, Manganactinolite, Hyalophane—adularia, Apatite, Green biotite, Chlorite, Fe-Ti-ore

(26) Xenolith of a rhodonite mass in a hornstone vein.

Pink rhodonite, Black hyalophane, Mangantremolite, Hornstone quartz

(27) Xenolith of *Azukiban* in a hornstone vein.

Hyalophane, Fe-Ti-ore, Manganphlogopite, Mangantremolite, Manganactinolite, Red garnet, Chlorite, Hornstone quartz

(28) Fine-grained quartz vein.

Ca-rhodochrosite B, Rhodonite, Fine-grained quartz

(29) The last carbonate ore.

Ca-rhodochrosite B—mangancalcite A, Quartz

(30) Ankerite adularia vein.

Ankerite, Adularia

(31) Penwithite vein.

Various varieties of penwithite

Period C_2: Pegmatitic quartz period.

(34) Pegmatitic quartz vein.

Pegmatitic quartz, Alkali-feldspar

(35) Contact-zone between a pegmatitic quartz vein and a *Azuki*-ore.

Carmine-red rhodonite, Tephroite, Ca-rhodochrosite B, Hyalophane

Period C_3: Rock-crystal period.

(36) Rock-crystal vein.

Rock-crystal, Pink rhodochrosite, Mangancalcite D

(36) Soapstone mass.

Soapstone

(37) Oxidized manganese ore.

Pyrolusite, Pyrochroite (?)

Part B

Mineralogy

Minerals found in the Kaso mine are very numerous and some of them, including a new mineral "kasoite", are particularly rare. In the following pages these minerals will be described in detail with special references to their genetical relationships.

Of the 85 minerals mentioned here 57 were analysed by the present writer along with the determination of the physical constants on the same specimens which were subjected to the chemical analyses.

The chemical analyses were generally performed after the customary way which needs no mention here. The determination of manganese was made by the gravitational method, precipitating manganese hydroxide in an ammoniacal solution under the oxidizing effect of hydrogenperoxide. This method required careful operations and some skill, especially when the amount of manganese to be treated was as large as 0.5 gramme. A small quantity of manganese missed by this precipitation was, without fail, detected and recovered volumetrically from the phosphate coprecipitate of magnesium and this manganese. Re-analysis was inevitable when the manganese to be recovered from the precipitated phosphate was more than 50 mg. To check the result, volumetric determination of total manganese was frequently made in parallel by the sodiumbismuthate method.

Specific gravity was determined by the pycnometer method, and in some rare cases by floating in Clerici's solution.

Refractive indices were measured by immersing in liquids of known refringence, and for specimens with indices higher than 1.7, the iodides(1)-melts in piperine were used after the determination of the refringences of these melts themselves performed by the prism-method. For refringences higher than 1.9, a comparison of them with that of molten sulphur was sometimes attempted.

Determinations of the optic orientations and measurements of the optic axial angles were made on the Fedorow's universal stage.

(1) Mixtures of SbI_3 and AsI_3 in varying proportions.

CHAPTER VIII

SULPHIDES

(a) Pyrrhotite.
(b) Chalcopyrite.
(c) Marmatite.
(d) Zincblende.
(e) Galena.
(f) Alabandite.
(g) Pyrite.

Various sulphide minerals are found in the Kaso deposit though not in a large quantity. Each of these sulphides has been formed successively in a rather restricted period of mineralization. They are arranged in the following Table 11 after the order of mineralization.

TABLE 11. Sulphide minerals of the Kaso mine.

Mineral.	Period.	Occurrence.
Pyrrhotite		In basic igneous rocks.
,,	A_1	In manganhedenbergite veins.
,,	A_1—A_3	In the *Tetuban*.
Marmatite	A_2	In knebelite masses.
,,	A_3	In the first carbonate ore.
Pyrrhotite	B_1	In rhodonite veins.
Chalcopyrite	B_1	,,
Ironzincblende	B_1	,,
Zincblende	B_2	In the *Hie*-ore.
Galena	B_2	,,
Alabandite	B_2	In massive form with alleghanyite.
,,	B_3	In the spotted *Azuki*-ore.
Pyrite	C_{1-3}	In various quartz veins.
,,	C_{1-3}	In the *Aburaban*.

(a) Pyrrhotite.

Pyrrhotite is the unique sulphide mineral found in company with the manganhedenbergite of A_1 period. It is also the one predominant sulphide constituent of the basic igneous rocks which themselves are probably related genetically to the manganese deposits.

Pyrrhotite occurs as irregular grains. The specific gravity and the chemical composition examined on a specimen collected from a manganhedenbergite vein are shown in Table 12.

TABLE 12. Specific gravity and chemical composition of pyrrhotite.

$d_4^{18} = 4.68$

	%		mol. %
Fe	49.36	Fe	46.2
Mn	—	S	53.8
Ni	—		(100.0)
Zn	—		
S	33.02	Formula;	
$CaCO_3$	6.98	Fe_6S_7	
Insoluble	12.35		
	101.71		

Pyrrhotite is also found very abundantly in the black *Tetuban* and, consequently, in some later minerals, for example the black hyalophane (cf. Table 45, p. 379), which have inherited this sulphide from the *Tetuban*. All these pyrrhotite crystals are very fine-grained and dusty. A considerable quantity of pyrrhotite is also suggested as a constituent of the black substances (cf. Chap. XVIII, g).

(b) Chalcopyrite.

Chalcopyrite occurs sparingly in the rhodonite vein of period B_1 as shapeless grains about 3 mm. across. In the oxidized zone one may see blue or green patches consisting of azurite or malachite crystals due to the alteration of chalcopyrite.

(c) Marmatite.

Strikingly iron-rich marmatite is found in association with minerals of A_2 and A_3 period (Pl. XLV (X), Fig. 1). It occurs as small crystals, often as large as 5 mm. across. Steel-black with subadamantine lustre. Only an exceedingly thin slice is transparent under the microscope, being deep reddish-brown and isotropic. Sp. gr. $d_4^{18} = 3.80$. An analysis was made of a material containing a considerable mixture of calcite (Table 13).

TABLE 13. Analysis of marmatite.

	%
Zn	31.8
Fe	20.7
S	24.6
Insoluble	10.8
$CaCO_3$	(12.1)
	(100.0)

	mol. %
ZnS	57.0
FeS	43.0
	(100.0)
S	Lack −5.2

(d) Zincblende.

A small quantity of zincblende is found in the products of B stage. Those of the earlier mineralization are iron-black, with shining lustre. Deep reddish-brown under the microscope. It may probably belong to a ferriferous variety of zincblende, though no decisive data are available to identify its iron content.

Zincblende of the later mineralization is found in the interspaces between tephroite crystals. It is amber-yellow and transparent, and may probably be a form of purest zincblende. It is highly probable that the zincblende can be traced in all its stages of development from marmatite.

(e) Galena.

Galena is rarely found, associated with zincblende in the interspaces between the tephroite crystals produced in B_2 period.

(f) Alabandite.

Alabandite is the most important mineral of the sulphide group found in the Kaso deposit. It is found abundantly as iron-black masses (B_2 period), often as large as one meter across.

Tephroite and alleghanyite are the chief minerals which have been deposited simultaneously with alabandite. The intimate mixture of these minerals are found strongly replaced by the rhodochrosite ore. As all these associated minerals were very soluble in acid, attempts to separate them chemically were unsuccessful, so the analysis was made on a material containing a considerable quantity of impurities with the following results (Table 14).

TABLE 14. Results of analysis of alabandite ore.

Sp. gr. $d_1^{18} = 3.81$

	%		mol. %
Mn	37.51	MnS	(100.0)
S	22.00	Impurities:	
SiO_2	9.97	Spessartine	3.2
TiO_2	0.18	Tephroite	17.8
Al_2O_3	2.51	Rhodochrosite	4.6
FeO	2.30	SiO_2 Lack	−5.0
MnO	19.45		
CaO	1.72		
MgO	1.26		
CO_2	1.50		
H_2O	0.20		
	98.60		

Distinct crystal forms of alabandite were not observed, it being, for the most part, granular massive. Under the microscope it is rather coarse-grained and is found replaced by rhodochrosite along its cleavage-planes (Pl. XXXVI (I), Fig. 4).

On a fresh surface it is iron-black with metallic lustre, but under exposure in the air it tarnishes rapidly to a matt brownish-black mass. Alabandite in thin section is yellowish-green only in a fresh portion, being changed for the most part deep brown owing to a kind of oxidation. Semitransparent and perfectly isotropic. Perfect cleavages are observed. It is soluble even in a very weak acid with effervescences of hydrogensulphide gas.

(g) Pyrite.

Pyrite occurs frequently in the products of C stage or the related altered rocks, as isolated crystals about 1 cm. across. Commonly fine cubic crystals, (100), with marked striations.

CHAPTER IX

OXIDES

(a) Magnetite.
(b) Ilmenite.
(c) Fe-Ti-ore.
(d) Manganosite.
(e) Quartz.

(f) Pyrochroite.
(g) Pyrolusite.

Oxide minerals are found in the Kaso mine only as accessory constituents, but they include a very interesting material which is tentatively termed Fe-Ti-ore in this paper. These minerals are arranged after the order of mineralization in Table 15 below:

TABLE 15. Oxide minerals of the Kaso mine.

Mineral.	Period.	Occurrence.
Magnetite		In basic igneous rocks.
Ilmenite		,,
Quartz		In green hornblende veins.
,,	A_1	In manganhedenbergite veins.
,,	A_1	In albite quartz veins.
,,	B_1	In quartz rhodonite veins.
Fe-Ti-ore (pyramidal type)	B_1	In rhodonite veins.
,,	B_{1-3}	In *Azukiban*.
Manganosite	B_3	In xenoliths enclosed in *Azuki*-ore.
Fe-Ti-ore (platy type)	C_1	In quartz rhodochrosite rhodonite veins.
,,	C_1	In hornstone veins.
Quartz	C_1	As hornstone veins.
,,	C_2	As pegmatitic quartz veins.
,,	C_3	As rock-crystal veins.
Pyrochroite	C_3	In oxidized garnet-fels.
Pyrolusite	C_3	On the outcrop of the deposit.

(a) Magnetite.

Magnetite occurs in a small quantity in autometamorphosed metadiabases, especially in *Kuroboku*. The remarkably abundant iron content of *Kuroboku* is partly due to this mineral.

(b) Ilmenite.

Characteristic skeletal growths indicative of ilmenite are frequently seen in a thin slice of metadiabase (Pl. XXXVI (I), Fig. 5). Remarkably high percentages of titanium and iron found in the compositions of metadiabase and *Kuroboku* given in Table 2, p. 323 are in harmony with the observations under the microscope.

(c) Fe-Ti-ore.

A strikingly titaniferous iron-ore occurs as minute crystals or grains widespread in the products of stages B and C. As it is most

unyielding to metasomatic alteration by a carbonate solution it remains unattacked as red pigments broadly in rhodonite veins or carbonate ores of later mineralizations.

The *Azukiban* and the *Azuki*-ore owe their reddish-brown colour to the content of Fe-Ti-ore. The black pigments found in the *Tetuban* leave a kind of such Fe-Ti-ore when they are attacked by the metasomatism of a carbonate solution.

Fe-Ti-ore occurs in two forms which are quite distinct: (i) As pyramidal crystals forming clusters in a rhodonite vein or in the *Azukiban;* (ii) As platy crystals enclosed in a pink rhodochrosite crystal of C_1 or C_3 period or disseminated in a hornstone vein.

(1) Pyramidal Fe-Ti-ore.

Pyramidal crystals presumably (111) with tetragonal symmetry, sometimes in combination with prismatic faces, are seen under the microscope. In Pl. XXXVI (I), Fig. 2 are shown several pyramidal crystals of relict Fe-Ti-ore found in the main rhodochrosite ore of B_3 period (the *Azuki*-ore), and in Fig. 3 in the same Plate are presented some tiny crystals found embedded in a blood-red rhodonite crystal. Owing to the too small size of the crystals no goniometric data could be obtained. Their forms as observed under the microscope seem to be very near to octahedra of the regular system, although their birefringences offer evidence to the contrary.

This pyramidal Fe-Ti-ore is similar in many respects to iron-rich octahedrite. Macroscopic pyramidal crystals of Fe-Ti-ore were rarely observed. They are black with metallic lustre. Nonmagnetic. The crystals disseminated as very tiny grains in the rhodonite vein or the *Azukiban* are brownish-red to vandyke-red (26 FE), and deep blood-red to carmine-red under the microscope. Uniaxial negative; refractive indices markedly higher than that of molten sulphur. An interesting corona structure of Fe-Ti-ore developed around a titanite(?) crystal is shown in Pl. LIV (XIX), Fig. 3.

(2) Platy Fe-Ti-ore.

This mineral is found enclosed in pink rhodochrosite crystals in a carbonate rhodonite vein of C_1 period. In Pl. XXXVII (II), Fig. 3 are shown trigonal platy crystals with well-developed basal planes, on which are seen striations intersecting at 120°. Similar crystals are found also as an essential constituent in a hornstone vein (Pl. XXXVII (II), Fig. 2). The platy Fe-Ti-ore is usually

carmine-red coloured under the microscope, but, sometimes, it is clear lemon-yellow. A splendid zonal structure is not rare consisting of narrow repetitions of lemon-yellow and carmine-red zones. This lemon-yellow colour remained unchanged even on heating to red heat.

Uniaxial negative interference figure was clearly observed, the optic axis lying perpendicular to the basal plane. Pleochroism weak. Sp. gr. d>4.4, heavier than Clerici's solution of its maximum density.

Chemical investigations were undertaken on a material separated from the pink rhodochrosite by treating with hydrochloric acid. Fe-Ti-ore was found to be rather soluble in hot sulphuric acid. The following results were obtained (Table 16).

TABLE 16. Chemical composition of Fe-Ti-ore.

	I.	II.	III.
Amount removed by acid.	4%	16%	20%
Composition of the removed portion.		wt %	
SiO_2	33	14	21
TiO_2	3	20	17
Fe_2O_3	44	13	20
Al_2O_3	18	32	25
MnO	2	21	17
	(100)	(100)	(100)

I. Soluble part in hot hydrochloric acid.

II. Soluble part removed from the residue of (I) by treating with hot sulphuric acid.

III. Sum of I and II, calculated.

Although the figures given in Table 16 are not satisfactory for use as the basis of further calculations owing to considerably abundant impurities of garnet and rhodonite, it is obvious that the mineral under consideration is remarkably rich in Fe and Ti. It may probably be a kind of a titaniferous hematite. The lemon-yellow variety of hematite, however, has not yet been reported, and will be worth recording as well as the interesting dimorphism(?) of the pyramidal and the platy forms of the Fe-Ti-ore. Mineralogical relationships of the Fe-Ti-ore to other Fe-Ti-minerals, such as ilmenite, crichtonite, pyrophanite, pseudobrookite and arizonite, were hard to make out owing to the lack of a satisfactory material for mineralogical investigations.

(d) Manganosite.

Manganosite is found occasionally as very tiny crystals (Pl. XXXVII (II), Fig. 6 and Pl. XXXVIII (III), Fig. 2). Octahedral crystals of this mineral are seen imbedded in an orbicular xenolithic patch composed of tephroite, alleghanyite, rhodochrosite and alabandite. The interspaces between such orbicular patches is filled with fine-grained rhodochrosite. The formation of the manganosite may possibly be due to the hydrothermal alteration of alabandite ore captured in a rhodochrosite mass.

The crystal of manganosite is transparent with a beautiful emerald-green to mountain-green colour. It is always pure and shows no sign of alteration. Fragments of the manganosite crystal detached from the globular patch have been converted completely into brown spots of superoxidized manganese ore due to a kind of hydrothermal alteration. Black substances accumulated on the border of the patch seem to have reacted as a protector against the alteration of manganosite. Perfectly isotropic and distinguishable from alabandite by its much lower refringence. Optic constants, however, were not measurable owing to the scarcity of a satisfactory material.

(e) Quartz.

Quartz is, as usual, an important mineral in this deposit, though found only as an accessory constituent except in the minerals which are products of C stage. Six modes of occurrence of the Kaso quartz can be distinguished as will be described in the following pages.

1) As the sole constituent of chert, sandstone and quartzite.
2) Chalcedonic quartz seen in the skeletal remains of *Radiolaria* in a Radiolarian slate.

A specimen showing round rings composed of such quartz was photographed in Pl. XXXVII (II), Fig. 4, their detailed skeletal structure, however, was undeterminable.

3) High temperature quartz.

It occurs sparingly as an accessory mineral in a rhodonite vein. In a drusy cavity contained in this vein were found numerous fine crystals, all in the hexagonal bipyramidal form, characteristic of the high temperature modification of quartz.

4) Hornstone.

Hornstone is a rock which consists monomineralically of very

fine-grained quartz. It is found in the Kaso mine as the dominant product mineralized in period C_1. Its mineralization has effected a remarkable hydrothermal metamorphism on almost all minerals previously formed, resulting in new-formed minerals such as manganotremolite, manganphlogopite etc. The hornstone-quartz is also found widely disseminated throughout the wall rock, thus forming a *Kakusekiban*. Minute lenses of hornstone quartz impregnated in *Kakusekiban* are shown in Pl. XXXVIII (III), Fig. 5.

In Pl. XXXVII (II), Fig. 1 is shown a piece of *Azukiban* in process of replacement by a hornstone vein. Garnet and actinolitic amphibole are observed as alteration products and the black substances originally found dispersed in *Azukiban* are seen coagulated into black spots. The hornstone usually occurs accompanied by a small quantity of pyrite, apatite and chlorite. Adularia and Fe-Ti-ore (hematite type) are also seen frequently associated with such quartz.

5) Pegmatitic quartz.

In a very late stage or even after the main mineralization had been finished a pegmatitic quartz vein was intruded into the Kaso deposit, and effected a peculiar contact-metamorphism. Its effects are seen selectively marked on the *Azuki*-ore (cf. Chap. XIV, f; "Carmine-red rhodonite"). The pegmatitic quartz vein seems to have been very dry as it is accompanied only by a small quantity of alkali-feldspar.

6) Rock-crystal.

Quartz is again the dominant product of C_3 period, being deposited as numerous quartz veinlets. The contemporaneous minerals accompanying this quartz are pink rhodochrosite and pyrite. Zonal overgrowths of these two minerals on a rock-crystal are frequently seen as a result of alternating depositions. The quartz here mineralized is a well-crystallized rock-crystal and belongs to a low temperature form.

An interesting twinning of rock-crystals on Japan-law was found, though very rare, in a drusy cavity of the quartz vein (Pl. XXXVII (II), Fig. 5).

(f) Pyrochroite.

In the oxidized zone were found some brown scaly crystals which may tentatively be identified with pyrochroite, but no numerical constants were available to identify it.

A hexagonal platy crystal, markedly striated on the basal plane is shown in Pl. XXXVIII (III), Fig. 1. Optically uniaxial negative, with remarkable pleochroism as follows:

E ..... reddish-brown
O ..... yellowish-brown
E>O.

Indices of refraction much lower than those of the Fe-Ti-ore, the unique resembling mineral of the Kaso deposit. Similar pyrochroite-like mineral is found rather abundantly in the manganese deposit of the Ōasi mine, as a product of hydrothermal alteration of manganosite.

(g) Pyrolusite.

A small quantity of oxidized manganese ore left unworked near the outcrop, consists chiefly of a kind of pyrolusite. This mineral is seemingly a devitrified product of psilomelane which gradually passes, as a rule, into pyrolusite, there being no sharp junctions. Analysis of a very impure specimen was made with the results given in Table 17 below.

TABLE 17. Analysis of an impure pyrolusite ore.

	wt %
MnO_2	55.99
SiO_2	11.82
TiO_2	tr
Al_2O_3	4.27
Fe_2O_3	8.03
CaO	2.62
MgO	3.60
BaO	—
H_2O^+	7.40
H_2O^-	5.38
	99.11

CHAPTER X

CARBONATES

Primary carbonates.

(a) Calcite A.
(b) Fe-Mn-calcite.
(c) Fe-rhodochrosite.

(d) Ca-rhodochrosite A.
(e) Rhodochrosite.
(f) Mangancalcite A.
(g) Ankerite.

Metamorphosed carbonates.

(h) Calcite B.
(i) Manganiferous calcite.
(j) Mangancalcite B.
(k) Mangancalcite C.
(l) Ca-rhodochrosite B.
(m) Mangancalcite D.

Secondary carbonate.

(n) Pink rhodochrosite.
(o) Malachite.
(p) Azurite.

Carbonate minerals found in the Kaso mine are various and abundant, especially the manganiferous carbonates which constitute the main part of the ore mined. They are arranged in Table 18 below after the sequence of mineralization.

TABLE 18. Carbonate minerals of the Kaso mine.

Mineral	Period	Occurrence
Calcite A.		In autometamorphosed igneous rocks.
,, B.	A_1	In manganhedenbergite veins.
Fe-Mn-calcite.	A_3	The first carbonate ore, early member.
Fe-rhodochrosite.	A_3	The first carbonate ore, late member.
Ca-rhodochrosite A.	B_1	In rhodonite carbonate veins.
Mangancalcite B.	B_2	As a product of contact-metamorphism.
Manganiferous calcite.	B_2	,,
Mangancalcite C.	B_2	As a white carbonate in *Hie* ore.
Rhodochrosite.	B_3	The main carbonate ore.
Ca-rhodochrosite B.	C_1	Altered carbonate ore.
Mangancalcite A.	C_1	The last carbonate ore.
Mangancalcite D.	C_3	As a relict mineral in a quartz carbonate vein.
Pink rhodochrosite.	C_3	A secondary carbonate.
Ankerite.	C_1–C_3	In adularia ankerite veins.
Malachite and azurite.		Surface alteration products.

Analyses were made of thirteen of these carbonate minerals, from which the molecular compositions were calculated with the results as compared in Tables 19 and 20 below. These analyses are

divided into two groups, the one including the analyses of primary carbonates and the other those of secondary minerals.

TABLE 19. Variation of molecular compositions of primary carbonates.

Period of mineralization	1 A_3	2 A_3	3 B_1	4 B_3	5 C_1	6 C_{1-3}
$FeCO_3$	24.6	12.7	7.2	2.4	3.4	10.6
$MnCO_3$	16.5	75.0	74.7	84.7	31.4	3.2
$CaCO_3$	53.6	6.9	11.8	8.4	59.6	65.5
$MgCO_3$	5.3	5.4	6.3	4.5	5.6	20.7

1. Fe-Mn calcite ; from Table 22.
2. Fe-rhodochrosite ; ,, ,, 23.
3. Ca-rhodochrosite A ; ,, ,, 24.
4. Rhodochrosite ; ,, ,, 25.
5. Mangancalcite A ; ,, ,, 26.
6. Ankerite ; ,, ,, 27.

TABLE 20. Variation of molecular composition of carbonate minerals recrystallized under the effect of metamorphism.

Period of mineralization	1 A_1	2 B_2	3 B_2	4 B_2	5 C_1	6 C_3	7 C_3
$FeCO_3$	1.5	2.4	1.6	2.0	4 3	5.9	8.3
$MnCO_3$	3.4	4.2	21.8	29.1	53.8	32 1	76 5
$CaCO_3$	91.7	91.2	75.1	62 8	37.5	47.6	11.3
$MgCO_3$	3.4	2.2	1.5	6.1	4.4	14.4	3.9

1. Calcite B ; from Table 28.
2. Manganiferous calcite ; ,, ,, 29.
3. Mangancalcite B ; ,, ,, 30.
4. Mangancalcite C ; ,, ,, 31.
5. Ca-rhodochrosite B ; ,, ,, 32.
6. Mangancalcite D ; ,, ,, 33.
7. Pink rhodochrcside ; ,, ,, 34.

Primary carbonates.

(a) Calcite A.

A kind of calcite occurs as a product of the autometamorphism of basic igneous rocks, but no analytical data have been available to identify it. It is also found in a scapolite salite aplite.

(b) Fe-Mn-calcite.

Calcite very rich in iron and manganese was produced as an early member of the carbonate ore of A_3, period. By the subsequent con-

tact-metamorphism it has lost the dominant portion of its iron and manganese and has been left as a saccharoidal mass, iron and manganese being embodied in knebelite, dannemorite, spessartine or some other contact minerals.

An impure material collected from the saccharoidal carbonate ore inclusive of a considerable quantity of contact minerals was analysed by the author with the results given in Table 21 below.

TABLE 21. Properties of an early member of impure carbonate of period A_3.

$d_4^{18} = 3.38$

wt. %		mol. %	
SiO_2	15.01	Mangancalcite $(MnCa)CO_3$	71.5
TiO_2	—	Dannemorite $(Fe, Mn)SiO_3$	2.1
Al_2O_3	1.72	Knebelite $(Fe, Mn)_2SiO_4$	24.3
FeO	17.51	Spessartine $Mn_3Al_2Si_3O_{12}$	2.1
MnO	11.67		(100.0)
CaO	30.35		
MgO	2.18	(Original carbonate; cf. Table 22)	
CO_2	23.34		
	101.78		

The approximate chemical composition of the original carbonate mineral may be calculated in the following way:— SiO_2 contained in dannemorite and knebelite molecules in Table 21 is removed from the analysis as an impurity along with the included spessartine, and the remaining bases are recalculated to 100 percents as corresponding carbonate molecules. The results of this calculation are given in Table 22.

TABLE 22. Estimated composition of the original carbonate.

	mol. %
$FeCO_3$	24.6
$MnCO_3$	16.5
$CaCO_3$	53.6
$MgCO_3$	5.3

(c) Fe-rhodochrosite.

Fe-rhodochrosite is probably the last product of the mineralization of period A_3. This mineral occurs as compact masses com-

posed of very fine-grained crystals with scarcely any impurities. Only a small quantity of amber-yellow garnet (cf. Chap. XII, a) and marmatite were observed as impurities. Under the microscope it is strikingly turbid, sometimes nearly opaque. Chemical analysis yielded the results shown in Table 23.

TABLE 23. Properties and analysis of Fe-rhodochrosite.

$d_4^{18} = 3.38$
$\omega_D = 1.790$

	wt. %		mol. %	
FeO	.....	7.26	$FeCO_3$	12.7
MnO	.....	43.18	$MnCO_3$	75.0
CaO	.....	3.10	$CaCO_3$	6.9
MgO	.....	2.50	$MgCO_3$	5.4
CO_2	.....	33.42		(100.0)
SiO_2	.....	5.38		
Al_2O_3	.....	1.28		
H_2O	.....	1.62		
Insoluble	.....	2.67		
		100.41		

(d) Ca-rhodochrosite A.

This mineral is found in the form of clusters of coarse-grained pink crystals in the interspaces between blood-red rhodonite crystals. Its physical properties and chemical composition as examined are presented in the following table (Table 24).

TABLE 24. Physical properties and chemical composition of Ca-rhodochrosite A.

Sp. gr. $d_4^{20} = 3.51$
$\omega_D = 1.795$

	wt. %		mol. %	
FeO	.....	4.39	$FeCO_3$	7.2
MnO	.....	44.49	$MnCO_3$	74.7
CaO	.....	5.62	$CaCO_3$	11.8
MgO	.....	2.17	$MgCO_3$	6.3
CO_2	.....	36.90		100.0
H_2O	.....	0.20		
Insoluble	.....	4.98	CO_2 Lack	−0.9
		98.75		

(e) Rhodochrosite.

Rhodochrosite is the dominant constituent of the manganese ore of the Kaso mine. It occurs mainly as a product of the mineralization of B_3 period, i.e. the main carbonate period or the *Azuki*-ore period. Some varieties of rhodochrosite are also found among the products of several other mineralizations. They are, however, varieties more or less rich in iron or lime, which are described in this article under the head of Fe- or Ca-rhodochrosite respectively. A pink-coloured rhodochrosite of presumably secondary origin will be described separately in section (n) of this chapter.

Rhodochrosite proper, though somewhat lime-rich, is found as the sole constituent of the main carbonate ore of B_3 period. This ore and its variegated modifications are called "the *Azuki*-ore." A specimen of the *Azuki*-ore proper with as little impurities as possible was analysed by the author with the following results (Table 25). The presence of a very small quantity of calculated impurity consisting of tephroite as shown in Table 25 is in harmony with the observations under the microscope.

TABLE 25. Composition of rhodochrosite, the pure *Azuki*-ore proper.

$d_4^{18} = 3.58$

	wt. %		mol. %	
FeO	.....	1.40	$FeCO_3$	2.4
MnO	.....	54.14	$MnCO_3$	84.7
CaO	.....	3.77	$CaCO_3$	8.4
MgO	.....	1.46	$MgCO_3$	4.5
CO_2	.....	35.35		(100.0)
SiO_2	.....	2.68	CO_2 Excess	1.2
H_2O	.....	0.12	Impurity: Tephroite	5.5
		98.92		

(f) Mangancalcite A.

The lime-rich carbonate ore of late mineralization of C stage is considered as the last carbonate ore in this deposit. This ore occurs as coarse-grained massive aggregates or as veinlets consisting of clear pink mangancalcite crystals. Paragenesis of quartz and pyrite is not uncommon in this ore. Physical and chemical properties of this mangancalcite were examined with the following results (Table 26).

TABLE 26. Physical constants and chemical composition of mangancalcite A of period C_1.

Sp. gr. $d_4^{20} = 3.00$
Refringence $\omega_D = 1.710-1.760$
Chiefly near 1.730

wt. %		mol. %	
FeO	2.38	$FeCO_3$	3.4
MnO	21 27	$MnCO_3$	31.4
CaO	32.11	$CaCO_3$	59 6
MgO	2.17	$MgCO_3$	5.6
CO_2	41.75		(100.0)
H_2O	0.20		
	99.88	CO_2 Lack	−1.5

(g) Ankerite.

Ankerite occurs as colourless transparent crystals forming narrow veinlets traversing the wall rock or the last carbonate ore. It is frequently found accompanied by adularia. Brown tarnishing due to exposure in air is a characteristic feature of this mineral. Physical constants and chemical composition as examined on a picked material are given in Table 27 below.

TABLE 27. Physical constants and chemical composition of ankerite.

Sp. gr. $d_4^{17} = 2.87$
Refringence $\omega_D = 1.700$

wt. %		mol. %	
FeO	8.05	$FeCO_3$	10.6
MnO	2.37	$MnCO_3$	3.2
CaO	38.50	$CaCO_3$	65.5
MgO	8.75	$MgCO_3$	20.7
(CO_2 calc.	42.33)		(100.0)
	(100.00)		

Metamorphosed carbonates.

(h) Calcite B.

Calcite occurs also in the manganhedenbergite vein as large crystals enclosing poikiloblastic tiny crystals of manganhedenbergite. This mineral was termed calcite B in order to discriminate it from calcite A found in autometamorphosed igneous rocks.

Colourless and transparent. $d_4^{18} = 2.75$. The results of analysis made by the author are presented in Table 28.

TABLE 28. Analysis of calcite B.

	wt. %		mol. %
CaO	50.00	$FeCO_3$	1.5
MgO	1.36	$MnCO_3$	3.4
FeO	1.06	$CaCO_3$	91.7
MnO	2.37	$MgCO_3$	3.4
CO_2	38.70		(100.0)
H_2O	0.56		
Insoluble	5.58		
	99.63		

(i) Manganiferous calcite.

Calcite slightly manganiferous, occurs as saccharoidal aggregates with some corroded crystals of relict manganhedenbergite among them (Pl. XXXVIII (III), Fig. 4). Its composition was calculated on the basis of the composition of the contact-metamorphosed carbonate ore of A_3 period presented in Table 21, by removals of corresponding compositions of admixed minerals (Table 29). The contact-metamorphism of this carbonate, which had probably been mineralized in period A_3, seems to have taken place later in period B_2 contemporaneously with mineralization of some other contact minerals.

TABLE 29. Calculated composition of saccharoidal manganiferous calcite of period B_2.

	mol. %
$FeCO_3$	2.4
$MnCO_3$	4.2
$CaCO_3$	91.2
$MgCO_3$	2.2
	(100.0)

(j) Mangancalcite B.

Several fragments of the first carbonate ore are seen enclosed in a rhodonite vein. They are comparatively pure being presumably derived from the Fe-rhodochrosite of late mineralization of A_3 period (Table 23). They have been completely changed to white saccharoidal masses surrounded by a rim of manganknebelite or knebelite.

These manganese silicates of the olivine group are apparently the product of contact-metamorphism, the details of which will be described in Chapter XIII. A few minute crystals of marmatite and celsian are seen sometimes as relict minerals free from the effect of contact-metamorphism. These impurities, though scanty and sporadic, show clearly the original character of this carbonate. The properties of this white saccharoidal carbonate were examined with the following results (Table 30).

TABLE 30. Properties of saccharoidal mangancalcite B.

Sp. gr. $d_4^{18} = 2.98$

wt. %		mol. %	
FeO	1.14	$FeCO_3$	1.6
MnO	15.05	$MnCO_3$	21.8
CaO	41.27	$CaCO_3$	75.1
MgO	0.61	$MgCO_3$	1.5
CO_2	40.83		(100.0)
Insoluble	0.20		
	99.10	CO_2 Lack −5.2	

(k) Mangancalcite C (white mangancalcite).

This mineral occurs as white turbid crystals embedded in an irontephroite mass (Pl. XXXVIII (III), Fig. 3), and are seemingly in equilibrium with irontephroite and rhodonite as the following diagram shows;

$$\underset{\text{(blood-red rhodonite)}}{MnSiO_3} + \underset{\text{(Fe-rhodochrosite)}}{(FeCaMn)CO_3} \longrightarrow \underset{\text{(irontephroite)}}{(FeMn)_2SiO_4} + \underset{\text{(Mn-calcite)}}{(MnCa)CO_3}.$$

The details of this reaction are also described in Chapter XIII in this paper.

Physical properties and chemical composition of this mineral are presented in the following Table 31. The lack of uniformity of its refringence shows that the white clot is really a mixture of carbonate corresponding to various grades of demanganisation. Under the microscope the mineral is intensely dusty and turbid owing to numerous minute inclusions (Pl. XXXIX (IV), Fig. 2). Sometimes strongly pleochroic crystals are found; $O \ll E$. Compare with the mangancalcite D shown in Figs. 3 and 4 in Pl. XXXIX (IV).

TABLE 31. Physical properties and chemical composition of white mangancalcite.

Sp. gr. $d_4^{16} = 3.00$
Refringence $\omega_D = 1.675—1.715$

	wt. %		mol. %	
FeO	.....	1.36	$FeCO_3$	2 0
MnO	.....	19.59	$MnCO_3$	29.1
CaO	.....	33.12	$CaCO_3$	62.8
MgO	.....	2.37	$MgCO_3$	6.1
CO_2	.....	37.69		(100.0)
H_2O	.....	0.23		
Insoluble	.....	3.62	CO_2 Lack —9.5	
		97.98		

(l) Ca-rhodochrosite B.

This mineral occurs as extremely fine-grained aggregates, replacing rhodonite and some other minerals previously formed (Pl. XL (V), Fig. 1). Macroscopically greyish-white, but under the microscope it is smoky-brown owing to its turbidity. Strikingly turbid, sometimes nearly opaque. Fragments of the wall rock captured in this ore are seen intensely altered and for the most part sericitized. Results of a chemical analysis along with the observed physical properties are given in Table 32 below.

TABLE 32. Physical constants and chemical composition of opaque Ca-rhodochrosite B.

Sp. gr. $d_4^{15} = 3.05$
Refringence $\omega_D = 1.731$

	wt. %		mol. %	
FeO	.....	2.31	$FeCO_3$	4.3
MnO	.....	29.33	$MnCO_3$	53.8
CaO	.....	15.61	$CaCO_3$	37.5
MgO	.....	2.56	$MgCO_3$	4.4
CO_2	.....	30.67		(100.0)
SiO_2	.....	4.37	CO_2 Lack —5.9	
Al_2O_3	.....	1.08	SiO_2 Excess 4.1	
H_2O	.....	0.95	Impurities:	
Insoluble	.....	12.86	Sericite 4 1	
		99.74	Quartz Insoluble	

Some specimens of such turbid ores are seen affected by the hydrothermal alteration of a siliceous solution, which has resulted

in a marked grain-growth of this carbonate. A semispherulitic structure looking like cabbage leaves is characteristic of such recrystallized carbonate as is shown in Pl. XXXIX (IV), Fig. 1. Strong pleochroism is also common. O; reddish-brown to smoky-purple, E; colourless. O$\gg$E.

The turbid Ca-rhodochrosite is probably an alteration product derived from the *Azuki*-ore, which has been demanganized by the hydrothermal solution of C_1 period.

(m) Mangancalcite D (pleochroic mangancalcite).

White clots of a relict carbonate mineral are seen sporadically distributed in a quartz carbonate vein of C_3 period accompanied by transparent pink rhodochrosite. This white mangancalcite D is also strongly pleochroic under the microscope (Pl. XXXIX (IV), Figs. 3 and 4). Such a peculiar pleochroism of a carbonate mineral may be due to minute inclusions which are arranged in the mother crystal in parallel position. The results of an analysis are given in Table 33.

TABLE 33. Analysis of pleochroic mangancalcite.

Sp. gr. $d_4^{18} = 2.95$

wt. %		mol. %	
FeO	3.95	$FeCO_3$	5.9
MnO	21.07	$MnCO_3$	32.1
CaO	24.85	$CaCO_3$	47.6
MgO	5.40	$MgCO_3$	14.4
CO_2	37.69		(100.0)
H_2O	0.26		
Insoluble	5.50	CO_2 Lack	−8.0
	98.72		

Secondary carbonates.

(n) Pink rhodochrosite.

Beautiful pink rhombohedra of lime-rich rhodochrosite are seen abundantly in a quartz carbonate vein of C_3 period as one of the last products of the Kaso mineralization. The dominant quartz is well-crystallized rock-crystals frequently forming beautiful druses

mounted with fine crystals of associated minerals. It is accompanied usually by pyrite crystals and clots of white pleochroic mangancalcite described above. Fibrous radiating crystals of this mineral are frequently observed in the druse (Pl. XL (V), Fig. 2). The results of investigations made on a pure specimen of this mineral are given below (Table 34).

TABLE 34. Density and composition of pink rhodochrosite.

Density $d_4^{13} = 3.51$

wt. %		mol. %	
FeO	5.34	$FeCO_3$	8.3
MnO	47.92	$MnCO_3$	76.5
CaO	5.63	$CaCO_3$	11.3
MgO	1.41	$MgCO_3$	3.9
CO_2	36.88		(100.0)
H_2O	0.06		
Insoluble	1.95	CO_2 Lack	−5.0
	99.19		

The genesis of this pink rhodochrosite leaves much to be investigated. A greater part of manganese leached from various manganese minerals by a hydrothermal solution of C stage might have been deposited in more advanced stages in forms of this new carbonate which was in equilibrium with the ultimate mineralizing solution. Rhodochrosite of B_3 period, for example, might have been left as white clots of mangancalcite D described in the preceding section, being deprived by the solution of C_3 period of the greater portion of its manganese content, which has again been deposited later as the pink rhodochrosite.

It is not fully ascertained that the pink rhodochrosite mentioned here is always a product of a hydrothermal metamorphism. No explanation, however, can be offered to account for the occurrence of a primary carbonate so rich in manganese from the ultimate mineralizing solution of C_3 period (cf. Tables 19 and 20).

(o) Malachite.

(p) Azurite.

These two associated minerals occur sparingly in the oxidized zone as an oxidation product of chalcopyrite.

CHAPTER XI

FELDSPARS

Barium feldspars.
Basic feldspars.
Solid-solution relationship.
Physical properties of barium feldspars.
Na:K ratio.

(a) Adularia.
(b) Alkalifeldspar.
(c) Hyalophane.
(d) Kasoite.
(e) Celsian.
(f) Bariumalbite.
(g) Albite.
(h) Plagioclase.

Minerals of the feldspar group found in the Kaso mine are numerous and noteworthy, although never found in a large quantity. Feldspars containing barium occur intimately associated with manganese ores as a product of contemporaneous mineralization.

The interesting evolution of these feldspars deserves mention here. Their composition varies in the following order: Bariumalbite → Celsian → Kasoite → Hyalophane → Alkalifeldspars including adularia. This sequence is approximately in order of decreasing barium and increasing potash. Feldspars from the Kaso mine are arranged in the following Table 35 after the order of mineralization.

TABLE 35. Minerals of the feldspar group found in the Kaso deposit.

Mineral.	Period.	Occurrence.
Plagioclase		In basic igneous rocks
Albite		,,
,,	A_1	As albite veinlets
Bariumalbite	A_1	In manganhedenbergite veins
Celsian	A_2	In picroknebelite masses
Kasoite	B_1	In kasoite rhodonite veins
Hyalophane	C_1	In mangantremolite rhodonite veins
Alkalifeldspar	C_2	In pegmatitic quartz veins
Adularia	C_{1-3}	In adularia ankerite veins

Barium feldspars.

A few general remarks will be made on barium feldspars, because some of them, especially the "kasoite," are the most characteristic minerals of the Kaso mine.

(i) Chemical composition.

All accessible analyses of barium-containing feldspars are compared in Table 36 below. Analyses with less barium than 2% BaO were omitted. Nos. 6, 7, 12 and 14 are those reported in the present article. The specimens are arranged from Nos. 1 to 20 in order of decrease in barium content.

TABLE 36. Chemical analyses of barium-containing feldspars.

	1.	2.	3.	4.	5.	**6.**	**7.**	8.	9.	10.
SiO_2	31.9	35.06	33.9	32.43	32.23	29.3	38.48	51.6	51.30	52.67
Al_2O_3	27.3	30.23	25.6	26.55	27.40	29.7	23.61	21.9	21.50	21.12
Fe_2O_3	—	0.60	—	0.12	0.32	—	0.60	—	—	—
CaO	—	—	—	0.23	0.39	—	0.85	—	—	0.46
MgO	—	—	—	0.11	0.13	—	0.97	—	0.84	0.04
BaO	40.8	34.38	37.7	39.72	36.45	34.5	25.50	16.4	15.11	15.05
Na_2O	—	—	—	0.16	0.77	2.5	1.85	—	0.55	2.14
K_2O	—	—	—	0.22	0.22	3.9	5.10	10.1	9.25	7.82
H_2O	—	0.21	—	0.64	1.02	—	0.98	—	0.58	0.58
MnO	—	—	—	—	0.24	—	2.67	—	—	—
TiO_2	—	—	—	—	—	—	—	—	—	—
Others ...	—	—	0.4(1)	0.64 —0.27(2)	0.12 —0.05(2)	—	—	—	—	—
	100.0	100.48	97.6	100.55	99.24	100.0	100.61	100.0	100.0	99.88

Locality.

1) Theoretical composition for $BaAl_2Si_2O_8$
2) Candoglia (so-called Paracelsian)
3) Alaska
4) Jakobsberg (in Mn-deposit)
5) ,, ,,
6) Kaso Mine (celsian B)
7) ,, ,, (kasoite)
8) Theoretical composition for Cn_1Or_2
9) Imfeld, Binnental
10) ,, ,,

Literature.

E. Tacconi: Zs. Kr., **43** 424 (1907).
S. T. Schaller: Am. Min., **14** 319 (1929).
Hj. Sjögren: G. För. Förh., **17** 578 (1895).
Strandmark: ,, ,, , **25** 289 (1903).
Present article, Table 51.
,, ,, , Table 48.
Urlaub: Pogg. Ann., **100** 549 (1859).
Stockar-Eschar: Kenngott: Ueb. 107 (1856).

(1) Insoluble. (2) F—(O).

TABLE 36. (*Continued*).

	11.	12.	13.	14.	15.	16.	17.	18.	19.	20.
SiO_2	61.90	50.52	45.40	59.52	51.14	53.53	55.10	62.95	62.60	59.69
Al_2O_3	15.80	16.58	20.82	15.76	22.86	23.33	23.20	19.82	19.97	21.07
Fe_2O_3	—	4.97(3)	1.54(3)	0.68	—	—	0.45	0.17	0.12	2.27(3)
CaO	0.40	1.23	2.70	0.73	4.28	—	1.83	0.25	0.19	0.95
MgO	1.30	3.09	0.76	1.68	3.10	3.23	0.56	—	—	—
BaO	9.58	9.02	10.58	7.60	9.56	7.30	7.30	3.95	3.71	2.27
Na_2O	6.02(2)	1.23	2.69	0.98	9.06	—	7.45	4.01	4.31	6.55
K_2O	—	6.35	7.54	8.80		11.71	0.83	8.57	8.95	8.61
H_2O	—	1.50	2.35	0.67	—	—	3.72	0.11	0.19	—
MnO	5.00(1)	5.75	2.67	1.15	—	—	—	—	—	—
TiO_2	—	0.22	—	1.10	—	—	—	—	—	—
Others....	—	—	3.50(4)	1.87(5)	—	—	—	—	—	0.36(6)
	100.00	100.95	100.55	100.12	100.00	99.10	100.44	99.83	100.04	101.74

Locality.	Literature.
11) Sjö Mine, Sweden	Igelström : G. För. Förh., **10** 416 (1888).
12) Kaso Mine (hyalophane A)	Present article, Table 44.
13) Franklin Furnace, N.J.	Jenkins & Bauer : Am. Min., **11** 172 (1926).
14) Kaso Mine (hyalophane C)	Present article, Table 46.
15) Jakobsberg, Sweden	Igelström : Ofv. Ak. Stockh, **24** 15 (1867).
16) ,, ,,	,, : B.S.F.M., **6** 139 (1883).
17) ,, ,,	Pisani : B.S.F.M., **1** 84 (1878).
18) Delaware, Pa. (cassinite)	Genth : Proc. Ac. Philad., 110 (1866).
19) ,, ,, ,,	Sperry : Am. J. Sci., **36** 326 (1888).
20) Vogelsberg	Knop : Jb. Min., 687 (1865).

Basic feldspars.

Some of the analyses given in Table 36 are remarkably poor in silica. It is more obvious in the calculated molecular percentages presented in Table 37 below. In this calculation the want of silica was embodied in corresponding amount of Ne + Kp (nepheline and kaliophilite molecules). Excess or want of alumina will not be touched upon in this paper.

(1) Including FeO. (2) Including K_2O. (3) FeO. (4) SO_3+PbO+ZnO.
(5) P_2O_5. (6) SrO.

TABLE 37. Molecular composition of barium-containing feldspars.

	Celsian———						———kasoite.
mol. %	1.	2.	3.	4.	5.	**6.**	**7.**
Cn	100	100	100	95.5	87.1	73.3	49.6
Or+Ab	0	0	0	2.0	4.2	0	8.5
Ne+Kp	0	0	0	2.5	8.7	26.7	41.9
Al_2O_3 Excess	0	+33	+2	0	+8	0	−5.6
SiO_2 Excess	0	+61	+29	0	0	0	0

	Hyalophane———											———adularia.
mol. %	8.	9.	10.	11.	**12.**	13.	**14.**	15.	16.	17.	18.	19.	20.
Cn	33	32.0	29.0	25.4	23.5	19.0	18.5	17.2	16.0	15.2	7.5	6.5	4.0
Or+Ab	67	68.0	71.0	74.6	62.0	44.0	81.5	55.0	64.3	84.8	92.5	93.5	64.5
Ne+Kp	0	0	0	0	14.5	37.0	0	27.8	19.7	0	0	0	31.5
Al_2O_3 Excess	0	+2	0	0	0	0	0	+3	0	α[1]	0	0	0
SiO_2 Excess	0	0	0	+65	0	0	+79	0	0	+11	+6	0	0

Nos. **6**, **7**, **12** and **14** are those from the Kaso mine.

The composition of barium-containing feldspar, consequently, will be more conveniently discussed as a member of the ternary system Cn − (Or + Ab) − (Ne + Kp). The specimens listed in Table 37 were plotted in the ternary diagram as shown in Fig. 6.

The existence of so many basic feldspars[2] is worthy of note. As the kasoite is one of the most basic feldspars a few words will be added here though it is not the aim of this paper to discuss the subject in detail.

Even in a well-known basic feldspar, "the anemousite", the paucity of the silica was only as much as was satisfied if 10% carnegieite molecules were considered in its molecular composition. The necessity of taking 42% (Ne + Kp) molecule in the calculation of the composition of kasoite will, therefore, be a striking fact. The showing of such a remarkable paucity of silica was not accidental as the analysis of the kasoite was made on a carefully picked material.

The paragenetic relations are also in harmony with the basisity of the kasoite. Of the four Kaso feldspars given in the above tables the silica-poor three, Nos. 6, 7 and 12, were never found associated

(1) α, reported as a mixture of anorthite.

(2) The author proposes to call such a silica-poor feldspar a "basic feldspar", although this name is sometimes used as a synonym of "calcic plagioclase".

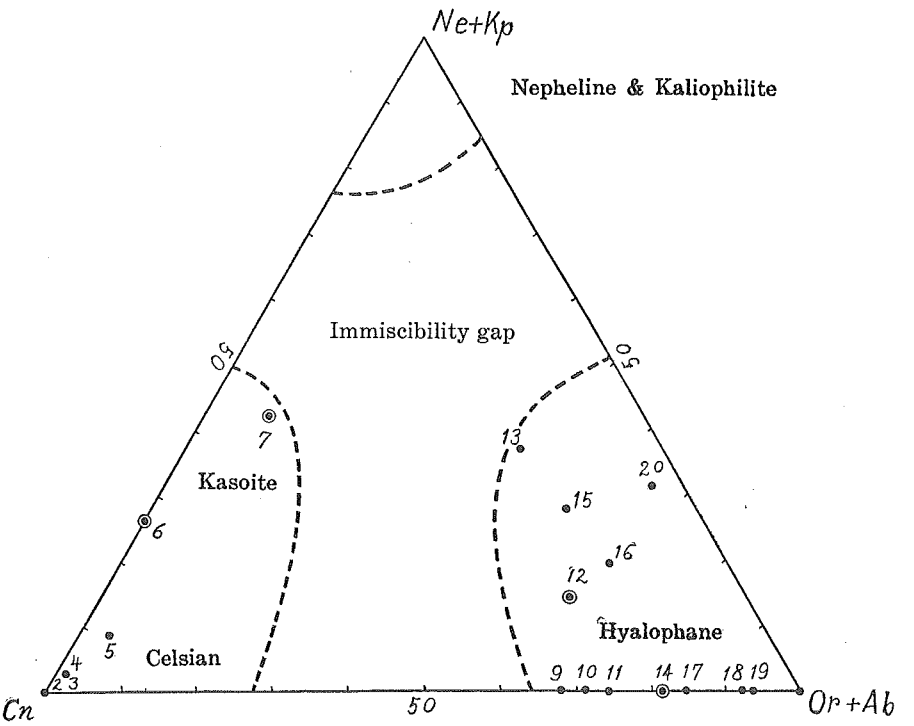

Fig. 6. Variations in composition of barium-containing feldspars.

with quartz, while No. 14, the hyalophane C which was the only silica-rich feldspar, was found closely associated with hornstone-quartz.

The solid-solution relationship.

It is believed that a complete series of mixed crystals exists between the two end members, celsian and adularia, the intermediate member being called a hyalophane. But it is more correct to say that the complete solid-solution relationship in this system is not yet fully ascertained as there is in this series a large range, the representatives of which have never been found in nature nor successfully synthesized.

The occurrence of kasoite, however, may throw little light upon this problem, as it is a kind of strikingly basic feldspar, but in connection with the basic barium feldspars, it has given a basis for a further elucidation of their solid-solution relationship.

It is unlikely that mixed crystals can occur in the silica-poor division of the ternary system (Ne + Kp) – (Or + Ab) – Cn; in other words, celsian which is poor in silica but rich in alkali (i.e. kasoite) and barium-containing basic alkalifeldspars are not isomorphous, with a rather broad range of non-mixing between them. Kasoite includes a part of the isomorphous group of silica-poor alkali-rich celsian, corresponding to the opposite extremity of this series against the pure celsian end.

The exact boundary of the non-mixing gap in the ternary system is not determined. Experimental data were not available for this problem. After their synthetic experiments on barium feldspars Dittler and Lasch[1] had little to say on such immiscibility. Whether the immiscibility gap in the ternary system reaches the Cn–Or line or not is the most important problem now remaining. Much more reliable and complete data are required regarding minerals of the hyalophane group, containing more barium than those previously known in hyalophanes.

Physical properties of barium feldspars.

The physical constants previously reported of the minerals, the analyses of which are given in Table 36, are listed in the following Table 38, with some additional data, 9′, 9″ 12′, 17′ and 18′ which are quoted from a text-book[2].

For the theoretical celsian proper, No. 1, the data measured by Eskola[3] on an artificial material are included in this table.

In Figs. 7–9, plotting the specific gravity, indices of refraction, birefringence, optic axial angle and extinction angle c ∧ X on (010), it will be noted that for most of the barium-containing feldspars a straight-line relationship here also exist against the molecular percentage of celsian Cn.

The break of curves seen near about a point on 40% Cn may presumably be due to the immiscibility related to the content of the basic feldspar molecules, Ne + Kp. Fig. 7 shows the variations in the specific gravity. The straight-line relationship is most apparent in this figure. The paucity of silica has little effect on the specific

(1) E. Dittler and H. Lasch: Sitzb. Wien Ak., **140** 633 (1931).
(2) Rosenbusch-Mügge: Mikroskopische Physiographie u.s.w. I. **2**, 686 (1927).
(3) P. Eskola: Am. J. Sc., **4** 367 (1922).

TABLE 38. Physical constants of barium-containing feldspars.

No.	Composition.			sp. gr. d	Optic orientations.	Indices of refraction.			Birefringence.	Optic axial angle.
	Cn	Or +Ab	Ne +Kp			α	β	γ	γ−α	2V
1	100	0	0	3.573	b≒Y, c∧X = +3°	1.587	1.593	1.600	0.013	(+) —
2	100	0	0	3.325		—	1.592	—	—	(+) 83°5
3	100	0	0	—	b≒Y, c∧X = +5°	1.584	1.589	1.596	0.012	90°
4	95.5	2.0	2.5	3.384	b≒Y, c∧X = +3°	1.5835	1.5886	1.5941	—	(+) 86°
5	87.1	4.2	8.7	—	b≒Y, c∧X = −3°	—	—	—	—	(+) —
6	73.3	0	26.7	—	b≒Y, c∧X = +2°	1.5795	1.5826	1.5862	0.0067	(+) 86°
7	49.6	8.5	41.9	3.003	b≒Y, c∧X = +2°	1.5645	1.5685	1.5720	0.0075	(−) 80°.5
9	32.0	68.0	0	2.80	b≒Z, a∧X = −5°	—	1.5392	—	—	(−) 79°.0
9′	30.0	70.0	0	2.818	—	1.5419	1.5451	1.5469	0.0050	(−) 78°.5
9″	24.0	76.0	0	2.756	— a∧X = −6°	—	—	1.5426	—	(−) 77°.5
12	23.5	62 0	14.5	2.78	b≒Z, a∧X = −5°	1.5378	1.5425	1.5460	0.0082	(−) 75°.5
12′	21.0	79.0	0	2.733	— a∧X = −2°	1.5373	1.5395	1.5416	0.0043	(−) 74°
13	19.0	44.0	37.0	—	—	—	1.54	—	—	(−)
14	18.5	81.5	0	2.73	b≒Z, a∧X = +5°	1.5380	1.5420	1.5445	0.0065	(−) 75°.0
17	15.2	84.8	0	—	— a∧X = +7°	—	—	—	—	—
17′	9.0	91.0	0	2.645	— a∧X = +5°	—	—	1.5335	—	—
18	7.5	92.5	0	2.692	b≒Z, a∧X = +6°	—	—	—	—	—
18′	5.0	95.0	0	2.593	—	1.5201	1.5240	1.5257	0.0056	(−) 71°.5

gravity, which shows that the end-members corresponding to $NaAlSiO_4$ or $KAlSiO_4$ may probably have specific gravities very near 2.6 if embodied in modal minerals.

The variations in the refringences are most noteworthy (Fig. 8). Their plots are divided clearly into two groups, (i) continues from the Cn-end, celsian to kasoite; and (ii) continues from the adularia-end, hyalophane to adularia; each of the groups arranged on a straight line independently.

That the plots of some basic hyalophanes deviate from the curve always on the upper side is in harmony with the assumption that Ne or Kp molecule, if it appears as a modal mineral, must have higher refringence, than orthoclase or albite. The refringence of such a hypothetical mineral may be extrapolated from the curve of Fig. 8 to be near 1.545 or higher.

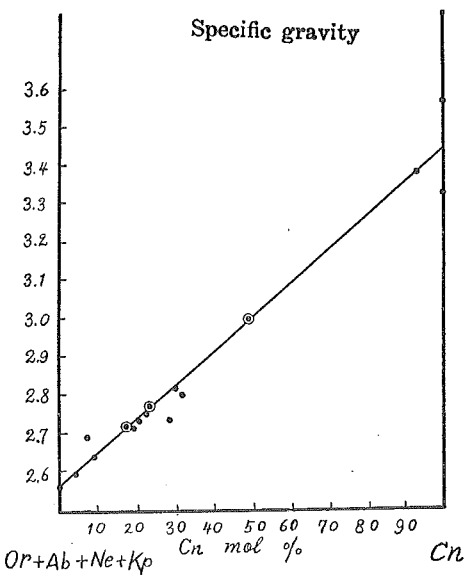

Fig. 7. Variation of the specific gravity of barium-containing feldspars.

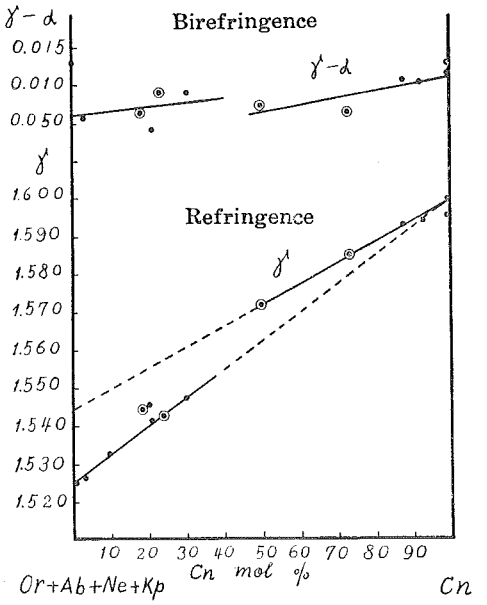

Fig. 8. Variations of refringence and birefringence.

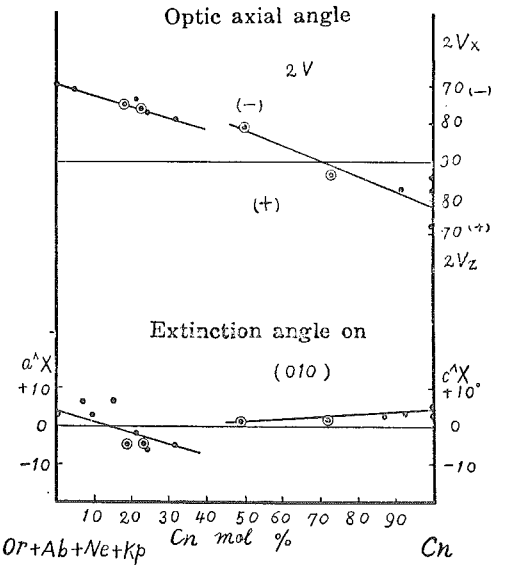

Fig. 9. Variations of the extinction and the optic axial angle.

⊙ Specimens from the Kaso Mine

Bieliankin[1] stated that the refringence of the end-member $NaAlSiO_4$ would be as high as $\beta = 1.57$, remarkably higher than that of carnegieite.

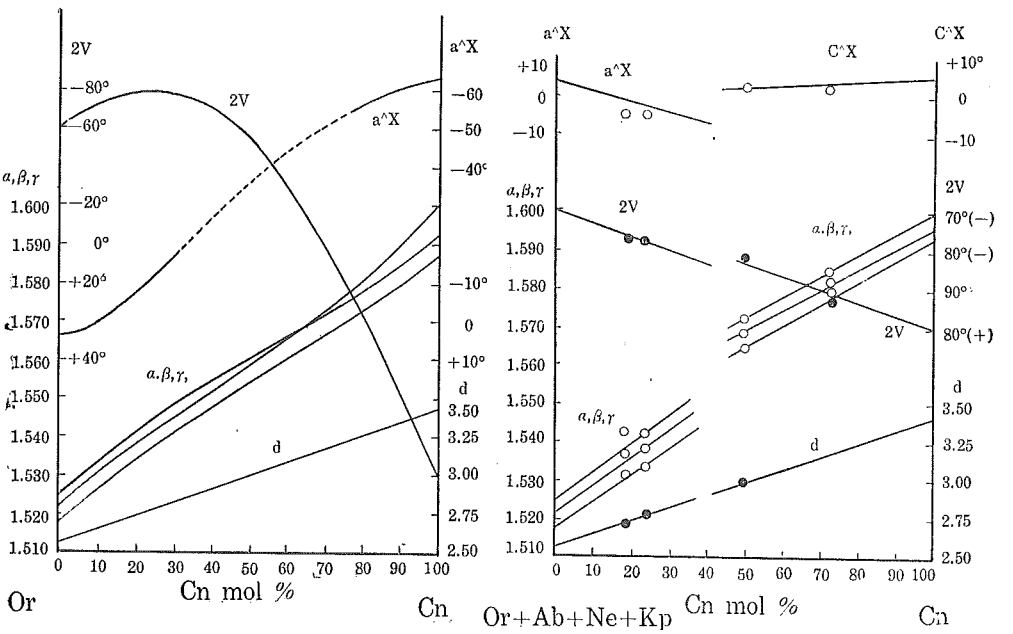

Fig. 10 a. Variations in composition and optic properties in the adularia-celsian series.

By A. N. Winchell.

Fig. 10b. The same as Fig. 10a, based on practical data inclusive of those known of some basic members.

By the present author.

The extinction angle c ^ X′ on 010 differs remarkably with the two groups of this system (Fig. 9). It is unlikely that the two can be connected by a smooth curve[2]. This discontinuity shows most clearly the gap of miscibility in this barium feldspar series. It is not certain whether the discontinuity in the transitions of the extinction still exists in the silica-rich system because no data are now available for a wide range of silica-rich members from $Cn_{30}\ Or_{70}$ to $Cn_{80}\ Or_{20}$.

---

(1) D. S. Bieliankin: Compt. Rend. Ac. Sci. U.R.S.S. (1931).

(2) STRANDMARK: G. För. Förh., **26** 97 (1907), reported a rapid rise of the extinction angle with the increase of Cn% in the hyalophane on basis of his observations on a zoned crystal. His records are not in accordance with other data and a further examination is required in this connection.

The optic axial angle (Fig. 9) and birefringence (Fig. 8) change more or less uniformly though nothing decisive can be concluded from their variations. It deserves mention here that the uniaxiality never occurs at 65% Cn in this series, though it has been stated in some text-books. The optic axial angle, on the contrary, is 90° and the optical character, changes from positive to negative at this point.

A diagram showing variations in composition and optic properties in the adularia-celsian series is graphed on the basis of the new data described above (Fig. 10b). The old diagram[1] and the new revised one are compared in Fig. 10. Some of the discrepancies between these two are inevitable, because the new diagram is, if more rigorously stated, not a graph of a binary system but a projection of the ternary system, Cn−(Ne + Kp)−(Or + Ab), on a binary line, Cn −(Or + Ab + Ne + Kp).

Basic feldspar molecules in kasoite.

Molecules reported as Ne and Kp in the calculation of the kasoite composition are represented by the following formulas.

Ne ..... $NaAlSiO_4$.
Kp ..... $KAlSiO_4$.

The reason why the nepheline molecule instead of the carnegieite molecule was considered will here be discussed in some detail. The solubility of the nepheline molecule in feldspars has frequently been discussed on the basis of reliable experimental data[2]. A wide range of mutual solubility has been established by some authors. Some of the considerations paid here on the variations in the physical properties of basic barium feldspars show that the molecules Ne and Kp, if embodied in modal minerals, must appear as minerals quite similar to nepheline and kaliophilite respectively.

Extrapolation based on the assumed linear relationship of physical constants against the percentage of the constituent molecule gives the following properties for these hypothetical minerals.

---

(1) A. N. WINCHELL: Elements of Optical Mineralogy, Part II (1927) p. 314.

(2) N. L. BOWEN: Am. J. Sc., **33** 551 (1912).
E. DITTLER & H. LASCHS. l.c (1931).
E. DITTLER: T. M. P. M., **39** 122 (1911).

Sp. gr.	$d = 2.6$
Refringence	$\gamma = 1.545$
Birefringence	very low
Optically negative	

These properties are in substantial agreement with those of the modal nepheline, and, on the other hand, differs notably from those of carnegieite.

Na : K Ratio.

Of the constituent molecules of barium feldspars given in Table 37, the numerical value of each Or, Ab, Ne and Kp was not obtainable because the distribution of alkalis between the feldspar and the nepheline molecules were out of estimation.

The ratio Or + Kp : Ab + Ne, however, is known from the Na : K ratio as shown in the following Table 39. As the calculation is referred to the simple formula $NaAlSiO_4$ for Ne and $KalSiO_4$ for Kp, the ratio Na : K corresponds as itself to the ratio Ab + Ne : Or + Kp.

TABLE 39. Na : K ratios in barium-containing feldspars compared with celsian percentages.

No.	(atomic ratio) Na : K.	Cn %.
1	—	100
2	—	100
3	—	100
4	1.25	95.5
5	0.52	87.1
6	1.25	73.3
7	0.55	49.6
8	—	33
9	0.08	32.0
10	0.27	29.0
11	—	25.4
12	0.41	23.5
13	0.55	19.0
14	0.14	18.5
15	—	17.5
16	—	16.0
17	13.6	15.2
18	0.71	7.5
19	0.73	6.5
20	1.14	4.0

The affinity of Ba and K is an evident fact frequently observed in their distribution in nature. The ratio Na:K is, consequently,

expected to be very small in barium feldspars, but the results of examination are quite the contrary as shown in Table 39 above.

It is, however, interesting to see a regularity in the variation of the ratios between the two alkalis and that of barium found in the Kaso feldspars. As is reproduced in the following Table 40, the ratio Na : K quickly decreases as Cn% decreases, showing an immediate replacement of Cn by Or. This is also an evident representation of a mode of paragenesis of Ba and K.

The paragenesis of barium with alkalis at the beginning of the mineralization of the Kaso mine is represented by the association of bariumalbite and celsian, but only a small amount of barium seems to be contained in the bariumalbite. Afterwards in stage B abundant barium was introduced accompanied by a large quantity of potash instead of soda and here produced a plenty of kasoite, in which mineral is represented the paragenesis of Na + K + Ba.

In stage C there was mineralized a series of hyalophanes in which the predominant bases are K and Ba. The mutual solubility of Cn and Or is seen to be remarkably larger than that existing between Cn and Ab.

TABLE 40. Paragenesis of alkalis and barium in barium feldspars from the Kaso mine.

Stage.	Mineral.	m.l. % Cn.	Mol. Ratio. Na : K.
A	Celsian B	73.3	1.25
B	Kasoite	49.6	0.55
C	Hyalophane A	23.5	0.41
,,	Hyalophane C	18.5	0.14

(a) Adularia.

Adularia occurs as well-developed crystals, with characteristic rhombus-shaped forms (110), (001) and ($\bar{1}01$). Colourless, sometimes with a pale-bluish tint. Transparent or milky. Pseudotetragonal twinnings are not rare.

The physical and the chemical properties examined are shown in Table 41.

Adularia is found forming narrow veinlets, which traverse almost all members of the Kaso deposit, and is usually accompanied by ankerite in varying proportions. Paragenesis of quartz are not seen frequently.

TABLE 41. Physical constants and chemical composition of adularia.

Sp. gr. $d_4^{16} = 2.57$
Indices of refraction;
$\alpha = 1.523$ $\gamma - \alpha = 0.006$
$\beta = 1.527$
$\gamma = 1.529$
Optically negative, $(-)$ $2V = 40°$.

	wt %		mol. %
SiO_2	63.63	Or ..... $KAlSi_3O_8$	82.9
TiO_2	—	Ab ..... $NaAlSi_3O_8$	5.8
Al_2O_3	20.09	An ..... $CaAl_2Si_2O_8$	11.3
Fe_2O_3	1.20		(100.0)
CaO	2.65	Al_2O_3 Excess	1.4
MgO	—	Impurities;	
BaO	—	Quartz	18.5
Na_2O	0.61	Calcite	2.2
K_2O	13.38	Limonite	2.1
CO_2	0.35		
H_2O	0.06		
	101.97		

(b) Alkalifeldspar.

In the Kaso deposit, barium-free alkalifeldspar is found sparingly in the marginal part of a pegmatitic quartz vein.

Photomicrographs of a specimen are shown in Pl. XL (V), Figs. 4 and 5. The central rhombus-shaped portion is the secondary hyalophane which is in process of replacing a kasoite crystal. Relict crystals of ferriferous rhodonite and veinlets of new-formed carmine-red rhodonite are shown in marked contrast with each other.

The following optical constants were obtained on a specimen consisting of such associating hyalophane and kasoite (Table 42). Unfortunately there was not sufficient material for a quantitative chemical analysis.

TABLE 42. Optical constants of kasoite and hyalophane, found associated in a pegmatitic quartz vein.

	Kasoite.	Hyalophane.
Extinction angle;		
X′∧trace of 001 (in the thin section given in Pl. XL (V) Figs. 4–5)	+63°	−3°
α	1.551	1.530
β	1.555	1.534
γ	1.560	1.536
$\gamma - \alpha$	0.009	0.006

(c) Hyalophane.

Hyalophane is found as a product of C_1 period, crystallized in three forms which are quite distinct:

(i) as idiomorphic crystals, either isolated or forming a cluster in an altered mangantremolite rhodonite vein (hyalophane A); (ii) as xenocrysts partly resorbed and partly recrystallized in a fragment of a kasoite rhodonite vein captured by a hornstone vein (hyalophane B); (iii) as the sole constituent of a hyalophanized wall rock enclosed in a hornstone vein of C_1 period (hyalophane C).

A few relict crystals of celsian and kasoite were found in the hyalophane crystal, particularly in hyalophanes B and C. It is worthy of note that no zonal structure nor gradual transition between these barium feldspars have been observed under the microscope.

(i) Hyalophane A.

Fine crystals of hyalophane A are found sporadically distributed in a mangantremolite rhodonite vein as shown in Pl. XLI (VI), Fig. 5.

A sketch of a well-developed crystal with signs denoting the optic orientations is shown in Fig. 11. The crystal habit of hyalophane A is like that commonly observed of orthoclase crystals, (010) and (110) being most prominent, and (001) and (101) also well-developed. Crystals of hyalophane C embedded in a pink rhodochrosite mass are sometimes idiomorphic and apparently of the adularia type (Pl. XLI (VI), Fig. 2).

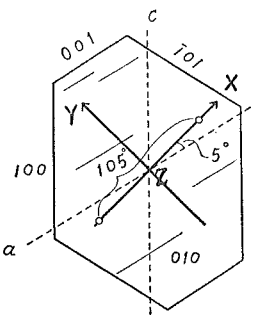

Fig. 11. Optic orientation of hyalophane A.

Hyalophane A and C are colourless transparent being free from inclusions, while hyalophane B is greyish-black to pitch-black as it contains a plenty of black impurities flocked together as shown in Pl. XL (V), Fig. 3.

The optic orientations of hyalophane are common to all specimens related to the three modes of occurrence as shown in Fig. 11, which are quite distinct from those of celsian and kasoite (cf. Fig. 12).

Very fine-grained crystals of hyalophane C occur sometimes as deep reddish-brown streaks in a hornstone vein (Pl. XLI (VI), Fig. 1). Its characteristic colour is due to a mixture of strikingly numerous minute crystals of Fe-Ti-ore, presumably inherited from the *Azukiban*.

The physical constants of these three hyalophanes were measured and analyses of the same specimens were made with the results presented in the following Tables 43–46.

The analysed specimen of the black hyalophane B was a large crystal, about 2 cm. across. Even though the cleavage flakes alone were picked by hand and subjected to analysis, the results show a plenty of admixtures. The analysis, on the other hand, is of interest as it makes it possible to calculate from its results the approximate composition of the black impurities (cf. Chap. XVIII, g). An additional analysis of the reddish-brown hyalophane B was made with the results compared in Table 45.

The physical properties of the three hyalophanes are compared in Table 43 below.

TABLE 43. Physical properties of hyalophanes.

	Hyalophane A	Hya. B (black).	Hya. C.
d	2.78	3.24[1]	2 78
Optic orientation;			
Optical plane	⊥010	⊥010	⊥010
	b = Z	b = Z	b = Z
a^X in acute β	+5°	—	—
c^X in acute β	+59°	—	—
α	1.537_8	1.539_5	1.538_0
β	1.542_5	1.543_5	1.542_0
γ	1.546_0	1.547_0	1.544_5
γ−α	0.008_2	0.007_5	0.006_5
$\alpha_F-\alpha_C$	0.008	0.007	0.007
2V	(−) 75.5 meas.	(−) 75.5 meas.	(−) 75.0 meas.
	(−) 84.0 calc.	(−) 86.0 calc.	(−) 76.0 calc.

The chemical compositions of hyalophanes A, B and C are given in the following three tables (Tables 44–46).

TABLE 44. Chemical composition of hyalophane A.

wt %		mol. %	
SiO_2	50.52	Cn	23.5
TiO_2	0.22	Or+Ab	62.0
Al_2O_3	16.58	Ne+Kp	14.5
BaO	9.02		
FeO	4.97	Impurity;	
MnO	5.75	Mangantremolite	14.0
MgO	3.09		
CaO	1.23		
K_2O	6.35		
Na_2O	1.72		
H_2O	1.50		
	100.95		

(1) Measured on a material with abundant black substances enclosed.

TABLE 45. Composition of hyalophane B.

	wt % I.	wt % II.	mol. % I.	mol. % II.
d	3.24	2.86		
SiO_2	39.64	49.26		
TiO_2	—	0.83		
Al_2O_3	12.09	19.80		
FeO	4.74	0.92		
MnO	8.72	2.56		
CaO	—	2.38		
MgO	3.67	2.12		
BaO	7.75	12.16		
Na_2O	1.37	0.92		
K_2O	6.02	8.02		
H_2O+	0.40	0.49		
H_2O-		0.20		
Fe	10.72	0.78[1]		
S	5.86	—		
	100.95	100.44		
Cn			23.6	25.8
Or			58.5	64.5
Ab			17.9	9.7
			(100.0)	(100.0)
Impurities;				
(Fe, Mn) SiO_3			30.0	27.0
Fe S			87.1	—
Mica			10.2	—
Apatite			—	7.0
Fe-Ti-ore			—	3.0

I. Hyalophane B (black) with black pigments.
II. ,, (reddish-brown) with Fe-Ti-ore.

TABLE 46. Composition of hyalophane C.

	wt %	mol. %
SiO_2	59.52	
TiO_2	1.10	
Al_2O_3	15.76	
Fe_2O_3	0.68	
CaO	0.73	
MnO	1.15	
MgO	1.68	
BaO	7.60	
K_2O	8.80	
Na_2O	0.98	
P_2O_5	1.87	
H_2O	0.67	
	100.54	
Cn		18.5
Or		69.8
Ab		11.7
		100.0
Impurities;		
Quartz		8
Fe-Ti-ore		9
Mn-tremolite		3

Minerals in paragenesis with the three hyalophanes differ a little in each case.

(i) With hyalophane A. { Pink rhodonite, Mangantremolite, Yellow garnet

1) P_2O_5.

(ii) With hyalophane B.
- Pink rhodonite
- Hornstone
- Black impurities
- Fe-Ti-ore (pyramidal type)

(iii) With hyalophane C.
- Pink rhodonite
- Rhodochrosite
- Mangantremolite
- Chlorite
- Fe-Ti-ore (platy type)
- Apatite
- Allanite

Hyalophane is distinguished from kasoite by a much lower refringence and the optical orientations. It differs from quartz in its very weak birefringence, its optic sign and the biaxial character. Note the marked difference of birefringence between quartz and hyalophane as shown in Pl. XLI (VI), Fig. 4.

The quantity of hyalophane which occurs disseminated in the wall rock seems to be enormous. It is, however, very hard to determine its distribution accurately because it is very fine-grained and, moreover, indistinguishable from quartz in such state.

Whether hyalophane A is a primary constituent emanating from the magma during period C_1 or whether it has been produced by the silicification of kasoite is an important and interesting problem. Hyalophanes B and C are apparently of secondary origin.

The hyalophanisation of kasoite under consideration was not a simple silicification but was accompanied by a considerable increase in the potash content as shown in Table 47.

TABLE 47. Comparison of kasoite and hyalophane.

	I. Kasoite. mol. %		II. Hyalophane.	
Cn = $BaAl_2Si_2O_8$	49.6		23.5	
Or = $KAlSi_3O_8$	—	32.5	54.2	54.2
Kp = $KAlSiO_4$	32.5		—	
Ab = $NaAlSi_3O_8$	8.5	17.9	22.3	22.3
Ne = $NaAlSiO_4$	9.4		—	

I. From Table 48. II. From Table 44.

(d) Kasoite.

Kasoite is the chief associate in rhodonite veins of period B_1. It also occurs as monomineralic veinlets or coarse crystalline ag-

gregates (Pl. XLI (VI), Fig. 3). Individual crystals as large as 5 mm. across are quite common. Some specimens embedded in a fine-grained rhodonite mass were perfectly idiomorphic as presented in Pl. XLII (VII), Fig. 1. The crystal-habit is of the adularia type, frequently showing rhombus sections in a thin slice. Forms (110) and (101) are observable. No twinning. Dusty inclusions are always seen, arranged parallel to the direction of the c-axis of the mother crystal.

Physical properties; Cleavage parallel to (001) is perfect, and to (010) distinct. Weak cleavage parallel to (110) is also seen.

Hardness: H = 5½. Sp. gr. $d_4^{16} = 3.003$. Fusibility: F = 4.

The optic orientations of kasoite shown in Fig. 12 correspond closely to those of celsian in spite of the marked differences between the chemical composition of these two minerals.

The optic axial plane is parallel to 010 (or, strictly speaking, nearly so).

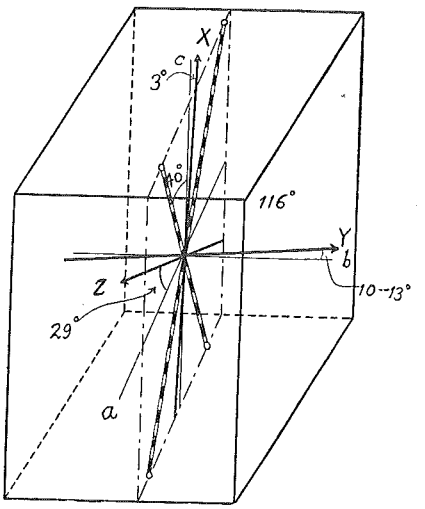

Fig. 12. Optic orientation of kasoite.

c∧X on 010 = 2°—3° in acute β.
a∧Z on 011 = 28–29° in obtuse β.

Extinction angle on 001 is 10–13° and not zero to the trace of 010[1]. If this oblique extinction of light on 001 is not accidental, the monoclinic symmetry of kasoite and celsian appears to be very doubtful. In Figure 12 these relationships were considered, drawing Y not coinciding with b-axis.

$\alpha = 1.564_5$
$\beta = 1.568_5$
$\gamma = 1.572_0$
$\gamma - \alpha = 0.007_5$
$\alpha_F - \alpha_C = 0.008$
Optically negative, (—)2V = 80°.5.

(1) Oblique extinction of light in a similar case was reported by STRANDMARK on a celsian crystal from Jackobsberg, Sweden.
X′∧ trace of 010 = 26°45′.
STRANDMARK: G. För. Förh., **25** 289 (1903).

Kasoite and celsian are distinguished from hyalophane and adularia by their much higher refringence. The optical orientation is also reliable especially when a rhombus-shaped outline is shown in a slice cut nearly normal to c-axis. It is done as follows:—In a celsian or a kasoite crystal Z′ (the vibration direction of the slower wave) is parallel to the shorter diagonal of the rhombus, and in case of a hyalophane or an adularia crystal it is parallel to the longer diagonal.

A small quantity of kasoite carefully picked from a kasoite vein was pure and homogeneous except for a slight admixture of rhodonite and rhodochrosite. Analysis of this material yielded the results given in Table 48.

TABLE 48. Analysis of kasoite.

wt. %		mol. %	
SiO_2	38.48	$BaAl_2Si_2O_8$	49.6
TiO_2	—	$NaAlSi_3O_8$	8.5
Al_2O_3	23.61	$NaAlSiO_4$	9.4
Fe_2O_3	0.60	$KAlSiO_4$	32.5
MgO	0.97		(100.0)
MnO	2.67	Impurities:	
CaO	0.85	(Mn, Fe, Ca) SiO_3	5.0
BaO	25.50	(Ca, Mn) CO_3	3.2
Na_2O	1.85		
K_2O	5.10		
Ign. loss	0.98		
	100.61		

If the above analysis is recalculated in terms of the constituent molecules the following figures are obtained (Table 49). Five different cases are observed as compared in this table, each based on a particular way of calculation of basic feldspar molecules.

TABLE 49. Calculations of the molecular composition of kasoite.

Chief element.	Molecule.	I.	II.	III. Molecular	IV. %	V.
Ba	Cn = $BaAl_2Si_2O_8$	49.6	59.5	66.9	62.8	49.6
Na	Ab = $NaAlSi_3O_8$	17.9	21.2	—	10.6	8.5
	Ne = $Na_2Al_2Si_2O_8$	—	—	11.9	6.2	—
	or $NaAlSiO_4$	—	—	—	—	9.4
K	Or = $KAlSi_3O_8$	32.5	—	—	—	—
	K_p = $K_2Al_2Si_2O_8$	—	19.3	21.2	20.4	—
	or $KAlSiO_4$	—	—	—	—	32.5
Total		(100.0)	(100.0)	(100.0)	(100.0)	(100.0)

Discrepancies.	SiO_2 Excess	—	—	22.9	0	0
	Lack	67.7	21.9	—	0	0
	Al_2O_3 Excess	—	—	—	—	—
	Lack	5.6	6.7	7.5	7.0	5.6

I. All Na_2O and K_2O were calculated into Ab and Or.
II. All Na_2O was calculated into Ab and all K_2O into Kp.
III. All K_2O in Kp, while Na_2O was divided into two parts, Ne and Ab, so as to satisfy the paucity of the silica.
IV. Similar with IV, but the monomolecular formulas were applied for Ne and Kp.

Kasoite is presumably a product of the early mineralization of B_1 period which has been continued from stage A, as shown by the gradual transition of the feldspar composition from celsian to kasoite. Ironrhodonite is the unique mineral produced contemporaneously with kasoite.

The wall rock impregnated with kasoite is the typical feldspathic *Azukiban* as described in Chapter VI. The chief change, on the other hand, observed on xenolithic fragments of the wall rock captured in a kasoite vein is the formation of green biotite and the resorption of hornfels-garnet.

Kasoite is also found as impregnations in the *Tetuban*, an altered country rock related to the mineralization of stage A (Pl. XLII (VII), Fig. 3).

(e) Celsian.

Celsian is found sporadically distributed through the products of A_2 period. An idiomorphic crystal observed in a thin slice of a picroknebelite mass is shown in Pl. XLII (VII), Fig. 2. Forms corresponding to (110), (101) and (001) were observed. The celsian found isolated as such idiomorphic crystals would be called "celsian A", and those found as irregular aggregates replacing picroknebelite crystals "celsian B" (Pl. XLIII (VIII), Fig. 5).

Celsian is stable in a mineralizing solution of the manganese carbonate period so it is found frequently as relict crystals in various rhodochrosite ores, especially in the black *Azuki*-ore.

The physical properties of the two kinds of celsian are compared in Table 50 below.

TABLE 50. Physical properties of celsian A and B.

	Celsian A.	Celsian B.
Optic axial plane	010 ?	010 ?
c^X	(—) 0-2°	(—) 3°
a^Z	(+) 28°	(+) 27°
$Z'_{(001)}$^trace of $010_{(001)}$	—	10°
α	1.582_7	1.579_5
β	1.586_3	1.582_6
γ	1.590_2	1.586_2
$\gamma-\alpha$	1.007_5	0.006_7
$\alpha_F-\alpha_C$	0.008	0.007
(+) 2V	88° calc.	86° calc.

A pure and homogeneous material was not available for the analysis. The chemical composition of celsian B was calculated from the results obtained by the analysis of the residue left from treatment of the black *Azuki*-ore with hot hydrochloric acid. It is highly probable that celsian itself has also been attacked by the acid. The results of the analysis and the calculation made by the author are given in the following Table 51.

TABLE 51. Chemical composition of celsian B.

	I.	II.
SiO_2	31.78	29.3
TiO_2	0.28	—
Al_2O_3	16.10	29.7
FeO	0.20	—
MnO	29.75	—
CaO	3.72	—
MgO	1.95	—
BaO	9.70	34.5
K_2O	2.15	3.9
Na_2O	1.40	2.5
Ign. loss	4.12	—
	101.15	(100.0)

I. Analysis of the residue left after the dissolution of the black *Azuki*-ore.

II. Feldspar constituents in I, calculated to 100 percents. They correspond to:

	mol. %
Cn	30
Ne+Kp	11
Mica	12
Picroknebelite	46

Analysis of celsian B shown in Table 51 corresponds approximately to the composition of $Cn_{74}(Ne + Kp)_{26}$.

It is obvious from the variations of the refractive indices as shown in Table 50 that the evolution of celsian is accompanied by the decrease of Cn% in the later stage.

(f) Bariumalbite.

Bariumalbite occurs as a minor constituent in a manganhedenbergite vein. It shows rhombic crystal outlines under the microscope with no twinning. Indices of refraction were measured on cleavage flakes as follows:

$$n_1 = 1.532$$
$$n_2 = 1.538$$

As bariumalbite is the unique impurity in the manganhedenbergite vein, those constituents in the analysis of the latter mineral given in Table 84, which have not been incorporated in the calculated pyroxene molecules, may correspond approximately to the composition of bariumalbite. They are calculated and set down in Table 52 below.

TABLE 52. Molecular composition of bariumalbite calculated from Table 84.

	mol. %
$NaAlSi_3O_8$	44
$KAlSi_3O_8$	42
$BaAl_2Si_2O_8$	14
	(100)
SiO_2	−11.5

(g) Albite.

Albite belongs to the earliest mineralization of stage A. Although it does not occur as a large mass or vein, its total amount intruded as small veinlets or disseminated through the mother rock might have been enormous (Pl. XLIII (VIII), Fig. 2). Albitization is also prominent as a phase of autometamorphism of basic igneous rocks which have probably an intimate genetical relationship to the manganese deposit.

Albite appears at first as minute lath-shaped crystals in albite-quartz veins, widespread through the country rocks. Such minute crystals show a simple twinning on albite-law. The maximum symmetrical extinction is 17° relative to the trace of the twinning-plane. Extinction $a \wedge X'$ on 010 is 10°; optically positive; (+) 2V large. The average of the refractive indices measured is $n_{1(010)} = 1.536$.

Albite laths of later mineralization are generally free from twinning, the refractive indices being a little higher. It seems to be

possible to trace all stages of development from albite to barium-albite described above.

Alterations of wall rocks related to the introduction of albite are worthy of notice. Four sorts of alteration will be enumerated here in this connection.

(i) Formation of green ironhornblende due to the alteration of the hornfels-biotite by an albitic residual solution with the cooperation of manganhedenbergite (cf. Chap. XV, d).

Biotite + Albite + Manganhedenbergite → Green ironhornblende + Albite vein.

(ii) Grain-growth of the hornfels-biotite enclosed in an albite veinlet. The biotite, in the meanwhile, becomes more strongly pleochroic and birefringent.

Biotite + Albite (dry) → Large deep-coloured biotite flakes + Albite veinlet.

(iii) Formation of epidote (cf. Chap. XVIII, e).

Biotite + Albite → Epidote + Albite.

(iv) Formation of green biotite, as a product of hydrothermal alteration of the hornfels-biotite (cf. Chap. XVI, c).

Biotite + Albite (wet) → Green biotite + Albite spots.

This green-biotitization is related to the introduction of volatile constituents emanating from the albite solution. Simple intrusion of a dry albite veinlet results usually in a mere grain-growth of the biotite (see ii), while the introduction of a highly wet albitic solution affects the wall rock remarkably converting it into aggregates of green biotite flakes disseminated heavily with albite spots.

(h) Plagioclase.

Calcic plagioclases occur as essential minerals in the basic igneous rocks found in the vicinity of the Kaso mine. They are seen so intensely albitized that their original characters are hard to make out. The most interesting feature of these albitized feldspars is that they are encroached upon gradually from their margin or along cracks by a much more calcic plagioclases. Such peculiar zonal

growths are of the reverse order to those familiar in the crystallization from a melt, a more albitic kernel being surrounded by a more anorthitic shell. This reverse order of evolution of the plagioclase feldspar may presumably be due to the autometamorphic character of the Kaso igneous intrusives as has already been discussed above in some detail in the section on the relationships of these igneous rocks (cf. Chap. III, c).

Formation of anorthitic plagioclase by the degradation of scapolite is also an interesting fact (cf. Chap. XVIII, b), but no reliable data were available to allow a discussion in more detail on this subject.

CHAPTER XII

GARNETS

Primary garnets.

(a) Spessartine A (amber-yellow garnet).
(b) Spessartine B (wine-yellow garnet).
(c) Fe-Ca-spessartine (cinnamon-yellow garnet).

Contact-garnets.

(d) Ca-Fe-spessartine (greyish-yellow garnet).
(e) Spessartine C (black garnet).
(f) Spessartine D (red garnet).

Garnets of the Kaso mine can be divided into two groups; (i) those formed as one of the chief constituents of mineral veins; (ii) those formed as the products of contact-metamorphism of wall rocks. They are compared in the following Table 53, arranged after the sequence of mineralization.

TABLE 53. Garnets of the Kaso mine.

Mineral	Period	Occurrence
Ca-Fe-spessartine		In garnet-hornfels.
Spessartine A	A_1	Primary, in manganhedenbergite veins.
Spessartine B	B_1	,, , in rhodonite veins.
Spessartine C		Contact-metam. *Tetuban*.
Spessartine D		,, *Azukiban*.
Fe-Ca-spessartine	C_1	Primary, in manganactinolite veins.

Chemical compositions of the three primary garnets are compared in Table 54.

TABLE 54. Comparison of three primary garnets.

Period of mineralization		1 A_1		2 B_1		3 C_1	
Chief associate.		Manganhedenbergite		Rhodonite		Mangantremolite	
Colour		Amber-yellow		Wine-yellow		Cinnamon-yellow	
d		4.04		4.12		3.97	
n_D		1.806		1.788		1.788	
	mol. %						
Sp.	$Mn_3Al_2Si_3O_{12}$	79.1		79.3		51.7	
Alm.	$Fe_3Al_2Si_3O_{12}$	5.2	86.9	6.5	88.8	15.5	69.5
Pyr.	$Mg_3Al_2Si_3O_{12}$	2.6		2.3		2.3	
And.	$Ca_3Fe_2Si_3O_{12}$	8.8		11.2		0.9	
Gross.	$Ca_3Al_2Si_3O_{12}$	4.3	13.1	—	11.2	29.6	30.5

Garnets of contact-metamorphic origin are similarly compared in Table 55.

TABLE 55. Comparison of the three contact-garnets.

Original rock		1 Grey hornfels		2 Black *Tetuban*		3 *Azukiban*	
Colour		Greyish-yellow		Black		Red	
d		3.83		4.11		4.09	
n_D		1.790		1.800		1.796	
	mol. %						
Sp.	$Mn_3Al_2Si_3O_{12}$	57.4		74.2		71.6	
Alm.	$Fe_3Al_2Si_3O_{12}$	17.7	76.3	12.8	89.3	11.0	86.4
Pyr.	$Mg_3Al_2Si_3O_{12}$	1.2		2.3		3.8	
And.	$Ca_3Fe_2Si_3O_{12}$	0.0		0.0		3.4	
Gross.	$Ca_3Al_2Si_3O_{12}$	23.7	23.7	10.7	10.7	10.2	13.6

The abundance of garnet is one of the characteristic features of the Kaso mine. Garnet is generally considered as an indicator of a considerably high grade of metamorphism, but this rule does not hold when the original rock contains a plenty of manganese. If sufficient alumina and silica are available, the manganese and the corresponding amounts of Al_2O_3 and SiO_2 are converted into garnet forming the spessartine molecule $Mn_3Al_2Si_3O_{12}$. Even the formation of the blythite molecule $Mn_3Mn_2Si_3O_{12}$ is sometimes postulated if there is a too great excess of manganese. It has been suggested by the author that in the Mituisi garnet[1] Al_2O_3 and SiO_2 were taken up as far as the necessary amount of manganese was available, and

(1) T. YOSIMURA: Garnet from Mituisi, Hidaka, Japan; Journ. Jap. Assoc. of Geol. Min. and Econ. Geologist, Vol. **14**, p. 197 (1935).

the garnet thus formed shows a uniform content of the spessartine molecule $Mn_3Al_2Si_3O_{12}$ notwithstanding the variable content of manganese in the original rock. The distribution of garnet crystals, therefore, indicated in itself that of manganese.

It was, moreover, mentioned that the limit of miscibility of lime-garnet $Ca_3Al_2Si_3O_{12}$ in spessartine or almandine was dependent upon the pressure prevailing during the contact-metamorphism. The miscibility advanced markedly as the prevailing pressure grew higher. The author has proposed to name those garnets which contain both "ugrandite" and "pyralspite" molecules mixed with each other to a considerable degree "a high-pressure-garnet", as they are the characteristic mineral of a high-grade metamorphic rock. Garnets found in various amphibolites and eclogites are exclusively "high-pressure-garnets", which, therefore, may be understood as a synonym of "eclogite-garnet". The mentioned garnet found in the quartz-garnet-amphibolite from Mituisi is the type of the "high-pressure-garnet".

Garnets of the Kaso mine are by no means "high-pressure-garnets", and, even though some stress-effects are seen in the products of C_1 period (cf. Chap. XIV, e) and also in a schistose basic igneous rock, a remarkably high pressure most probably did not prevail during metamorphism.

An interesting feature, in this connection, that deserves mention here is the miscibility of lime-garnet in the manganese-garnet (cf. Tables 54 and 55).

It must be remembered that the original country rocks are all poor in lime and manganese, so these two elements found in the contact-garnets must have been introduced from the mineralizing solution before or during the metamorphism. The greyish-yellow garnet, which is found as the dominant constituent of the garnet-biotite-hornfels and is presumably related to the early contact-metamorphism due to the intrusion of metadiabases, has evidently more lime than the garnets which are related to later metamorphisms.

It is also noticeable that the various garnets, spessartines A, B, C and D, show an almost uniform content of manganese notwithstanding the unequal manganese content of the original rock. This is an example which shows that similar genetical conditions, temperature and pressure, result in uniform miscibility of garnet molecules regardless of the original bulk composition.

One of the marked differences between the contact and the vein garnets is the kind and distribution of inclusions. All of the three

vein garnets show almost no inclusions, while the three contact garnets are all dusty, containing numerous and abundant inclusions inherited from their original rocks. It is also noticeable that the inclusions found in the contact garnets disappear almost completely if their mother crystals are soaked in and reacted upon by a later feldspathic mineralizing solution.

Contact garnets are seen strongly corroded if captured in a feldspathic vein. This is an interesting evidence of the unstability of contact garnet in a vein. In Pl. XLIII (VIII), Fig. 4 are shown remarkably corroded crystals of greyish-yellow hornfels-garnet found in a wall rock heavily disseminated with kasoite spots.

Those given in Pl. XLIII (VIII), Fig. 1 are the corroded crystals of black garnet, from which the black pigmental inclusions are seen wholly swept away. Such corrosion and clarification are apparently due to the intrusion of a kasoite vein, the effects of which are conspicuous only on the half side of a train of black garnet crystals soaked in the kasoite vein.

On the contrary these contact garnets are very stable in the carbonate solution. They remain intact as relict crystals in various carbonate ores. Also the garnets in the carbonate *Azukiban* show no trace of corrosion as presented, for example, in Pl. XLIII (VIII), Fig. 6, in marked contrast with the corroded garnet in the feldspathic *Azukiban* given in Fig. 4 in the same Plate.

Primary garnets.

(a) Spessartine A (amber-yellow garnet).

This garnet is found in all mineral assemblages produced in stage A. Always transparent, containing scarcely any inclusion. Often fine crystals, (211) without exception, are observed. Under the microscope it is colourless or slightly brown, showing anomalous birefringence. The outline of the birefringent portion divides the crystal after the dodecahedral type of the garnet-anomaly previously reported.

$$d_4^{20} = 4.04$$
$$n_D = 1.806$$
$$n_F - n_C = 0.015$$

A pure material collected from transparent crystals was analysed by the author with the following results (Table 56):

TABLE 56. Analysis of amber-yellow garnet.

	%
SiO_2	34.93
TiO_2	--
Al_2O_3	20.06
Fe_2O_3	2.53
FeO	2.01
MnO	32.91
CaO	5.74
MgO	0.59
Na_2O	0.45
K_2O	tr
CO_2	1.30
H_2O	0.05
	100.57

	mol. %
$3CaO.Fe_2O_3.3SiO_2$	8.8
$3CaO.Al_2O_3.3SiO_2$	4.3
$3MnO.Al_2O_3.3SiO_2$	79.1
$3MgO.Al_2O_3.3SiO_2$	2.6
$3FeO.Al_2O_3.3SiO_2$	5.2
	(100.0)

Al_2O_3 Excess 22.0

Impurity: $CaCO_3$ 15.0

(b) Spessartine B (wine-yellow garnet).

Wine-yellow garnet is a frequent constituent of the rhodonite vein of period B_1. It is also found in later mineralized assemblages as a relict mineral. Crystals not rare, always in a trapezohedral form (211). Crystal faces markedly striated. Optical anomalies are common, the anomalous divisions being arranged after the trapezohedral type.

The physical constants and the chemical composition examined are presented in Table 57.

TABLE 57. Physical constants and results of analysis of wine-yellow garnet.

Sp. gr. $d_4^{20} = 4.10$

Refringence; $n_D = 1.788$

wt. %	
SiO_2	35.52
TiO_2	0.60
Al_2O_3	18.42
Fe_2O_3	4.12
FeO	2.70
MnO	32 45
CaO	3.63
MgO	0.67
K_2O	0.01
Na_2O	0.45
H_2O^+	1.01
H_2O^-	0.16
	99.74

	mol. %
$3CaO.Fe_2O_3\ 3SiO_2$	11.2
$3FeO.Al_2O_3.3SiO_2$	6.5
$3MnO.Al_2O_3.3SiO_2$	79.3
$3MgO.Al_2O_3.3SiO_2$	3.0
	(100.0)

Impurity;

Mica 3

(c) Fe-Ca-spessartine (cinnamon-yellow garnet).

Cinnamon-yellow garnet is presumably the unique garnet produced in the C_1 period contemporaneously with manganactinolite and mangantremolite. Crystal form always (211). Colour cinnamon-yellow. Under the microscope it is pale-brown, with distinct anisotropism.

Sp. gr. $d_4^{18} = 3.97$
Refringence; $n_D = 1.788$

The results of chemical analysis are given in Table 58.

TABLE 58. Analysis of cinnamon-yellow garnet.

	wt. %
SiO_2	36.40
TiO_2	0.15
Al_2O_3	21.97
Fe_2O_3	0.30
FeO	7.15
MnO	23.37
CaO	11.42
MgO	0.68
CO_2	0.21
H_2O	—
	101.65

	mol. %
$Ca_3Fe_2Si_3O_{12}$	0.9
$Fe_3Al_2Si\ O_{12}$	15.5
$Ca_3Al_2Si_3O_{12}$	29.6
$Mn_3Al_2Si_3O_{12}$	51.7
$Mg\ Al_2Si_3O_{12}$	2.3
	(100.0)

SiO_2 Lack −20.0
RO Lack −2.0
Impurity;
Carbonate 2.0

Contact garnets.

(d) Ca-Fe-spessartine (greyish-yellow garnet).

Greyish-yellow garnet is one of the chief constituents of the garnet-biotite-hornfels which is found well-preserved as a wall rock

TABLE 59. Properties of greyish-yellow garnet.

$d_4^{18} = 3.83$
$n_D = 1.790$

	wt. %
SiO_2	43.75
TiO_2	0.44
Al_2O_3	19.80
Fe_2O_3	—
FeO	7.16
MnO	22.92
CaO	7.35
MgO	0.31
BaO	—
Na_2O	0.10
K_2O	—
H_2O	0.13
	101.96

	mol. %
$3CaO.Fe_2O_3.3SiO_2$	—
$3CaO.Al_2O_3.3SiO_2$	23.7
$3FeO.Al_2O_3.3SiO_2$	17.7
$3MnO.Al_2O_3.3SiO_2$	57.4
$3MgO.Al_2O_3.3SiO_2$	1.2
	(100.0)

R O −10

Impurities;
Quartz 79
Feldspar 1

of the manganhedenbergite vein. Similar yellow garnets were found in a strongly altered country rock and were easily separated from the associated minerals, such as chlorite, soapstone and sericite, by floating in a heavy liquid. The results of analysis and the physical constants measured are tabulated in Table 59.

(e) Spessartine C (black garnet).

Some fragments of *Tetuban* captured in a rhodonite vein of period B_1 are seen metamorphosed completely into pitch-black masses looking like some xenoliths of pitchstone. They consist exclusively of black garnets, each garnet grain being so intimately aggregated as to leave no interspaces between them and, consequently, they show as a whole a conchoidal fracture with a smooth glassy surface. The outlines of each garnet grain are indistinct even under the microscope.

Submicroscopic inclusions of black substances uniformly distributed in each garnet grain give smoky brown colour to this mineral even in thin slices and it is almost opaque in thick slices. The results of chemical analysis with some physical constants measured are presented in Table 60.

TABLE 60. Physical constants and chemical composition of black garnet.

wt. %	
SiO_2	35.28
TiO_2	1.03
Al_2O_3	20.62
Fe_2O_3	—
FeO	5.32
MnO	31.64
CaO	3.98
MgO	0.50
BaO	—
Na_2O	0.35
K_2O	0.26
CO_2	0.40
H_2O	0.12
	99.50

Sp. gr. $d_4^{18} = 4.11$

Refringence; $n_D = 1.800$

mol. %	
$3CaO.Fe_2O_3.3SiO_2$	—
$3CaO.Al_2O_3.3SiO_2$	10.7
$3FeO.Al_2O_3.3SiO_2$	12.8
$3MnO.Al_2O_3.3SiO_2$	74.2
$3MgO.Al_2O_3.3SiO_2$	2.3
	(100.0)

SiO_2 Lack —13.0

Impurities;

Feldspar	3
Calcite	5

Although the *Tetuban* contains plenty of barium (cf. Table 7, p. 335), the black garnet derived therefrom does not show even a trace of barium, in spite of the so complete and thorough conversion of the *Tetuban* into garnet. Barium and alkalis seem to have escaped

completely before or during the metamorphism. The red garnet, which will be described in the following section, also contains no barium, notwithstanding that it is similarly derived from the exceedingly barium-rich *Azukiban*.

Although it may be impossible to deny the existence of a barium garnet molecule which may be expressed by the formula $Ba_3Al_2Si_3O_{12}$ it is clear that such a molecule cannot be expected as a result of such a mere thermal metamorphism as has taken place in the Kaso mine.

Garnet with a black core.

Some of the *Tetuban* not completely garnetized contains numerous peculiar crystals of black garnet as shown in Pl. XLIV (IX), Fig. 5. Each garnet crystal has a black core. Fig. 6 in Pl. XLIV (IX) shows the garnet crystals of more advanced stage of garnetization, each garnet grain being much enlarged. Coalescence of two or three grains is conspicuous, resulting in larger individuals containing two or three black pupils in their center. The black material in the core was removed by treating with hot hydrochloric acid and analysed with the results given in Table 61.

TABLE 61. Analysis of the black substance in the core of the black garnet.

	wt. %
SiO_2	29.9
TiO_2	1.5
Al_2O_3	23.1
Fe_2O_3	3.8
Mn_3O_4	39.6
CaO	4.5
MgO	0.3
	102.7

$RO : Al_2O_3 : SiO_2 = 3.0 : 1 : 2.5$

The black substance soluble in hydrochloric acid is, therefore, chemically very near to a kind of spessartine. The only explanation for this unexpected result is that the black core consists chiefly of a fragile garnet-like material which is partly decomposed by acid and looks black and opaque owing to the presence a small quantity of contaminated black substances. These latter will be described in Chapter XVIII, g.

Two modes of occurrence of the black substance in garnet are worthy of note. The perfect dispersion of the black pigments ob-

served in a homogeneously black garnet crystal may probably be due to the rapid and complete garnetization which has taken place at high temperature in the presence of a supply of a sufficient quantity of manganese.

In Pl. XLIII (VIII), Fig. 3 is shown an interesting zoned crystal of black garnet observed in a contact-metamorphosed *Tetuban*. The central zone consists of an amber-yellow garnet produced in stage A. The outer zone seems to have been formed by the later contact-metamorphism. It is necessary to assume a severe fracturing of the early mineralized product to explain the existence of an isolated round fragment of a vein garnet in the wall rock.

The black substance in the original wall rock which might have been a kind of *Tetuban* is seen partly concentrated and partly dispersed in the new-formed garnet of the outer zone.

The anisotropy of the garnets formed in a vein and the reverse character of the contact garnet, as interestingly contrasted in the single specimen of the zoned crystal here mentioned, are phenomena quite contrary to the customary understanding concerning the optical anomaly of garnet. Such an unusual relationship was observed to hold throughout various garnets found in the Kaso mine.

(f) Spessartine D (red garnet).

Red or eugenia-red garnet is found abundantly in the Kaso deposit. This mineral is the product of contact-metamorphism of the *Azukiban,* and is deeply coloured by numerous inclusions of tiny grains of Fe-Ti-ore. Figure 2 in Pl. XLIV (IX), shows the embryo stage of the red garnet, formed in a slightly metamorphosed *Azukiban,* the unresorbed Fe-Ti-ore inclusions being distinctly seen in the core of the new-formed garnet. Garnet itself is colourless under the microscope. It is also clearly seen in this photograph that the intrusion of the hornstone vein is evidently later than that of the rhodonite vein and the formation of the *Azukiban.* In Pl. XLIV (IX), Fig. 3 is shown an example of a more completely garnetized wall rock.

Crystals always (110). Zonal growth and optical anisotropy are seen, though not frequently. Some zoned crystals are shown in Pl. XLIV (IX), Fig. 1, the boundary of each zone being replaced by carbonate ores.

Sp. gr. $d_4^{19} = 4.09.$
Refringence; $n_D = 1.796.$

The results of chemical analysis are given in the following Table 62.

TABLE 62. Analysis of red garnet.

	wt. %		mol. %
SiO_2	35.53	$Ca_3Fe_2Si_3O_{12}$	3.4
TiO_2	1.07	$Fe_3Al_2Si_3O_{12}$	11.0
Al_2O_3	20.44	$Mn_3Al_2Si_3O_{12}$	71.6
Fe_2O_3	1.05	$Ca_3Al_2Si_3O_{12}$	10.2
FeO	5.06	$Mg_3Al_2Si_3O_{12}$	3.0
MnO	31.65		(100.0)
CaO	4.77		
MgO	1.08	Impurity;	
BaO	0.41	Kasoite	1.4
Na_2O	0.25		
K_2O	0.15		
H_2O	0.10		
	101.56		

CHAPTER XIII

TEPHROITES

Genesis of the vein tephroite.
Genesis of the contact tephroite.
The system Fe_2SiO_4–Mn_2SiO_4.

(a) Ironknebelite.
(b) Picroknebelite.
(c) Knebelite.
(d) Manganknebelite.
(e) Irontephroite.
(f) Tephroite.

Manganese minerals of the tephroite group are the predominant and characteristic constituents of the Kaso deposit. Some of them are found in large quantity and are mined as a part of useful ores.

The study of these minerals possesses more than local interest for two reasons: (a) Rare iron-rich members are included; (b) A noteworthy relationship is suggested between the primary iron-poor group (tephroites) and the contact-metamorphosed iron-rich group (knebelites).

Continuous variation of composition most probably exists between the most iron-rich early member and the least iron-rich late member of this mineral group of the Kaso mine, of which, however,

only the following five specimens were analysed by the author (Table 63).

TABLE 63. Representatives of the knebelite-tephroite series of the Kaso mine.

Mineral	Period	Occurrence
Ironknebelite	A_2	As fragments of a monomineralic vein.
Picroknebelite	A_2	,, ,,
Manganknebelite	B_2	As a contact-mineral.
Irontephroite	B_2	,,
Tephroite	B_2	Abundantly as a constituent of the *Hiė*-ore.

Two modes of occurrence were observed of the minerals of the tephroite group; (i) as a primary vein; and (ii) as a product of contact-metamorphism.

The later produced mineral was, without exception, the less ferriferous one similarly in both cases, and those of metamorphic origin were richer in iron, compared with the contemporaneous member of the vein tephroite.

It may, however, be open to question whether all minerals of the tephroite group found at the Kaso mine are of metamorphic origin. The following explanations do not support such an opinion, though the evidences enumerated here may not be decisive enough.

(i) The amount of demanganised carbonate which is expected to be left as the unincorporated remains of the original carbonate is too little to account for the formation of all of the tephroites.

(ii) The dominant carbonate ore is obviously a product of later mineralization than the formation of tephroites.

(iii) Minerals of the rhodonite group are usually found replaced by the tephroites but the reverse case is quite rare.

(iv) The contact tephroite which has been derived from the most iron-poor carbonate ore must necessarily be the most iron-poor variety if the intruding rhodonite vein is also the most iron-poor member. Specimens which seem to have been produced under such circumstances have proved to be irontephroite, so the much iron-poorer tephroite which is found abundantly associated with the rhodochrosite ore is certainly of primary origin.

Genesis of the vein tephroite.

The occurrence of minerals of the tephroite group is very suggestive as to the temperature prevailing during deposition of the manganese ore.

Formation of tephroite may be expressed by such reactions as:

$$\underset{\text{(rhodonite)}}{MnSiO_3} + \underset{\text{(rhodochrosite)}}{MnCO_3} = \underset{\text{(tephroite)}}{Mn_2SiO_4} + CO_2$$

(low temperature) (high temperature)

If the crystallization proceeds at high temperature there will be produced mainly tephroite, but at temperatures lower than a certain limit no tephroite will be formed as a primary and stable mineral. This limit of temperature will be termed the "tephroite-limit".

Distribution of the manganese deposits which contain tephroite as one of the chief constituents will probably indicate the region in which the mineralizing temperature was higher than the tephroite-limit. It is of much interest that the occurrence of tephroite in the district here mentioned is limited to a nearly circular area with the Ashio igneous complex at its center. The Kaso mine and others in its vicinity are situated in the eastern part of this area. Manganese mines located in this area are generally rich in tephroites while those on the out-side of this circle contain scarcely any tephroites.

It is worthy of note that a small quantity of pink Ca-rhodochrosite is found closely associated with blood-red rhodonite which crystallizes just before the crystallization of knebelite begins.

The formation of knebelite seems to be a result of a reaction between the rhodonite molecule and the enriched rhodochrosite molecule at a temperature higher than the tephroite-limit. The equilibrium which may exist between the mentioned molcules may be expressed by the following equation.

$$m\,(\text{blood-red rhodonite}) + n\,(\text{Ca-rhodochrosite}) = p\,(\text{irontephroite}) + q\,(\text{white mangancalcite}).$$

With a view to explaining this relation numerically, analyses of the four minerals concerned are given in the following Table 64 in atomic percentages.

TABLE 64. Atomic composition of four minerals which participated in the formation of vein tephroite.

	I. Blood-red rhodonite	II. Ca-rhodochrosite	III Irontephroite	IV. White mangancalcite
Fe	11.9	7.2	16.3	2.0
Mn	71.6	74.7	76.7	29.1
Ca	6.0	11.8	—	62.8
Mg	10.5	6.3	7.0	6.1

I, from Table 88. III, from Table 78.
II, „ „ 24. IV, „ „ 31.

Substitute for the coefficients as follows:

$$\begin{cases} m = 1 \\ n = 5 \end{cases} \qquad \begin{cases} p = 5 \\ q = 1 \end{cases}$$

Then the above equation is proven to hold, practically, by comparison of the calculations as presented in Table 65.

TABLE 65. Comparison of the calculated compositions.

	1×(blood-red rhodonite) +5×(Ca-rhodochrosite)	5×(irontephroite) +1×(white mangancalcite)
Fe	8.0	13.9
Mn	74.2	68.8
Ca	10.8	10.5
Mg	7.0	6.8

Except for a slight increase in the iron-content the total composition was proven to remain nearly unchanged after the formation of irontephroite, which may probably be due to a sudden rise in temperature or a rapid exudation of carbonic acid. The numerical values of the quotients m, n, p, q are also in substantial accordance with the proportions of materials engaged in this reaction.

Genesis of the contact tephroite.—Manganknebelite and tephroite as the products of contact-metamorphism.

Minerals of the tephroite group are found frequently as a product of contact-metamorphism which has taken place between the rhodochrosite ore and the intruded rhodonite vein. Such contact-reaction may be expressed by an equation as:

$$\underset{\text{(carbonate ore)}}{(Fe, Ca, Mn)CO_3} + \underset{\text{(rhodonite)}}{(Ca, Fe, Mn)SiO_3} = \underset{\text{(tephroites)}}{(Mn, Fe)_2SiO} + \underset{\text{(metamorphosed carbonate)}}{(Mn, Ca)CO_3}$$

Two different modes of formation were observed in the Kaso deposit; (i) the contact-metamorphism between the first carbonate ore and the blood-red rhodonite vein, and (ii) the contact between the *Azuki*-ore and the pink rhodonite vein.

(i) Contact-metamorphism of the first carbonate ore.

By this metamorphism the first carbonate ore and a corresponding amount of the intruded blood-red rhodonite are made over into manganknebelite leaving a considerable quantity of white saccharoidal mangancalcite as the unincorporated residue. The following equation is expected to hold between the two sets of mineral assemblages.

m(blood-red rhodonite) + n(the first carbonate ore)
= p(manganknebelite) + q(saccharoidal mangancalcite).

Specimens representative of these four members were analysed by the author, with the results compared in the following Table 66.

TABLE 66. Four minerals which participated in the contact-metamorphism of Type (i).

	I. Blood-red rhodonite	II. The first carbonate ore	III. Mangan-knebelite	IV. Saccharoidal mangancalcite
Fe	11.9	12.7	24.0	1.6
Mn	71.6	75.0	68.2	21.8
Ca	6.0	6.9	0.6	75.1
Mg	10.5	5.4	7.2	1.5

I, from Table 88. III, from Table 76.
II, ,, ,, 23. IV, ,, ,, 30.

The above equation of the metamorphic change will be proved to hold if the following coefficients are multiplied.

$$\begin{cases} m = 5 \\ n = 5 \end{cases} \qquad \begin{cases} p = 9 \\ q = 1 \end{cases}$$

The results of such calculation are given in Table 67.

TABLE 67. Comparison of the calculated atomic compositions before and after the metamorphism.

	5×(blood-red rhodonite) +5×(the first carbonate ore)	9×(manganknebelite) +1×(saccharoidal mangancalcite)
Fe	12.3	12.5
Mn	73.3	70.8
Ca	6.4	8.6
Mg	8.0	8.3

(ii) Contact-metamorphism of the *Azuki*-ore.

The second mode of formation of tephroite is through the contact-metamorphism of the *Azuki*-ore of period B_3 by the pink rhodonite vein of period B_1.

Although the crystallization of the rhodonite is, as a rule, earlier than the deposition of the main carbonate ore, some exceptional cases are seen in which the latest member of the rhodonite vein traverses the *Azuki*-ore, i.e. the main carbonate ore of period B_3 (Pl. XLV (X), Figs. 5 and 6).

This irregularity may probably be due to an exceptionally long continuation of a part of the mineralization of B_1 period which survived the rather rapid evolution of the main carbonate-rich part of B_3 period. Two different ways must, therefore, be assumed as the course of evolution of the ironrhodonite vein as presented schematically by the following diagram:

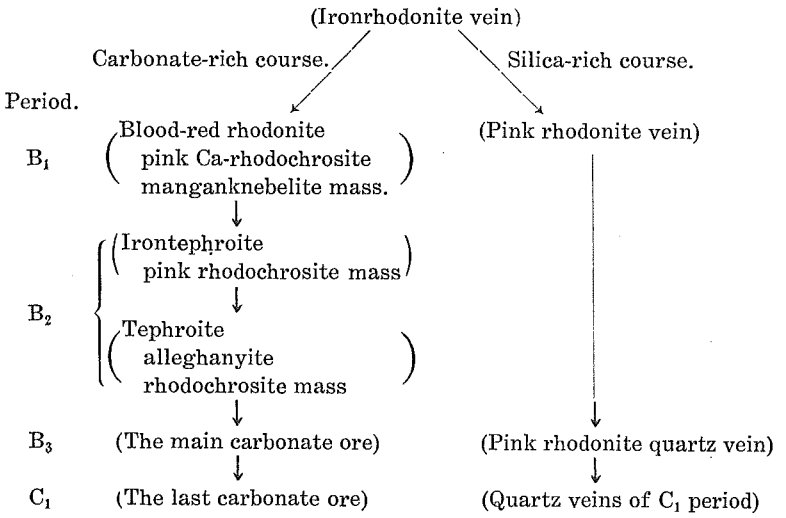

The following equation is expected to hold between the four constituents which have participated in this reaction.

$$m\,(\text{pink rhodonite}) + n\,(\textit{Azuki}\text{-ore}) = p\,(\text{tephroite}) + q\,(\text{white mangancalcite}).$$

The atomic composition of the four members were recalculated from the analyses described elsewhere in this article with the results compared in the following Table 68.

TABLE 68. Four components which participated in the reaction of Type (ii).

	I. Pink rhodonite	II. *Azuki*-ore	III. Tephroite	IV. White mangancalcite
	atom. %			
Fe	5.8	2.4	6.1	1.6
Mn	81.0	84.7	85.4	21.8
Ca	8.7	8.4	3.5	75.1
Mg	4.5	4.5	5.0	1.5

I, from Table 90. III, from Table 80.
II, ,, ,, 25. IV, ,, ,, 30.

Substitute the following figures for the coefficients in the above equation:

$$\begin{cases} m = 8 \\ n = 6 \end{cases} \qquad \begin{cases} p = 13 \\ q = 1 \end{cases}$$

The accordance of the calculations of both sides of this equation was remarkably good as shown in Table 69.

TABLE 69. Calculations in order to compare both sides of the equation of Type (ii) reaction described above.

	8×(pink rhodonite) +6×(*Azuki*-ore)	13×(tephroite) +1×(white mangancalcite)
	atom. %	
Fe	4.4	5.7
Mn	84.7	81.0
Ca	8.4	8.6
Mg	4.5	4.7

The three modes of formation of knebelite and tephroite described above are all common in the following three respects.

(i) The iron is intensely enriched in the tephroites which are embodied in knebelite, manganknebelite or irontephroite.

(ii) The lime is retained almost completely in the carbonate.

(iii) The original carbonate mineral is deprived of its iron and manganese contents by these reactions and remains as iron-poor mangancalcite.

As shown in the previous sections concerning the mangancalcite (cf. Chap. X), the removal of iron from the carbonate ore is complete in both the manganhedenbergite formation and the knebelite formation, while the complete removal of manganese occurs only in the former case being incomplete in case of the knebelite formation.

The amount of the residual carbonate depends chiefly upon the lime-content of the original carbonate ore. The saccharoidal carbonate which remains after the contact-metamorphism of the first carbonate ore is consequently the most abundant among the allied carbonates.

The system Fe_2SiO_4—Mn_2SiO_4.

Minerals of the tephroite—fayalite series may be classified in the following seven varieties from the chemical point of view (Table 70).

TABLE 70. Minerals of the Fe_2SiO_4–Mn_2SiO_4 series.

Mineral	Fe_2SiO_4 (mol. %)
Fayalite	100–95
Manganfayalite	95–80
Ironknebelite	80–60
Knebelite	60–40
Manganknebelite	40–20
Irontephroite	20–5
Tephroite	5–0

At the Kaso mine five varieties belonging to this series, from ironknebelite to tephroite, were found and their properties studied. As the manganknebelite and irontephroite have been found for the first time from the Kaso mine the continuous relationship in this series has acquired an another support in the natural mineral group. The variations in the physical properties in respect to the content of tephroite molecules are very irregular, because even the inferior contents of Ca_2SiO_4 and Mg_2SiO_4 affect their physical properties to a remarkable degree. This system must be treated in this connection as a quaternary system Ca_2SiO_4–Mg_2SiO_4–Mn_2SiO_4–Fe_2SiO_4, for the consideration of which much more reliable data are required beyond those now accessible.

(a) Ironknebelite.

Ironknebelite is a dark olive-green mineral, occurring fragmentarily in a mass of the first carbonate ore. No crystal forms are usually observed, but some of them found in a garnet rhodonite vein are rather distinct as shown in Pl. XLIV (IX), Fig. 4.

It is hard to make out the genetical condition of this mineral as it is found only as fragments distributed sporadically in later mineralized products. The physical properties examined are presented in Table 71, and the results of chemical analysis in Table 72.

TABLE 71. Physical constants of ironknebelite.

Sp. gr. $d_4^{18} = 4.16$

$\alpha = 1.796$ $\quad \gamma - \alpha = 0.049$

$\beta = 1.830$ $\quad \alpha_F - \alpha_C = 0.080$

$\gamma = 1.845$

Optically negative, $(-)2V = 50°$.

$\rho > v$ distinct.

TABLE 72. Chemical composition of ironknebelite.

	wt. %		mol. %
SiO_2	30.04	Fe_2SiO_4	57.0
TiO_2	tr	Mn_2SiO_4	29.1
Al_2O_3	1.27	Ca_2SiO_4	4.5
Fe_2O_3	1.65	Mg_2SiO_4	9.4
FeO	33.20		(100.0)
MnO	20.12		
CaO	6.58		
MgO	3.36	Impurities;	
CO_2	3.56	$CaCO_3$ 20.5	
H_2O	0.10	$Mn_3Al_2Si_3O_{12}$ 5.0	
	99.88		

(b) Picroknebelite.

Picroknebelite occurs as lenses or as fragments of a vein in an intensely fractured country rock. Some of the lenses consist of a single crystal of picroknebelite, which is as large as 5 cm. across (Pl. XLV (X), Fig. 3). Crystal forms indistinct. Characteristic parting parallel to 100 is strikingly well-developed (Pl. XLV (X), Fig. 2), to the trace of which it shows straight extinction of light under the microscope. A small amount of mangancalcite and celsian are seen closely in association with picroknebelite.

The physical properties and the chemical composition examined are given in Tables 73 and 74 respectively.

(c) Knebelite.

This mineral seems to occur frequently in the Kaso mine as a primary mineral or a product of contact-metamorphism. No decisive

TABLE 73. Physical properties of picroknebelite.

Cleavages distinct parallel to 010, 001.
Parting highly developed parallel to 100.
Colour greyish-brown.
Lustre greasy.
Sp. gr. $d_4^{16} = 3.98$.
Under the microscope, colourless.
$\alpha = 1.787$ $\gamma - \alpha = 0.043$
$\beta = 1.815$ $\alpha_F - \alpha_C = 0.030$
$\gamma = 1.830$
Optically negative; (−) $2V = 56°$.

TABLE 74. Analysis of picroknebelite.

	wt. %		mol. %	
SiO_2	.....	29.24	Fe_2SiO_4	26.3
TiO_2	.....	—	Mn_2SiO_4	59.0
Al_2O_3	.....	1.68	Ca_2SiO_4	4.2
Fe_2O_3	.....	1.66	Mg_2SiO_4	10.5
FeO	.....	17.98		(100.0)
MnO	.....	40.02		
BaO	.....	1.68		
CaO	.....	2.51	Impurities	
MgO	.....	4.02	$(Mn,Ca)CO_3$	9.
Na_2O	.....	0.04		
K_2O	.....	0.15	$Ba\ Al_2Si_2O_8$	2
CO_2	.....	0.60	$(Na,K)AlSi_3O_8$	2
H_2O	.....	0.13		
		100.07		

data, however, were available for a certain determination of this point. Some granular crystals of knebelite presumably formed by the contact-metamorphism of an impure carbonate ore of period A_3 are presented in Pl. XLV (X), Fig. 1.

(d) Manganknebelite.

Manganknebelite is found associated with white turbid manganocalcite as a product of contact-metamorphism of B_2 period. It has presumably been produced as a result of the assimilation of manganese of the first carbonate ore, caused by the contact of a rhodonite vein.

It is dark olive-coloured, with a slight yellowish-brown tinge. Lustre greasy. Only indistinct cleavages are observed. The physical constants and the chemical composition examined are presented in the following Tables 75 and 76 respectively.

TABLE 75. Physical constants of manganknebelite.

Sp. gr. $d_4^{18} = 4.01$.
Optic orientations; X = b, Y = c, Z = a.
$\alpha = 1.795$
$\beta = 1.830$
$\gamma = 1.840$
$\gamma - \alpha = 0.045$
$\alpha_F - \alpha_C = 0.028$
Optically negative, $(-)2V = 50°$.

TABLE 76. Analysis of manganknebelite.

	wt. %		mol. %	
SiO_2	29.21	Fe_2SiO_4		24.0
TiO_2	—	Mn_2SiO_4		68.2
Al_2O_3	0.20	Ca_2SiO_4		0.6
FeO	16.92	Mg_2SiO_4		7.2
MnO	43.23			(100.0)
CaO	0.35			
MgO	2.64	SiO_2 excess	5.0	
Fe	2.59			
S	1.41	Impurities;		
CO_2	2.80	FeS	4.5	
H_2O	0.12	Carbonate	6.0	
	99.47			

(e) Irontephroite.

Irontephroite occurs as irregular-shaped masses, almost monomineralically. It is also found as a product of the contact-metamorphism bordering a xenolith consisting of the white saccharoidal carbonate. Lustre greasy to resinous. Colour deep olive-grey with a greenish tinge. Under the microscope it is colourless, and shows rather distinct cleavages. The weak cleavages parallel to (001) and (100) were observed as usual, and, moreover, the cleavage parallel to (140) was also exceptionally distinct (Pl. XLV (X), Fig. 4). Physical properties and the chemical composition of irontephroite examined by the author are presented in the following Tables 77 and 78.

TABLE 77. Physical properties of irontephroite.

Sp. gr. $d_4^{15} = 3.96$.

Optic orientations;

X = b

Y = c

Z = a

Refractive indices;

$\alpha = 1.787$

$\beta = 1.811$

$\gamma = 1.819$

Optically negative, (−) $2V = 60°$.

TABLE 78. Analysis of irontephroite.

wt. %		mol. %	
SiO_2	27.97	Fe_2SiO_4	16.3
TiO_2	0.15	Mn_2SiO_4	76.7
Al_2O_3	tr.	Ca_2SiO_4	—
FeO	10.99	Mg_2SiO_4	7.0
MnO	52.45		(100.0)
CaO	0.94		
MgO	2.73	Impurities;	
CO_2	1.04	(Ca, Mn) CO_3	4.6
H_2O	4.02	Mn_2O_3, nH_2O	2.0
	100.29		

Irontephroite occurs nearly monomineralically as a vein and is accompanied only by a small amount of ferriferous zincblende and some relict crystals of rhodonite. Irontephroite as a contact mineral is accompanied by sporadic crystals of white turbid mangancalcite (cf. Chap. X).

Irontephroite is rather easily altered hydrothermally, resulting in a kind of penwithite. An example of such alteration is shown in Pl. XLV (X), Fig. 4, proceeding along (140) cleavages (cf. Chap. XVII, e).

(f) Tephroite.

Tephroite is one of the most important minerals of the Kaso deposit, being also important economically because of its high manganese content. It occurs abundantly as massive aggregates in the main ore body, especially where the latter is remarkably enlarged. Olive-grey to light grey with a slight greenish tinge. A coarse-grained aggregate of grey tephroite crystals looks, sometimes, like sandstone.

Tephroite masses contain a plenty of relict minerals such as rhodonite and wine-yellow garnet. Tephroite crystals, on the other hand, are found replaced metasomatically by the main rhodochrosite ore i.e., the *Azuki*-ore. A small amount of galena and zincblende frequently accompanies the tephroite (Pl. XLVI (XI), Fig. 6).

Crystallization of the tephroite is the most important mineralization of the Kaso deposit and seems to be a characteristic feature common to most of the promising manganese deposits of similar origin.

The physical properties and the chemical composition of tephroite are given in the following Tables 79 and 80 respectively.

TABLE 79. Physical properties of tephroite.

Cleavage ..... weak || to (001).
Sp. gr. $d_4^{18} = 3.98$.
$\alpha = 1.788$
$\beta = 1.810$
$\gamma = 1.817$
$\gamma - \alpha = 0.029$
$\alpha_F - \alpha_C = 0.023$
Optically negative, (−) 2V = 68°.

TABLE 80. Analysis of tephroite.

	wt. %		mol. %	
SiO_2	28.78	Fe_2SiO_4	6.1
TiO_2	—	Mn_2SiO_4	85.4
Al_2O_3	0.10	Ca_2SiO_4	3.5
FeO	4.57	Mg_2SiO_4	5.0
MnO	62.12		(100.0)
CaO	2.08		
MgO	2.10	SiO_2 Lack	6.5
CO_2	0.50	Impurity;	
H_2O	—	Carbonate 1.2	
	100.25		

CHAPTER XIV

PYROXENES

(a) Salite.
(b) Manganhedenbergite.
(c) Ironrhodonite.
(d) Blood-red rhodonite.
(e) Pink rhodonite.
(f) Carmine-red rhodonite.

Minerals of the pyroxene group, especially several varieties of rhodonite which are characteristic of the manganese deposit, are found abundantly in the Kaso mine. They are arranged below in Table 81 according to the order of mineralization.

TABLE 81. Minerals of the pyroxene group.

Minerals.	Period.	Occurrence.
Salite		In a scapolite salite aplite.
Manganhedenbergite	A_1	Independently as veins.
Ironrhodonite	B_1	,,
Blood-red rhodonite	B_{1-2}	,,
Pink rhodonite	B_{1-3}	,,
Carmine-red rhodonite	C_2	As a contact mineral related to a pegmatitic quartz vein.

Except for the last mineralized one, the carmine-red rhodonite, all minerals of the pyroxene group seem to be of primary origin. Their evolutional change is principally represented by the decrease of the lime and the iron contents, for example, from salite to pink rhodonite.

Variations in the physical properties against such change of the chemical composition are of much interest, which, however, will not be discussed in detail in this report.

Variations of a few diagnostic physical properties along with that of the chemical composition are presented in the following Table 82.

TABLE 82. Variations of some physical constants and the chemical composition of the pyroxenes.

	1.	2.	3.	4.	5.	6.
Mineral.	Salite.	Mangan-hedenbergite.	Iron-rhodonite.	Blood-red rhodonite.	Pink rhodonite.	Carmine-red rhodonite.
Colour.	green	green	greyish pink	blood-red	pink	carmine-red
d	n.d	3.50	3.73	3.68	3.58	3.70
γ	1.700	1.750	1.743	1.747	1.729	1.730
$\gamma-\alpha$	0.030	0.025	0.020	0.020	0.017	0.014
(+) 2V	62°	63°	39°	42°	44°	73°
c∧Z′ on (110)	40°	30°	31°	28°	28°	22°
c∧Z′ on (1$\bar{1}$0)	40°	30°	19°	16°	15°	13°
		mol. %				
$FeSiO_3$	n.d	36.8	13.3	11.9	5.8	1.5
$MnSiO_3$	n.d	7.1	73.0	71.6	81.0	91.9
$CaSiO_3$	n.d	46.8	7.6	6.0	8.7	4.9
$MgSiO_3$	n.d	9.3	6.1	10.5	4.5	1.7

(a) Salite.

Salite occurs in a scapolite salite aplite as small green crystals. Colourless under the microscope. The optical constants measured are given below:

$Y = b$
$c \wedge Z = 43°$
$\alpha = 1.670$ $\quad n_1(110) = 1.673$
$\beta = 1.681$ $\quad n_2(110) = 1.695$
$\gamma = 1.700$
$\gamma - \alpha = 0.030$
$\alpha_F - \alpha_C = 0.017$
Optically positive, (+) $2V = 62°$.

(b) Manganhedenbergite.

Manganhedenbergite is the chief constituent of the product of period A_1. It occurs in two forms; (i) granular massive aggregates; and (ii) veins about 4 cm. in thickness. Crystals as long as 2 cm. are not rare, but no good crystal forms are seen. Olive-green to pistacio-green, with glassy lustre.

Hardness H = 6; fusibility F = 3.

The physical constants (Table 83) and the chemical composition (Table 84) are not strictly equal in the two specimens examined, as their modes of occurrence are not the same.

TABLE 83. Physical constants of manganhedenbergites.

	(Type A)	(Type B)
Occurrence.	Veins.	Granular massive.
Sp. gravity	3.50	3.50
Optic axial plane	010	010
$c \wedge Z$	32°	33°
α	1.716	1.720
β	1.729	1.731
γ	1.746	1.750
$n_1(110)$	1.720	1.724
$n_2(110)$	1.735	1.734
$\gamma - \alpha$	0.030	0.030
$\alpha_F - \alpha_C$	0.018	0.018
2V	(+) 64°	(+) 62°
Dispersion	$\rho > v$ distinct	$\rho > v$ distinct.

TABLE 84. Chemical composition of manganhedenbergite.

wt. %	Type A.	Type B.
SiO_2	48.47	44.68
TiO_2	0.04	—
Al_2O_3	3 40	0.35
Fe_2O_3	4.36	4.32
FeO	15.23	17.40
MnO	3.26	4.40
BaO	1.28	—
CaO	18.06	23.96
MgO	3.55	2.19
Na_2O	0.82	0.22
K_2O	1.01	0.18
CO_2	—	1.76
H_2O+	0.86	0.24
H_2O-	0.32	
	100.66	99.70
mol. %		
(Na, K) $Fe^{III} Si_2O_6$	—	2.4
Ca $(Fe, Al)_2 SiO_6$	8.0	6.3
Mn $Mn_2 SiO_6$	4.4	—
Ca Fe Si_2O_6	62.2	61.2
Ca Mn Si_2O_6	—	16.1
Ca Mg Si_2O_6	14.0	25.4
	(100.0)	(100.0)

	Impurities; Bariumalbite		Calcite
	Type A	Type B	mean
	mol. %		
$FeSiO_3$	36.8	36.8	36.8
$MnSiO_3$	6.2	8.0	7.1
$CaSiO_3$	45.1	48.4	46.8
$MgSiO_3$	11.9	6.8	9.3
	(100.0)	(100.0)	(100.0)

Manganhedenbergite is also found as xenocrysts in a rhodonite vein of B_1 period. It looks almost unchanged if embedded in a crystal of rhodonite (Pl. XLVI (XI), Fig. 3), but it is found as strongly corroded crystals if affected by the metasomatic replacement of a kasoite rhodonite vein (Pl. XLVI (XI), Fig. 5).

In Pl. XLVI (XI), Fig. 1 are shown two pieces of closely aggregated manganhedenbergite mass which have been enclosed in an *Azukiban* and have been affected by a carbonate solution of the advanced stage. They have been altered gradually from their sur-

face and are seen surrounded by a rim of a new-formed colourless carbonate mineral.

(c) Ironrhodonite.

The pioneer of the rhodonites of B_1 period is a ferriferous one. Pale pink on a fresh surface. Under exposure even in the room it tarnishes rather rapidly and a remarkably rapid change of colour is observed on heating a wet sample to dry in the air. The tarnish is brownish-grey quite distinct from the pink colour characteristic of rhodonite.

Under the microscope it occurs as distorted dirty crystals showing a rather high birefringence. The physical properties examined and the results of chemical analysis are shown in Tables 85 and 86.

TABLE 85. Physical properties of ironrhodonite.

$d_4^{12} = 3.73$

Extinction angle $c\wedge Z'$ on $110 = 31°$

,, $c\wedge Z'$ on $1\bar{1}0 = 19°$

$(c\wedge Z')_\rho > (c\wedge Z')_v$

$\alpha = 1.723$	$\gamma - \alpha = 0.020$
$\beta = 1.730$	$\alpha_F - \alpha_C = 0.020$
$\gamma = 1.743$	

(+) $2V = 39.°$

TABLE 86. Chemical analysis of ironrhodonite.

	wt. %		mol. %
SiO_2	44.55	$Fe_2Si_2O_6$	10.0
TiO_2	—	$Mn_2Si_2O_6$	73.0
Al_2O_3	2.53	$Ca_2Si_2O_6$	7.6
Fe_2O_3	0.90	$Mg_2Si_2O_6$	6.1
FeO	5.06	$Na\,Fe\,Si_2O_6$	3.3
MnO	38.13		(100.0)
CaO	3.57		
MgO	1.84		
BaO	2.06	Impurities;	
K_2O	0.47	Kasoite 9.0	
Na_2O	0.67	Rhodochrosite 6.0	
CO_2	1.00		
H_2O	0.30		
	101.08		

The analysis shown in Table 86 contains the lower limit of iron necessary if a material is to be called ironrhodonite. It is, however, highly probable that some other specimens may be more ferriferous

than the analysed material, so this mineral was termed "iron-rhodonite", with special reference to its remarkable tarnishing under exposure in the air.

Ironrhodonite is found frequently replaced along cleavages or partings by a less ferriferous rhodonite (Pl. XLVI (XI), Fig. 4). The later mineralized iron-poor rhodonite is a fine clear crystal, not distorted, with a smaller extinction angle on a cleavage-flake and a considerably lower birefringence (cf. Table 82 and Pl. XLVII (XII), Fig. 2).

In Pl. XLVI (XI), Fig. 2 is reproduced the polished surface of a specimen showing successive intrusions of ironrhodonite veins and a rhodonite vein, the latter being always later than the former.

The later intruded rhodonite vein is lighter-coloured than the earlier ironrhodonites. A rhodonite veinlet traversing the wall rock is shown in Pl. XLVII (XII), Fig. 3 which has been strongly affected by a later mineralizing solution. This is a piece of decisive evidence that the hydrothermal alteration of the wall rock in B stage, i.e. the formation of *Azukiban,* has been anteceded by the intrusion of rhodonite veinlets. Three different modes of hydrothermal alteration of the ferriferous rhodonite were observed as the results of intrusions of various quartz veins. The most prominent effect is the formation of mangantremolite which will be described in detail in a succeeding section. The second is the purification of a turbid ironrhodonite crystal due to the removal of dusty inclusions as well as an extraction of the dominant portion of the component ironsilicate. The removed ferrosilicate molecule, $FeSiO_3$, is not substituted by a rhodonite molecule $MnSiO_3$, but is replaced, in this case, simply by quartz grains which are seen poikilitically distributed in the purified rhodonite (Pl. XLVII (XII), Fig. 1).

This is an interesting example of a poikilitic structure due to a hydrothermal alteration. The third mode of alteration is the complete replacement of rhodonite by a newly formed rhodochrosite. This alteration seems to be caused by a siliceous solution of the more advanced stage which has been remarkably enriched in volatile substances. Some of the new-formed rhodochrosite appears in peculiar worm-like forms as shown in Pl. XLVII (XII), Figs. 4 and 5.

They are probably a kind of "*Streckungshöfe*"[1], which has been reported not infrequently as a product of a stress-metamorphism. It

(1) U. GRUBENMANN & P. NIGGLI: Die Gesteinsmetamorphose s. 466 (1924).

is also noteworthy that the quartz vein which contains such peculiar shaped crystals of rhodochrosite shows a distinct schistosity under the microscope as reproduced in Pl. XLVII (XII), Fig. 6. It is also shown that such "*Streckungshöfe*" is always accompanied by a grain of iron-ore from which its development started.

(d) Blood-red rhodonite.

Blood-red rhodonite is an important mineral formed at the end of period B_1, when the residual solution has been considerably enriched in a carbonate constituent. This mineral occurs as large platy crystals, often as large as 10 cm. across. The interspaces between such large crystals are occupied by a mixture of manganknebelite and pink Ca-rhodochrosite. Some spaces left unoccupied by such primary minerals are seen full of black penwithite which is presumably a product of later mineralization of C_1 period.

Beautiful blood-red and transparent crystals are found abundantly in the Kaso deposit, being often replaced by a less iron-rich and, consequently, less double-refracting rhodonite along cracks or cleavage-planes.

Crystal forms (110) ($1\bar{1}0$) (001) are distinct.

Physical constants measured are given in Table 87.

TABLE 87. Physical constants of blood-red rhodonite.

Sp. gr. $d_4^{18} = 3.68$
c^Z′ on 110 = 28°
c^Z′ on $1\bar{1}0$ = 16°

$\alpha = 1.730$
$\beta = 1.735$
$\gamma = 1.747$
$\gamma - \alpha = 0.017$
$\alpha_F - \alpha_C = 0.020$
(+) $2V = 42.°$

In Table 88 below are given the results of chemical analysis, which correspond to the composition of a highly ferriferous rhodonite. Although the blood-red rhodonite shows a high content of iron the colour change on exposure in the air is almost negligible, compared with that of the ironrhodonite.

TABLE 88. Chemical analysis of blood-red rhodonite.

	wt. %
SiO_2	45.95
TiO_2	—
Al_2O_3	0.10
FeO	6.85
MnO	40.22
CaO	2.70
MgO	3.34
H_2O	0.11
	99.27

	mol. %
$FeSiO_3$	11.9
$MnSiO_3$	71.6
$CaSiO_3$	6.0
$MgSiO_3$	10.5
	(1000.0)
SiO_2 Lack	−3.6

(e) Pink rhodonite.

Pink rhodonite is the most important mineral of the rhodonite group, as it is found in almost every manganese deposit of Kaso type. It occurs in the Kaso deposit in an enormous quantity. It is a slightly ferriferous variety showing a very slow fading of a pink colour on exposure in the air. It is usually found as a monomineralic vein, or as massive aggregates accompanied by a considerable quantity of hornstone-quartz. A few conspicuous features of this mineral will be mentioned here under the following three heads.

(i) Corona structure.

A corona structure of pink rhodonite with a core of iron-rhodonite is seen sometimes in a quartz-rich pink rhodonite vein (Pl. XLVII (XII), Fig. 2). This structure may be regarded as one of the evidences that a reaction relation can be expected between the early-formed ironrhodonite and the late-formed iron-poor pink rhodonite.

(ii) Schiller inclusions.

Filmy or ribbon-shaped inclusions are sometimes found in a pink rhodonite crystal quite in a similar manner as is observed in a bronzite crystal (Pl. XLVIII (XIII), Figs. 1 and 2). A weak schillerization rarely observed in a rhodonite crystal may possibly be due to such inclusions.

(iii) Twinning.

Twinning of rhodonite crystals is said to be a very rare phenomenon. Numerous examples of twinned crystals, however, are observed in thin slices of the Kaso rhodonites, especially in those of the pink rhodonite (Pl. XLIX (XIV), Figs. 1 and 2).

Lamellar twinning was also observed in a thin slice of a carmine-red rhodonite (Pl. L (XV), Fig. 3). The cleavage traces are not

disturbed at all by these twinnings, so the twinning plane may be 100. The composition plane, on the other hand, does not coincide with 100, because the junctions of the twinned individuals is oblique to the trace of (110) cleavage. In a thin slice cut nearly perpendicular to c-axis this contact line is seen bisecting the intersecting angle of the traces of 110 and $1\bar{1}0$ as shown in Pl. XLIX (XIV), Fig. 2. The composition plane may, therefore, be parallel to 101 or some other domatic planes in zone [010].

The physical properties and the chemical composition of pink rhodonite are set down in the following two tables (Tables 89 and 90).

TABLE 89. Physical properties of pink rhodonite.

$d_4^{18} = 3.58$
$c\wedge Z'$ on $110 = 28°$
$c\wedge Z'$ on $1\bar{1}0 = 15°$
$\alpha = 1.712$
$\beta = 1.719$
$\gamma = 1.729$
$\gamma - \alpha = 0.017$
$\alpha_F - \alpha_C = 0.020$
Optically positive, (+) $2V = 44.°$

TABLE 90. Analysis of pink rhodonite.

	wt. %
SiO_2	45.61
TiO_2	—
Al_2O_3	0.08
FeO	3.30
MnO	44.85
CaO	3.97
MgO	1.75
H_2O	0.12
	99.68

	mol. %
$FeSiO_3$	5.8
$MnSiO_3$	81.0
$CaSiO_3$	8.7
$MgSiO_3$	4.5
	(100.0)
SiO_2 Lack	−2.5

Minerals associating with pink rhodonite are rare and scarce except for quartz. Wine-yellow garnet and Fe-Ti-ore are found occasionally in a pink rhodonite vein, sometimes with a bit of allanite.

Pink rhodonite of the advanced stage, probably even later in a practical time relation than the deposition of the main carbonate ore of period B_3, consists solely of very fine fibrous crystals, sometimes so intimately interwoven as to be tough and tenaceous enough to be sculptured. The texture under the microscope (Pl. XLIX (XIV), Figs. 4 and 5) is like those usually observed in a thin section of jade. Such a mass has a beautiful ruby colour and is translucent. These

fibrous rhodonite crystals are, sometimes seen being accompanied by a large amount of black substance (Pl. XLVIII (XIII), Figs. 3 and 4), which may presumably be a product contemporaneous with the black substance contained in the black *Azuki*-ore. Such black substances are also seen in coarse-grained rhodonite mass as shown in Pl. XLIX (XIV), Fig. 3, which shows that the impregnation of the black substance is at least prior to the recrystallization of pink rhodonite.

Two different ways of the evolution of the rhodonitic mineralizing solution are also evident in the paragenesis of minerals related to the deposition of the black substances (cf. Chap. XIII, p. 401). The scheme of such evolution, a little modified, is reproduced here for ease of reference.

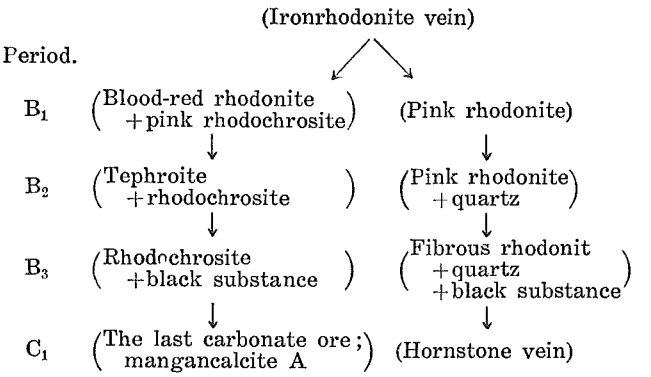

(f) Carmine-red rhodonite.

A very beautiful carmine-red rhodonite is found along the border of a pegmatitic quartz vein which has been intruded into the rhodochrosite ore. Figure 2 in Plate L (XV) shows an example of such occurrence. Three different mineral-zones can be seen symmetrically developed on either side of the quartz vein as shown schematically in the following diagram:

3. Rhodochrosite.
2. Tephroite.
1. Carmine-red rhodonite.

Pegmatitic quartz vein.

1. Carmine-red rhodonite.
2. Tephroite.
3. Rhodochrosite.

The pegmatitic quartz vein continues further as a beautiful rhodonite vein after the quartz has been consumed by the reaction between it and the carbonate ore, resulting in a new-formed rhodonite. The carmine-red rhodonite is, therefore, apparently a product of contact-metamorphism, and the tephroite zone seems to have also been formed by a contact-reaction between the newly formed rhodonite and the original carbonate ore. Such newly formed rhodonite veins are sometimes as thick as 5 cm.

Under the microscope this mineral is very clear and transparent, often showing peculiar polysynthetic twinning as already mentioned in the preceding section (Pl. L (XV)., Fig. 3). Chemical analysis and determination of the optical constants yielded the results given in Table 91. This rhodonite is an unusually pure variety, containing as much $MnSiO_3$ as 92 mol. percent.

TABLE 91. Physical constants and the results of chemical analysis of carmine-red rhodonite.

Sp. gr. $d_4^{18} = 3.70$
Extinction angles;
$c\wedge Z'$ $(110) = 22°$
$c\wedge Z'$ $(1\bar{1}0) = 13°$
Refractive indices;
$\alpha = 1.716$
$\beta = 1.722$
$\gamma = 1.730$
$\gamma - \alpha = 0.014$
$\alpha_F - \alpha_C = 0.025$
Optically positive, (+) $2V = 73.°$

	wt. %		mol. %
SiO_2	45.64	$FeSiO_3$	1.5
TiO_2	—	$MnSiO_3$	91.9
Al_2O_3	0.09	$CaSiO_3$	4.9
FeO	0.90	$MgSiO_3$	1,7
MnO	50.23		(100.0)
CaO	2.14		
MgO	0.54	SiO_2 Lack	−1.5
H_2O^+	0.27		
H_2O^-	0.32		
	100.13		

CHAPTER XV

AMPHIBOLES

(a) Common hornblende.
(b) Green hornblende.
(c) Actinolitic hornblende.
(d) Green ironhornblende.
(e) Dannemorite.
(f) Manganactinolite.
(g) Mangantremolite.

Minerals of the amphibole group are found frequently in the Kaso mine, chiefly as a product of hydrothermal alterations related to the mineralization of C_1 period. They are arranged in Table 92, after the order of mineralization with reference to their occurrences.

TABLE 92. Minerals of the amphibole group.

Minerals.	Period.	Occurrence.
Common hornblende		As altered phenocrysts in porphyritic metadiabasses.
Green hornblende		As a monomineralic veinlet traversing the *Kuroboku*.
Actinolitic hornblende		As a contact mineral in hornfelses.
Green ironhornblende	A_1	In a contact zone between biotite-hornfels and a manganhedenbergite vein.
Dannemorite	A_3	In a contact-metamorphosed carbonate ore of A_4 period.
Manganactinolite	C_1	As an independent vein or mass, probably of primary origin.
Mangantremolite	C_1	As a product of hydrothermal alteration of rhodonite.

Variations in the physical properties of the Kaso amphiboles against their chemical compositions are of much mineralogical interest, but as they are related to so diverse and rather independent mineralizations, it may not deserve much notice from the genetical point of view to compare them in detail.

(a) Common hornblende.

Common hornblende occurs as prismatic phenocrysts about 4 cm. long in porphyritic metadiabase. The original character of this

mineral is hard to make out owing to the intense alterations which are seemingly due to the autometamorphism characteristic of such basic igneous rocks. Some chloritic and serpentinic minerals and a plenty of iron ore are seen as the alteration product.

(b) Green hornblende.

Green hornblende is found constituting a nearly monomineralic vein which traverses the metadiabase dikes or other allied rocks (Pl. L (XV), Fig. 4). It occurs as acicular crystals up to 5 mm. in length. It is greenish-black macroscopically and under the microscope pale bluish-green with distinct pleochroism.

X = colourless,
Y, Z = pale bluish-green.
X<Y, Z.

Physical constants measured are given in Table 93.

TABLE 93. Physical constants of green hornblende.

Optic axial plane; (010). $c \wedge Z = 16.°$
$\alpha = 1.640$
$\beta = 1.652$ $\quad \gamma - \alpha = 0.020$
$\gamma = 1.660$ $\quad \alpha_F - \alpha_C = 0.016$
$n_1(110) = 1.649$
$n_2(110) = 1.658$
Optically negative, $(-)2V = 70.°$
Sp. gr. $\ldots\ldots d_4^{18} = 3.11$

From the results of the analysis of a green hornblende vein already given in Table 2, VI, the molecular composition and the formula of this mineral were calculated as follows (Table 94).

TABLE 94. Molecular composition and formula of green hornblende.

	mol. %
$MgAl_2SiO_6$	15.1
$MgFe_2^{III}SiO_6$	2.9
$CaMgSi_2O_6$	51.5
$Mg_2Si_2O_6$	6.3
$Fe_2Si_2O_6$	21.7
$Mn_2Si_2O_6$	0.5
$H_4Si_2O_6$	2.0
	(100.0)

$9\ \{(H_2)_5\ Ca_{63}\ Mg_{77}\ Fe_{53}\ Mn_2\}\ Si_{200}\ O_{600}$.
$2Mg_{100}\ (Al_{165}\ Fe_{35}^{III})\ Si_{100}\ O_{600}$.

(c) Actinolitic hornblende.

Actinolitic hornblende occurs abundantly as a contact mineral in a contact-metamorphosed diabase (cf. Chap. III, c). It forms green spots in close association with hornfels-biotite (Pl. LI (XVI), Fig. 4). Pure and homogeneous material was not available for a chemical analysis, but the refractive indices and some other physical properties examined are in good accordance with those reported of actinolitic hornblende.

Indices of refraction of this mineral were measured as follows:

$$n_{1(110)} = 1.650,$$
$$n_{2(110)} = 1.660.$$

(d) Green ironhornblende.

A black wall rock penetrated by a manganhedenbergite vein was found to consist of garnet-biotite-hornfels which had remained unaffected by all of the later hydrothermal alterations. As the manganhedenbergite vein is related to the earliest mineralization, of the Kaso mine it is an important fact that the country rock had already been metamorphosed into garnet-biotite-hornfels before the intrusion of this vein occurred.

Flakes of biotite derived from the hornfels, enclosed in an albite vein, have been made over into green ironhornblende here described. In a similar manner a few milimeters of the wall rock bordering the manganhedenbergite vein have been completely metamorphosed into green ironhornblende. But the borders of the albite veinlet itself are not at all hornblendized. Albite veinlets are apparently the offsets deposited from the last mineralizing solution which has precipitated all of its constituent manganhedenbergite at the end of its intrusion.

Green ironhornblende occurs as aggregates of prismatic crystals, and shows no good crystal forms except those which are found isolated in the metamorphosed wall rock. In Pl. L (XV), Fig. 5 are shown some isolated crystals of green ironhornblende developed in a biotite-hornfels. Traces of prismatic faces (110) (010) are seen and the intense pleochroism is also very distinct in this figure.

It is greenish-black with glistening lustre, and strongly pleochroic under the microscope.

X.....light yellow,
Y.....deep brownish-green,
Z.....deep bluish-green.
$X \ll Y < Z$.

A specimen picked up from nearly monomineralic aggregates was subjected to a chemical analysis. Some associated crystals of amber-yellow garnet were removed by hand before powdering. Physical constants and the chemical composition of this mineral are presented in Tables 95 and 96 respectively.

TABLE 95. Physical constants of green ironhornblende.

Sp. gr. ..... $d_4^{20} = 3.29$.
$Y = b$. Optic axial plane parallel to 010.
$c \wedge Z = 24.°$
$\alpha = 1.682$ $\quad \gamma - \alpha = 0.026$
$\beta = 1.697$ $\quad \alpha_F - \alpha_C = 0.014$
$\gamma = 1.708$
$n_1(110) = 1.695$
$n_2(110) = 1.707$
Optically negative; $\quad (-)\ 2V = 66.°$

TABLE 96. Chemical composition of green ironhornblende.

	wt. %
SiO_2	43.34
TiO_2	0.15
Al_2O_3	8.00
Fe_2O_3	8.05
FeO	17.09
MnO	2.63
CaO	12.40
MgO	5.25
Na_2O	0.18
K_2O	1.59
H_2O^+	0.93
H_2O^-	0.06
	99.67

	mol. %
$(Mg, Ca, Mn, Fe)SiO_3$	75.8
$Mg(Al, Fe)_2SiO_6$	15.8
$(Na, K)Fe^{III}Si_2O_6$	5.8
H_2SiO_3	2.6
	(100.0)

or

$FeSiO_3$	38.6
$MnSiO_3$	5.9
$CaSiO_3$	36.2
$MgSiO_3$	19.3
	(100.0)

Inclusive of

Fe_2O_3	6.2
Al_2O_3	9.8
$(Na, K)_2O$	2.5
SiO_2	20.0

The green ironhornblende is the product of a reaction between the hornfels-biotite and the introduced manganhedenbergitic solution. This reaction may be expressed by the following equation;

$$\underset{\text{(biotite)}}{SiO_2 + 2(Na, K)H_2(Mg, Fe)_3Al(SiO_4)_3} + \underset{\text{(manganhedenbergite)}}{5(Fe, Ca, Mg, Mn)SiO_3}$$

$$= \underset{\text{(green ironhornblende)}}{(Na, K)_2H_2(Fe, Mg, Mn, Ca)_8Si_9O_{27}} + \underset{\text{(garnet)}}{(Mg, Fe, Mn)_3Al_2Si_3O_{12}}.$$

Albite participates in this reaction only as a catalysor, or more correctly termed, as a "solvent-mineralizor". It is a great regret of the author that he has not succeeded in collecting a sufficient quantity of the pure hornfels-biotite for analysis' sake. An analysis of a contact-biotite reported by Prof. S. Tsuboi and Dr. K. Sugi is, therefore, reproduced in Table 97, No. 4. In this table are compared the composition of minerals representative of the four members included in the above equation. Such comparison offers a good explanation of the distribution of the elements which participated in this metamorphism. Remarkable enrichment of manganese in garnet is also worthy of note (cf. Chap. XII).

TABLE 97. Chemical composition of four minerals participated in the formation of green ironhornblende.

	1.	2.	3.	4.
SiO_2	48.47	43.34	34.93	34.13
TiO_2	0.04	0.15	—	2.62
Al_2O_3	3.40	8.00	20.06	19.74
Fe_2O_3	4.36	8.05	2.53	2.07
FeO	15.23	17.09	2.01	18.97
MnO	3.26	2.63	32.91	0.33
BaO	1.28	—	—	—
CaO	18.06	12.40	5.74	—
MgO	3.55	5.25	0.59	7.76
Na_2O	0.82	0.18	0.45	0.21
K_2O	1.01	1.59	—	9.15
H_2O^+	0.86	0.93	1.30(1)	4.30
H_2O^-	0.32	0.06	0.05	0.18
	100.66	99.67	100.57	99.46

(1) Manganhedenbergite ..... from Table 84.
(2) Green ironhornblende ..... from Table 96.
(3) Amber-yellow garnet ..... from Table 56.
(4) Reddish-brown biotite in injection gneiss from Usugi, Hukusima Pref.; Analysed by S Tanaka; Reported by S. Tsuboi and K. Sugi; Journ. Geol. Soc. Japan, **42** 292 (1935).

(e) Dannemorite.

Dannemorite occurs as a product of contact-metamorphism in a saccharoidal carbonate ore of period A_3 (Pl. L (XV), Fig. 1). It is also found in the interspaces between the manganhedenbergite

(1) CO_2.

crystals of A_1 period. It consists of minute fibrous crystals. Colourless with silky lustre, often stained brown. Cleavage traces parallel to (110) intersecting at 120° visible under the microscope. The optical constants measured are shown in the accompanying Table 98, but, to the author's regret, there was not sufficient material for a quantitative chemical analysis.

TABLE 98. Optical constants of dannemorite.

Optic axial plane parallel to 010.
$c \wedge Z = 17°$.
$\alpha = 1.677$
$\beta = 1.692$
$\gamma = 1.698$
$\gamma - \alpha = 0.021$
$\alpha_F - \alpha_C = 0.016$.

Dannemorite was observed to occur rarely intermingled with knebelite though these two minerals had been formed contemporaneously as contact-products. It was formed probably in a carbonate ore containing enough silica to convert the iron and manganese-contents of the ore into metasilicate, i.e. the dannemorite. If the silica is not sufficient to form metasilicate there appears the corresponding amount of knebelite. The distribution of dannemorite, therefore may be an indication of silicification which the carbonate ore had undergone prior to the contact-metamorphism.

(f) Manganactinolite.

Manganactinolite occurs as irregular grains forming veins often as thick as 5 cm. across. Prismatic crystals are not rare but not measurable. Dark green to greyish-green. Under the microscope it is light green with distinct pleochroism.

X = light yellow,
Y = Z = yellowish-green.
Y, Z, > X.

Cleavages parallel to (110) are perfect. The optic axial plane is parallel to 010.

$c \wedge Z = 16°$
$\alpha = 1.648$
$\beta = 1.661$
$\gamma = 1.668$
$(-) 2V = 74°$.

Dispersion of the extinction position is indistinct.
n_1 (110) = 1.656
n_2 (110) = 1.667
$\gamma - \alpha = 0.020$

The results of chemical analysis are given in Table 99. Fluorine was determined by the method of decolouration of the standard titanic solution.

TABLE 99. Analysis of manganactinolite.

	wt. %		mol. %	
SiO_2	49.79	$Fe_2Si_2O_6$	26.8
TiO_2	0.16	$Mn_2Si_2O_6$	11.0
Al_2O_3	2.42	$Ca_2Si_2O_6$	26.7
Fe_2O_3	3.46	$Mg_2Si_2O_6$	35.5
FeO	14.40		(100.0)
MnO	5.79		
CaO	11.19	$NaFe^{III}Si_2O_6$	9.2
MgO	10.62	$MgAl_2SiO_6$	6.5
BaO	—	$(H,F)_4Si_2O_6$	0.8
Na_2O	0.96		
K_2O	0.25		
H_2O^+	1.52		
H_2O^-	0.20		
F	0.17		
	100.93		
$-O = F_2$	0.07		
	100.86.		

Manganactinolite is usually accompanied by several varieties of garnet. Garnets previously formed are all stable in a manganactinolitic solution. Some of them, moreover, show evidences of secondary growth (Pl. LI (XVI), Fig. 5).

Garnet produced contemporaneously with manganactinolite is the cinnamon-yellow garnet. Well-developed crystals of allanite are seen in the manganactinolite vein with conspicuous pleochroic haloes around them (Pl. LII (XVII), Fig. 6.

(g) Mangantremolite.

Mangantremolite is the dominant mineral of C_1 period. It is white or colourless, with silky lustre and it resembles sericite. This mineral was produced by the hydrothermal metamorphism of rhodonite (Pl. LI (XVI), Fig. 2) and various other silicate minerals. It has also been derived from actinolitic hornblende formed in hornfelses. Manganactinolite was similarly altered into mangantremolite by the hydrothermal solution of C_1 period. Important minerals found closely associated with mangantremolite are brown garnet and manganphlogopite.

Crystals of mangantremolite were found well-preserved in an oxidized manganese ore. Some of them were separated by treating the manganese oxide with hydrochloric acid to which hydrogen peroxide had been added (Pl. LI (XVI), Fig. 1.). Colourless transparent crystals thus separated were examined with the following results;

Morphology.—Terminal faces were not observed. Faces of the forms (100) (110) (010) gave good reflections on the goniometer, the interfacial angles being measured as follows;

$$110\wedge 100 = 27°15'. \quad 110\wedge 110 = 54°30'.$$

Twinning on 100 with the composition-plane parallel to 101 was not uncommon. The physical properties examined are given in Table 100.

TABLE 100. Physical properties of mangantremolite.

Sp. gr. $d_4^{12} = 3.17$.
Optic axial plane; 010.
$c\wedge Z = 20°$
$c\wedge Z'$ on $110 = 15°$
$\alpha = 1.637$ $\quad n_1\,(110) = 1.644$
$\beta = 1.650$ $\quad n_2\,(110) = 1.658$
$\gamma = 1.660$
$\gamma - \alpha = 0.023$
$\alpha_F - \alpha_C = 0.011$
Optically negative, $(-)\ 2V = 84°$.
Dispersion; $\rho < v$ about X.

The analysed specimen has proved to be considerably ferriferous, even though it is colourless and transparent. From the chemical composition alone it may possibly be identified with manganactinolite. The results of analysis are given in Table 101.

TABLE 101. Analysis of mangantremolite.

	wt. %		mol. %	
SiO_2	54.18	$FeSiO_3$	18.3	
TiO_2	0.28	$MnSiO_3$	13.1	
Al_2O_3	tr	$CaSiO_3$	25.3	
Fe_2O_3	0.50	$MgSiO_3$	43.3	
FeO	10.34			(100.0)
MnO	7.38			
CaO	11.50	Fe_2O_3	0.5	
MgO	13.23	H_2SiO_3	15.7	
Na_2O	—			
K_2O	—			
H_2O^+	2.84			
H_2O^-	0.16			
	100.42			

Mangantremolite which was found as inclusions in a crystal of hyalophane A was examined on its physical properties and chemical composition with the results given in Table 102.

TABLE 102. Physical properties and chemical composition of mangantremolite found enclosed in hyalophane A.

Sp. gr. $d_4^{14} = 3.27$ (by floating in Clerici's solution).

Refractive indices;

$\alpha = 1.646$	$n_1\,(110) = 1.654$
$\beta = 1.658$	$n_2\,(110) = 1.665$
$\gamma = 1.667$	
$\gamma - \alpha = 0.021$	
$\alpha_F - \alpha_C = 0.016$.	

	mol. %
$FeSiO_3$	29.3
$MnSiO_3$	32.2
$CaSiO_3$	8 2
$MgSiO_3$	30.3
	(100.0)

CHAPTER XVI

MICAS

(a) Micas
(b) Green phlogopite.
(c) Green biotite.
(d) Manganphlogopite.
(e) Sericite.

Micas of the Kaso mine are not primary minerals in a rigorous sense, as they have been derived chiefly from the contact-biotite of hornfelses. It requires further research to explain the details of their genetical relations as they occur only sporadically and not in any large amount.

Two kinds of manganiferous micas, green biotite and manganphlogopite, have been analysed and are described in this report. These minerals may be worthy of note as the manganiferous micas have previously been reported rather infrequently. The micas of th Kaso mine are arranged in Table 103 below.

TABLE 103. Minerals of the mica group found in the Kaso mine.

Minerals.	Period.	Occurrence.
Biotite		In hornfelses
Green phlogopite	A_3	In a contact-metamorphosed carbonate ore of A_3 period.
Green biotite	B_1	As xenoliths in a kasoite rhodonite vein.
Manganphlogopite	C_1	As veins or xenoliths in the last carbonate ore.

(a) Biotite.

Biotite is the dominant constituent of hornfelses derived from argillaceous rocks. A pure material suitable for analysis was not available. Refractive index was measured as:

$\gamma = 1.625$–1.630
X = light brownish-yellow, $Y = Z$ = reddish-brown.

The indices of refraction of the contact-biotite found in a contact-metamorphosed diabase were measured as;

$$\beta \fallingdotseq \gamma = 1.635.$$

Various modes of alteration of biotite deserve mention here.

(i) Hornfels-biotite gives place to a cordierite spot as the result of the later contact-metamorphism. In Pl. LI (XVI), Fig. 3 are presented several quartz biotite spots in a metamorphosed argillaceous rock, some of them being now in process of degradation due to assimilation by a larger porphyroblast of cordierite.

(ii) Formation of green ironhornblende by the reaction between biotite and manganhedenbergite (cf. Chap. XV, d).

(iii) Alteration of hornfels-biotite into green biotite, when captured in a kasoite rhodonite vein.

(iv) Grain-growth of biotite crystals and the formation of minute allanite or epidote crystals among them, when enclosed in an albite quartz vein.

Allanite crystals segregated in the hornfels-biotite are radioactive, being accompanied by prominent pleochroic haloes around them (Pl. LII (XVII), Fig. 1). These haloes are always doubled, as shown in this Figure, though they have not been successfully photographed. The dimensions of such haloes were measured as:

Radius of the outer ring ..... 0.035 mm.
„ inner ring ..... 0.018 mm.

Similar haloes have been reported and explained as due to the radioactivity of Ra and RaC[1].

It is a characteristic feature of the Kaso deposit that the wall rock altered by a mineralizing solution has again been affected by a contact-metamorphism of later stage. A kind of biotite is seen as a product of such contact-metamorphism. It is reddish-brown and moderately pleochroic. It forms peculiar spots as shown in Pl. LII (XVII), Figs. 3 and 4.

The core of such a round spot consists of an aggregate of mangantremolite crystals and on its margin is seen a shell of the contact-biotite sprinkled with crystals of newly formed garnet. If attacked by a siliceous solution of the advanced stage these spots are destroyed and the biotite alone is resorbed leaving sporadic crystals of amphibole and garnet (Pl. LII (XVII), Figs. 3 and 4).

Another example of biotite-actinolite spots is shown in Pl. LII (XVII), Fig. 2, where they are irregular-shaped as is usually observed in hornfelses.

(b) Green phlogopite.

Deep green or malachite-green mica was observed in the saccharoidal carbonate ore of period A_3.

Under the microscope it consists of minute flakes of phlogopitic mica. It is usually colourless, but sometimes bright green, with prominent pleochroism.

X ..... colourless to brownish-yellow,
$Y = Z$ ..... bright bluish-green to deep yellowish-green.

Deep colour and intense pleochroism are apparently related to the paragenesis of marmatite.

Optically negative, 2V nearly zero.
$\alpha = 1.575$
$\beta \fallingdotseq \gamma = 1.605$
$\gamma - \alpha = 0.030$
$\alpha_F - \alpha_C = 0.013$.

There was not sufficient material for a chemical analysis.

(1) S. IIMORI & J. YOSHIMURA: Sci. Pap., I. P.C.R., **5** 11–24 (1926).

(c) Green biotite.

Green biotite occurs as minute flakes 0.1 mm. across or smaller. They are found as aggregates in a kasoite vein. This mineral is also seen in an altered wall rock which is found heavily contaminated with numerous minute crystals of kasoite. A satisfactory material for chemical analysis was collected from specimens found as nearly monomineralic masses.

It is deep green to blackish-green. Under the microscope it is light green with moderate pleochroism.

Sp. gr. $d_4^{18} = 3.05$.
$\alpha = 1.575$
$\beta \fallingdotseq \gamma = 1.607$
$\gamma - \alpha = 0.032$
Optically negative, (−) $2V \fallingdotseq 0$.

Acute bisectrix X lies perpendicular to the basal cleavage.

The chemical analysis yielded the results given in Table 104.

TABLE 104. Chemical analysis of green biotite.

	wt. %
SiO_2	34.76
TiO_2	tr.
Al_2O_3	16.18
Fe_2O_3	4.05
FeO	8·75
MnO	3.90
CaO	—
MgO	16.15
BaO	4.18
Na_2O	2.32
K_2O	8.25
H_2O	1.41
	99.95

	mol. %
Phlogopite $H_4K_2Mg_6Al_2Si_6O_{24}$	65.3
Siderophyllite $H_4(Na)_2Fe_5(Al, Fe)_4Si_5O_{24}$	23.5
"Manganophyllite[1]" $H_4K_2Mn_5Al_4Si_5O_{24}$	11.2
	(100.0)
SiO_2 Excess	5.0
Al_2O_3 Lack	−3.1

Green biotite occurs also in a metamorphosed biotite-hornfels as a product of alteration due to the contamination of albite spots (cf. Chap. XI, g).

(1) The "manganophyllite" molecule was calculated as an analogous molecule to that of siderophyllite, and no mineralogical relationship with the so-called "manganophyll" is suggested here, which is a synonym of "ganophyllite".

(d) Manganphlogopite.

Manganphlogopite occurs as irregular-shaped aggregates of foliated crystals. Dark grey and soft masses were found nearly monomineralic and were satisfactory as a material for analysis. Colourless under the microscope. The acute bisectrix X is nearly perpendicular to the plane of micaceous cleavage. The physical properties and the results of analysis are given in the following Table 105.

TABLE 105. Physical constants and chemical composition of manganphlogopite.

Sp. gr. $d_4^{16} = 3.21$
Indices of refraction;
$\alpha = 1.552$
$\alpha \fallingdotseq \gamma = 1.586$
$\gamma - \alpha = 0.034$
Optically negative, $(-)\ 2E \fallingdotseq 0$.

wt. %		mol. %	
SiO_2	37.16	Phlogopite	
TiO_2	0.46	$H_4K_2Mg_6Al_2Si_5O_{24}$	66.0
Al_2O_3	15.17	Siderophyllite	
FeO	2.52	$H_4(Na, K)_2Fe_5Al_4Si_5O_{24}$	8.1
MnO	18.24	Manganophyllite	
CaO	0.95	$H_4K_2Mn_5Al_4Si_5O_{24}$	25.9
MgO	17.58		(100.0)
BaO	—		
Na_2O	1.18	Alkali Lack	−32.5
K_2O	4.55		
H_2O^+	2.18	Impurity;	
H_2O^-	0.13	$Mn_3Al_2Si_3O_{12}$	21.0
	100.29		

Manganphlogopite has probably been deposited from the mineralizing solution of C_1 period, which has been remarkably enriched in such materials as magnesia or alumina, owing to the assimilation of wall rocks.

(e) Sericite.

Sericite is found frequently as a product of hydrothermal alteration of wall rocks. It occurs very sparingly although widely disseminated as minute flakes and, consequently, offers only a few scanty materials for investigation.

CHAPTER XVII

HYDROUS SILICATES

(a) Heulandite.
(b) Serpentine.
(c) Bementite.
(d) Chlorite.
(e) Penwithite.
(f) Soapstone.

Of the hydrous silicate minerals found in the Kaso mine chlorite and penwithite are the most important. Soapstone occurs also widespread through the deposit, though not in large amount.

These minerals are arranged in the following Table 106, after the order of mineralization. Each of them, however, belongs to a rather independent mineralization.

TABLE 106. Hydrous silicate minerals of the Kaso mine.

Mineral.	Period.	Occurrence.
Heulandite		In an altered scapolite veinlet traversing the *Kuroboku*.
Serpentine		In the *Kuroboku*.
Bementite	B_1	In a rhodonite vein, but scarce and uncertain.
Chlorite	C_1	In a hornstone vein
,,	C_1	As the chief constituent of *Aburaban*
Penwithite	C_{1-2}	As isolated masses.
Soapstone	C_3	In cracks or fissures widespread through the deposit.

(a) Heulandite.

This mineral, a member of the zeolite group, is found occupying fissures in a metadiabase dike or the *Kuroboku*. It appears to be one of the degradation products of scapolite.

Perfect micaceous cleavage is developed, normal to which lies the acute bisectrix *Z*. Lustre pearly on the cleavage-face. Mica-law-twinning on the cleavage-plane is very common, so it is usually difficult to determine the exact optic axial angle. Measurements vary with each specimen from 0° to 20°. The optical properties examined were as follows:

$\alpha \fallingdotseq \beta = 1.502$,
$\gamma = 1.511$, $\gamma - \alpha = 0.009$.
$\alpha_F - \alpha_C = 0.006$.
Optically positive; (+) $2V = 20°$.
Dispersion strong, $\rho < v$.

These optical data are in accordance with heulandite except for the character of dispersion of the optic axes. This conversion of scapolite into heulandite may be expressed by a reaction such as:

$$m3NaAlSi_3O_8 . NaCl . n3CaAl_2Si_2O_8 . CaCO_3$$
(scapolite)
$$\rightarrow mNaCa_3Al_{11}Si_{29}O_{80} . 25H_2O . nNa_2Ca_4Al_{10}Si_{30}O_{80} . 25H_2O.$$
(heulandite)

(b) Serpentine.

Serpentine occurs as an accessory constituent in the auto-metamorphosed metadiabase. It may probably be an alteration product of some ferromagnesian mineral, for example, hornblende.

(c) Bementite.

Bementite is an important mineral in the manganese deposit. This mineral seems to occur widespread in the Kaso deposit, though no numerical constants were available to identify it.

Thin micaceous crystal-flakes of this mineral, colourless and moderately refringent, show nearly uniaxial interference figures between crossed nicols. Optically negative. Scaly or fibrous minerals found as alteration products of penwithite (cf. section e), may also belong to a kind of bementite. The results of chemical analysis of an altered penwithite suggest a formula $MnSiO_3 \cdot H_2O$ for this alteration product which corresponds approximately to the previously known composition of bementite.

(d) Chlorite.

Wall rocks altered by the mineralizing solution of C_1 period are very rich in chlorite forming a noteworthy rock *Aburaban*. Chlorite occurs as minute flakes, with micaceous cleavage, with the acute bisectrix X lying perpendicular to it. Though it is found widespread and abundant only a small quantity of pure material picked up from a chlorite veinlet traversing the *Aburaban* was available for chemical analysis.

The physical properties and the results of chemical analysis are shown in Table 107.

TABLE 107. Physical properties and chemical composition of chlorite.

Sp. gr. $d_4^{18} = 2.79$

Pleochroism;

X = light brown,

Y = Z = greenish-brown,

X < Y = Z.

Indices of refraction;

$\alpha = 1.588$

$\beta = 1.606$

$\gamma = 1.607$

$\gamma - \alpha = 0.019$

wt. %	
SiO_2	28.99
TiO_2	0.10
Al_2O_3	12.97
Fe_2O_3	8.97
FeO	17.85
MnO	2.28
CaO	0.84
MgO	12.91
H_2O^+	10.95
H_2O^-	3.35
	99.21

mol. %	
$H_4(Fe, Mg, Mn, Ca)_2(Al, Fe)_2SiO_9$	72.5
$H_4(Fe, Mg, Mn, Ca)_3Si_2O_9$	27.5
	(100.0)
SiO_2	−25.0
Impurity;	
$Mn_3Al_2Si_3O_{12}$	11.5

Chlorite is also found in a hornstone vein as anhedral foliated crystals. Colour pale bluish-green, with faint pleochroism. Inclusions of allanite are not infrequent, which are seen surrounded by distinct pleochroic haloes (Pl. LIII (XVIII), Figs. 5 and 6).

These haloes are very dark-coloured, sometimes nearly opaque and show peculiar abnormal birefringence in marked contrast with the chlorite crystal itself. Purplish-indigo interference colour, and a remarkably higher birefringence characterize these haloes. Outlines of the haloes are always doubled, each halo-ring showing a radius of 0.018 or 0.040 mm. respectively, which is in substantial agreement with that of the halo produced in biotite due to Ra or RaC.

(e) Penwithite.

An amorphous manganese ore found widespread in the Kaso deposit consists of a mineral of the neotocite group which is usually termed "penwithite" in Japan.

Three varieties were distinguished.

(i) Opaline penwithite.
(ii) Brown penwithite.
(iii) Black penwithite.

They are found abundantly as veinlets or patches in the Kaso deposit and are seemingly one of the characteristic products of C_1 period. They are more or less manganiferous, though any of them can be used as a manganese ore independently.

The opaline penwithite is colourless, sometimes with pale greenish or yellowish tinge. The brown and the black penwithites were also colourless when they were collected in the underground workings, but rapidly changed their colour in the air, especially when exposed to daylight. These penwithites are all amorphous and isotropic though the brown penwithite alone shows some effects of devitrification, resulting in a fibrous or scaly mineral which may probably be a kind of bementite.

Penwithite is usually deposited from a mineralizing solution of a very late stage, but sometimes it is found as an alteration product of tephroite and alleghanyite (Pl. LII (XVII), Fig. 5).

Thin films of brown penwithite are found frequently intercalated in the cleavage-planes or partings of a manganhedenbergite crystal which shows consequently inner reflections of light similar to those of bastite or tiger-eye. In a few drusy cavities rarely found in a vein of black penwithite were observed peculiar surface markings characteristic of an amorphous mineral. Such are shown in Pl. LIV (XIX), Fig. 2.

The chemical composition along with some physical constants of the three varieties of penwithite are compared in Table 108.

TABLE 108. Physical constants and chemical composition of penwithites.

		I.	II.	III.
Hardness:	H	6	4	2-3
Sp. gr.	d_4^{16}	2.24	2.44	2.02
Refringence	n_D	1.450±	1.548-1.569	1.492-1.569

TABLE 108. (*Continued*)

	I.	II.	III.
	wt. %		
SiO_2	83.06	36.50	27.28
TiO_2	—	—	—
Al_2O_3	1.02	1.07	0.82
Fe_2O_3	0.99	1.47	2.78
MnO	4.35	36.85	24.38
CaO	—	—	3.86
MgO	3.97	6.02	5.68
H_2O^+	5.37	11.87	14.90
H_2O^-	2.96	6.72	9.89
	101.72	100.50	99.84(1)

I. Opaline penwithite. II. Brown penwithite. III. Black penwithite.

(f) Soapstone.

In drusy cavities of a rock-crystal vein was found a considerable quantity of soapstone. It is a soft clayey mineral, yielding white powders if dehydrated with absolute alcohol. It is white or grey when fresh but gradually changes to brownish-black if exposed in the air. It is very greasy to the touch and is used for a cleanser.

The results of chemical analysis, presented in Table 109, correspond closely to those previously reported of soapstone. There were no decisive data to account for the origin of the magnesia embodied in this mineral. It requires further research to determine whether it was primary or derived from the wall rock by assimilation.

TABLE 109. Analysis of soapstone dried in the air.

wt. %		mol. %	
SiO_2	51.81	$H_4Mg_4Si_5O_{15}$	92.3
TiO_2	—	$H_4Mn_4Si_5O_{15}$	4.2
Al_2O_3	0.18	$H_4Ca_4Si_5O_{15}$	3.5
Fe_2O_3	1.14		(100.0)
MnO	1.94		
CaO	1.29	H_2SiO_3 Excess	3
MgO	24.53	$(Na, K)_2SiO_3$	2
Na_2O	0.73		
K_2O	0.21		
H_2O^+	6.22		
H_2O^-	12.47		
	100.52		

(1) Including 0.25% active oxygen.

CHAPTER XVIII

MISCELLANEOUS MINERALS

(a) Apatite.
(b) Scapolite.
(c) Tourmaline.
(d) Zircon.
(e) Epidote.
(f) Titanite.
(g) Black substances.
(h) Alleghanyite.
(i) Andalusite.
(j) Allanite.
(k) Cordierite.

Various minerals which have not been described in the preceding sections are included here. Some of them have not been thoroughly investigated owing to the lack of satisfactory specimens.

As they possess no genetical relationship to each other, it is only a matter of convenience that they are arranged after the sequence of mineralization in Table 110 below.

TABLE 110. Miscellaneous minerals.

Mineral.	Period.	Occurrence.
Apatite		In various metadiabases.
Scapolite		In a scapolite salite aplite.
Tourmaline		In hornfelses.
Zircon		In hornfelses.
Epidote	A_1	In albite veinlets.
Titanite	A_3(?)	As xenocrysts in the products of B_2 period.
Black substances	A_3-B_3	Widespread as black pigments.
Alleghanyite	B_2-B_3	As a constituent of the *Azuki*-ore.
Andalusite	B_3	In a contact-metamorphosed *Tetuban*.
Allanite	B_2	In a mineralized wall rock or in rhodonite veins.
		In a manganactinolite vein.
Cordierite	C_1	In hornfelses presumably related to the intrusion of a granitic rock.

(a) Apatite.

Apatite is one of the characteristic ingredients of basic igneous rocks found in the vicinity of the Kaso mine. It is contained abundantly and is always left unaffected by alterations of various stages.

(b) Scapolite.

Scapolite occurs as prismatic crystals with good tetragonal cleavages. No measurable crystals were obtained (Pl. LIII (XVIII), Fig. 3). It is the chief constituent of the scapolite salite aplite, including small crystals of green salite abundantly (cf. Chap. III, c).

Optical constants of the scapolite were measured as follows;

$$\begin{aligned} \epsilon_D &= 1.556 \\ \omega_D &= 1.572 \\ \epsilon-\omega &= -0.016 \\ \omega_F-\omega_C &= 0.011 \end{aligned}$$

Optically uniaxial and negative. Indices of refraction correspond to the composition of $Ma_{40}Me_{60}$[1]. Of the scapolite of later mineralization forming a monomineralic vein the following optical constants were measured:—

$$\epsilon_D = 1.548 \qquad \epsilon-\omega = -0.010$$
$$\omega_D = 1.558 \qquad \omega_F-\omega_C = 0.012$$

They correspond to the composition of $Ma_{60}Me_{40}$. The scapolite experienced an evolution from $Ma_{40}Me_{60}$ to $Ma_{60}ME_{40}$, i.e., from a calcic scapolite to a sodic one quite in a similar manner with the evolution of the plagioclase feldspar.

Some of the scapolites of later crystallization have undergone hydrothermal alterations which have converted them into plagioclase or zeolite (cf. Chap. XVII, a).

Feldspathization of scapolite was observed in some part of a scapolite salite aplite where a considerable quantity of calcite was found associated. This alteration may probably be a kind of autometamorphism which would be caused by a reaction as expressed by the equation:

$$\underset{\text{(scapolite)}}{Ca_4Al_6Si_6O_{25}} + CO_2 = \underset{\text{(anorthite)}}{3CaAl_2Si_2O_8} + \underset{\text{(calcite)}}{CaCO_3}.$$

(1) After A. N. WINCHELL: Elements of Optical Mineralogy, Part II, (1927) p. 346.

(c) Tourmaline.

Tourmaline is found as minute brown crystals in hornfelses. This mineral may probably have no genetical relationship to the manganese deposit.

(d) Zircon.

Zircon is found sparingly as minute crystals in a contact-metamorphosed wall rock, surrounded by characteristic pleochroic haloes similar to those observed around allanite crystals.

(e) Epidote.

Epidote is found sparingly in an albite veinlet (cf. Chap. XI, g). Light yellowish-green, with weak pleochroism. High indices of refraction and abnormal bluish-indigo interference colour are characteristic of this mineral. It is presumably an alteration product of hornfels-biotite, embodying in it the rare elements left unincorporated after the recrystallization of biotite. It is also surrounded by pleochroic haloes when embedded in a biotite crystal.

(f) Titanite.

Titanite was found as crystals surrounded by Fe-Ti-ore showing a corona-structure (Pl. LIV (XIX), Fig. 3). This mineral seems to occur not infrequently in metamorphosed basic igneous rocks, but no numerical constants were obtained to identify it.

(g) Black substances.

Black substances are seen frequently in the manganese deposit. *Tetuban*, one of the altered wall rocks, is the most characteristic black rock rich in black substances mentioned here. Black pigments of the *Tetuban* were proved to consist mainly of fine-grained pyrrhotite or some other sulphide of iron. Rhodochrosite ore stained black by these black substances is also found abundantly, being termed as a black *Azuki*-ore in this report.

It is an interesting fact that the black *Azuki*-ore has been produced usually in later stages than the other variegated *Azuki*-ore. Fragments of the pink Azuki-ore proper are seen cemented by the later black *Azuki*-ore as shown in Pl. LIII (XVIII), Fig. 2.

The nature of these black substances has not been wholly made out. Low-grade graphite ore deposited abundantly along fractured zones in the Palaeozoic formations of Japan, may possibly be related to such black substances mentioned here.

Fragments of an albite quartz veinlet contained in a fractured black *Tetuban* are presented in Pl. LIV (XIX), Fig. 1. In this figure is shown how densely and homogeneously the black substances are distributed in the *Tetuban* and, moreover, how the segregation of these substances is facilitated by the fracturing of the rock.

Although these black substances were found widespread and abundantly, no satisfactory material was available for a chemical analysis. Two incomplete analyses were made on impure materials with the results given in Table 111.

TABLE 111. Composition of black substances.

	I.	II.
Fe_2O_3	60.3	11.9
FeS	7.2	68.3
Mn_2O_3	6.8	19.8
Insoluble	20.4	—
	94.7	(100.0)

I. The black residue which was left after the dissolution of the black *Azuki*-ore in dilute nitric acid. The insoluble material in this table consists chiefly of graphitic carbonaceous substance left after the treatment of the specimen with hydrochloric acid. Sulphur was determined on a separate material.

II. The black substance found as impurities in a black hyalophane B. Recalculated from the analysis given in Table 45, I.

(h) Alleghanyite.

Alleghanyite occurs as tiny crystals disseminated through the main carbonate ore. It is practically impossible to distinguish alleghanyite from the iron-poor tephroite if the former lacks its characteristic twinning.

At the end of period B_2 the mineralization proceeded, resulting in a gradual transition from tephroite to alleghanyite which might be expressed by the following scheme;

$$\underset{\text{(tephroite)}}{Mn_2SiO_4} \rightarrow \underset{\text{(alleghanyite)}}{Mn(OH)_2 . Mn_2SiO_4}$$

Alabandite is the most important mineral occurring closely associated with alleghanyite.

Alleghanyite is found most abundantly in the grey *Azuki*-ore (cf. Chap. V, a). The change of such bluish-grey ore into a brown ore is chiefly due to the alteration of alleghanyite into brown penwithite.

Satisfactory material of alleghanyite for chemical analysis was not obtainable owing to the small size of the crystals and to the unseparable impurities. The reader is referred to the analysis of the bluish-grey *Azuki*-ore given in Table 6, p. 331, as it is suggestive of the composition of alleghanyite. The fluorine-content of alleghanyite was carefully sought, but unsuccessfully.

Polysynthetic twinning is frequently seen (Pl. LIV (XIX), Figs. 5 and 6). The optic orientations of this mineral are quite distinct from those of tephroite as shown in Fig. 13.

In this figure is shown the optic orientation of elongated sections perpendicular to the obtuse bisectrix for polysynthetic twins of alleghanyite. If the principal cleavage be taken as (001), which is also parallel to the twinning-plane, the orientation is Z = b, c ∧ Y = 27°, c ∧ X = 63°.

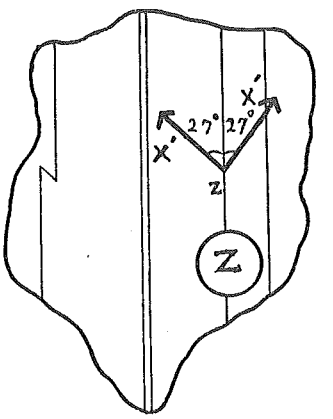

Fig. 13. Optic orientation of alleghanyite.

Sections parallel to 001 show high interference-tints and possess straight extinction with reference to the subordinate cleavages on (010) and (100). Remarkably oblique extinction against traces of the dominant cleavage-plane gives a triclinic appearance to alleghanyite crystals in a thin slice.

The physical properties observed are compared in Table 112 with those previously reported of the alleghanyite from Alleghany[1].

(1) C. S. Ross and P. F. Kerr: Am. Min., **17** 1 (1932).
A. F. Rogers: Am. Min., **20** 25 (1935).

TABLE 112. Comparison of the physical properties of alleghanyites.

Locality	Alleghany	Kaso mine
Colour	Pink	Grey or greyish-brown
Pleochroism	Weak	none
Sp. gr.	4.02	n.d.
X^X′ on twinned crystals	44°–70°	54°
α	1.756	1.740
β	1.780	1.758
γ	1.792	1.768
γ-α	0.036	0.028
(—) 2V	72°	75°

(i) Andalusite.

Only minute embryonic crystals of andalusite were found in a contact-metamorphosed *Tetuban*. Segregation of black substances around the new-formed crystal is manifest in Pl. LIV (XIX), Fig. 4. Numerous black spots of similar character are shown in Pl. LII (XVII), Fig. 2.

(j) Allanite.

A strongly pleochroic mineral of the epidote group is found associated with hexagonal platy crystals of Fe-Ti-ore. Zonal structure is common, the central part being always deeper-coloured and more strongly pleochroic. An example of such a crystal is shown in Pl. LIII (XVIII), Fig. 4.

X ..... colourless to brownish-pink,
Y ..... brownish-red to greenish-brown,
Z ..... dark-brown to nearly opaque.
$Z \gg Y \gg X$.
Optically negative, (−)2V moderate.
Dispersion strong. Birefringence, about 0.03.
Optic axial plane is normal to (010).
$Z = b$. This is an unusual optical orientation rarely reported of a mineral of the epidote group.

(k) Cordierite.

Cordierite occurs widespread in the argillaceous country rocks as porphyroblasts due to the contact-metamorphism which may probably be related to the intrusion of a large batholith of porphyritic

granite. The distribution of cordierite spots is irregular and restricted. Those found near the very contact-zone of the granite are generally larger in size.

As shown in Pl. LIII (XVIII), Fig. 1, such cordierite porphyroblast has no distinct crystal outlines, although it consists of a single crystal. The extinction of light under the microscope is neat and homogeneous.

An isotropic rim developed on the margin of the cordierite porphyroblast may be worthy of notice. Another ring-shaped outermost zone consisting of greenish-brown chloritic mineral is also noteworthy. Stepwise alteration from biotite to cordierite has probably taken place as follows:

Biotite → Chlorite → Isotropic mineral → Cordierite.

Refractive indices determined of these minerals are given below.

Central anisotropic portion.

$\alpha = 1.545$
$\beta = 1.551$
$\gamma = 1.554$
$\gamma - \alpha = 0.009.$

Peripherial isotropic portion

$n_D = 1.548.$

The genetical relation of the cordierite with the biotite has already been described in some detail in a preceding section (cf. Chap. III, b).

Pseudohexagonal twinnings of cordierite, noted as "cerasite", have been described by Y. KIKUCHI[1] on specimens collected from contact-metamorphosed slate in the adjacent valley north of the Kaso mine. In the vicinity of the Kaso mine they are found only in xenoliths of the hornfels captured in a quartz vein. Cordierite spots formed by the simple thermal metamorphism consist, without exception, of these anhedral crystals mentioned above.

Acknowledgments.—The author is greatly indebted for their cordial co-operation to Mr. E. IMAI, the owner of the Kaso mine, and to Mr. S. AKIYAMA, the mine manager, whose personal courtesies added to the comforts of the work, and also to Prof. Z. HARADA and Prof. J. SUZUKI for their advice and suggestions.

(1) Y. KIKUCHI: Journ. Coll. Sci. Tōkyō Imp. Univ., Vol. 3, (1889).

EXPLANATION OF THE PLATES

Plate XXXVI (I)

Fig. 1. Octahedral cleavage pieces of slate. × ½.

Fig. 2. Pyramidal crystals of Fe-Ti-ore in *Azuki*-ore.
Parallel nicols, × 150.

Fig. 3. Pyramidal crystals of Fe-Ti-ore embedded in a blood-red rhodonite crystal.
Parallel nicols, × 230.

Fig. 4. Alabandite crystals (black), replacement by rhodochrosite being in process.
Parallel nicols, × 45.

Fig. 5. Porphyritic metadiabase. Skeletal crystals of ilmenite and strongly altered idiomorphic phenocrysts of common hornblende embedded in a groundmass consisting wholly of lath-shaped crystals of strikingly albitized plagioclase.
Parallel nicols, × 14.

Plate XXXVII (II)

Fig. 1. *Azukiban* (upper) in process of replacement by a hornstone vein (lower) with newly formed garnet and manganactinolite crystals (middle).
Parallel nicols, × 52.

Fig. 2. Platy crystals of Fe-Ti-ore in a hornstone vein.
Parallel nicols, × 112.

Fig. 3. Platy crystals of Fe-Ti-ore.
× 150.

Fig. 4. Ring-shaped skeletal remains of *Radiolaria* in a Radiolarian slate.
Parallel nicols, × 42.

Fig. 5. A drusy cavity with clustered aggregates of rock-crystals. Crystals twinned on Japan-law are seen in the center.
× 3.

Fig. 6. A part of Fig. 2 in Pl. XXXVIII (III), magnified.
Parallel nicols, × 135.

Plate XXXVIII (III)

Fig. 1. A pyrochroite crystal formed in an interspace between garnet crystals.
Parallel nicols, × 114.

Fig. 2. Orbicular patches which contain numerous manganosite crystals.
Parallel nicols, × 52.

Fig. 3. A polished specimen of "*Hiê*" ore, with sporadic white crystals of mangancalcite C.
× ½.

Fig. 4. Saccharoidal manganiferous calcite, mineralized in B_2 period. With some corroded crystals of manganhedenbergite.
Parallel nicols, × 52.

Fig. 5. Lenses of impregnated hornstone quartz in *Kakusekiban*.
Parallel nicols, × 40.

Plate XXXIX (IV)

Fig. 1. Semispherulitic aggregates of crystals of Ca-rhodochrosite B. Effects of grain-growth and remarkable pleochroism are shown. Intruded quartz veinlet (white) in the center.
Parallel nicols, × 52.

Fig. 2. Two crystals of mangancalcite C which are turbid owing to numerous minute inclusions.
Parallel nicols, × 31.

Fig. 3. A peculiar-shaped crystal of relict mangancalcite D, embedded in newly formed pink rhodochrosite.
Parallel nicols, × 40.

Fig. 4. The same as Fig. 3 rotated 90 degrees in order to show the strong pleochroism.
Parallel nicols, × 40.

Plate XL (V)

Fig. 1. Ca-rhodochrosite B (dark) in process of replacing pink rhodonite (white).
Parallel nicols, × 47.

Fig. 2. Fibrous radiating crystals of pink rhodochrosite.
Natural size.

Fig. 3. A large crystal of hyalophane B (white) with numerous patches of black substance.
Parallel nicols, × 114.

Fig. 4. A large zoned crystal of barium-containing alkalifeldspar. Relict crystals of ironrhodonite (isolated) and a veinlet of new-formed carmine-red rhodonite are seen enclosed.
Parallel nicols, × 42.

Fig. 5. The same as Fig. 4. Introduced alkalifeldspar is seen as a net-work traversing both hyalophane (inner zone) and kasoite (outer zone). The parallel optical orientation of hyalophane to that of alkalifeldspar is worthy of note.
Crossed nicols, × 38.

Plate XLI (VI)

Fig. 1. A piece of exceedingly hyalophanized wall rock in process of replacement by a hornstone vein. It appears dark in this figure owing to numerous minute inclusions of Fe-Ti-ore.
Parallel nicols, × 12.

Fig. 2. Crystals of hyalophane C embedded in a pink rhodochrosite hornstone vein.
Parallel nicols, × 60.

Fig. 3. Kasoite veinlets and some kasoite rhodonite veins traversing *Azuki-ban*. A polished surface.
Nat. size.

Fig. 4. Fine-grained aggregate of hyalophane C (middle) penetrated by a quartz vein (right). Note the contrast of birefringenses of quartz and hyalophane. The upper and lower portions are mixtures of these two minerals.
Crossed nicols, × 12.

Fig. 5. Crystals of hyalophane A in a mangantremolite rhodonite vein.
Parallel nicols, × 18.

Plate XLII (VII)

Fig. 1. Idiomorphic crystals of kasoite embedded in a fine-grained aggregate of ironrhodonite.
Parallel nicols, × 110.

Fig. 2. Crystals of celsian A, embedded in a picroknebelite mass.
Parallel nicols, × 150.

Fig. 3. Photomicrograph of a thin slice of *Tetuban* with numerous impregnated crystals of kasoite.
Parallel nicols, × 42.

Plate XLIII (VIII)

Fig. 1. Garnet crystals in a contact-metamorphosed *Tetuban* traversed by a kasoite vein (right, upper; white). Crystals enclosed in the kasoite vein are seen clarified adjoining the unclarified portions with sharp junctions.
Parallel nicols, × 42.

Fig. 2. Numerous veinlets of albite intruding into biotite-garnet-hornfels.
Parallel nicols, × 42.

Fig. 3. A zoned crystal of garnet. Uninterrupted continuation of the distribution of black inclusions in both the outer zone and the matrix are worthy of notice.
Parallel nicols, × 18.

Fig. 4. Corroded crystals of greyish-yellow garnet in feldspathic *Azukiban* disseminated with numerous white spots of kasoite.
Parallel nicols, × 42.

Fig. 5. Celsian B (white) in process of replacing picroknebelite crystals (grey).
Parallel nicols, × 20.

Fig. 6. Fine crystals of greyish-yellow garnet found as a relict mineral in a carbonate *Azukiban*.
Parallel nicols, × 42.

Plate XLIV (IX)

Fig. 1. Zonal structure of red garnet markedly replaced by rhodochrosite ores.
Crossed nicols, × 38.

Fig. 2. *Azukiban* (right) with embryonic crystals of new-formed garnet, a hornstone vein (middle) and a rhodonite vein (left).
Parallel nicols, × 42.

Fig. 3. Exceedingly garnetized *Azukiban*.
Parallel nicols, × 42.

Fig. 4. Crystals of ironknebelite enclosed in a garnet rhodonite vein.
Parallel nicols, × 11.

Fig. 5. Garnet crystals with black core.
Parallel nicols, × 40.

Fig. 6. Garnetfels of advanced stage of garnetization. The grain-growth of garnet and the complete recrystallization of matrix differ from those in the case shown in Fig. 5.
Parallel nicols, × 42.

Plate XLV (X)

Fig. 1. Contact-metamorphosed carbonate ore of A_3 period. First carbonate ore, early member. Granular crystals of knebelite (grey) and skeletal growths of marmatite (black) are seen in a saccharoidal carbonate mass.
Parallel nicols, × 42.

Fig. 2. A part of picroknebelite vein.
Parallel nicols, × 12.

Fig. 3. Fragment of a large crystal of picroknebelite. (cleavage planes illuminated)
Nat. size.

Fig. 4. A crystal of irontephroite (grey) with exceptionally distinct cleavage traces. Somewhat altered into penwithite (black).
Parallel nicols, × 64.

Fig. 5. A polished surface of a contact-zone.
Right: *Azuki*-ore with black patches of alabandite (c).
Middle { Right zone: Demanganized white mangancalcite (d).
Left zone: Tephroite or irontephroite (i).
Left: Intruded rhodonite vein (p_1, p_2) with sporadic crystals of garnet (s).
× 2/3.

Fig. 6. A sketch of Fig. 5.
Notations explained in the preceding note.

Plate XLVI (XI)

Fig. 1. Two fragments of a fine-grained manganhedenbergite vein enclosed in a carbonate *Azukiban*.
Parallel nicols, × 42.

Fig. 2. A polished surface showing successive intrusions of rhodonite veins. The portion to the right is a silicified chert; the left portion is an *Azukiban* cut into two parts of which the lower half alone has been completely changed into red garnet, while the upper half has remained quite unchanged.
Nat. size.

Fig. 4. Relics of ironrhodonite largely replaced by a less ferriferous rhodonite (the latter in extinction position).
Crossed nicols, × 40.

Fig. 5. Corroded crystals of manganhedenbergite in a kasoite green-biotite rhodonite vein.
Parallel nicols, × 42.

Fig. 6. Tephroite crystals with interstitial sulphide minerals.
Parallel nicols, × 45.

Plate XLVII (XII)

Fig. 1. Poikiloblastic inclusions of quartz in a purified rhodonite crystal.
Parallel nicols, × 42.

Fig. 2. A corona structure of pink rhodonite (outer zone) and ironrhodonite (inner zone) in a garnet rhodonite quartz vein.
Parallel nicols, × 42.

Fig. 3. Fragments of ironrhodonite veins strongly altered by a mineralizing solution which has effected the formation of *Azukiban*.
Parallel nicols, × 42.

Fig. 4. Peculiar form of recrystallized rhodochrosite in a schistose quartz vein. It is found attached to a grain of iron ore.
Parallel nicols, × 110.

Fig. 5. Worm-shaped crystals of the recrystallized rhodochrosite. Relics of ferriferous rhodonite are also seen.
Parallel nicols, × 52.

Fig. 6. The same as Fig. 5, showing the schistosity of the quartz vein.
Crossed nicols, × 45.

Plate XLVIII (XIII)

Fig. 1. Filmy or ribbon-shaped inclusions in a rhodonite crystal.
Parallel nicols, × 62.

Fig. 2. The same as Fig. 1, illustrating the optical anisotropism of the inclusions.
Crossed nicols, × 56.

Fig. 3. Fibrous rhodonite crystals accompanied by abundant black substance. A colourless hornstone vein is seen in the lower portion.
Parallel nicols, × 52.

Fig. 4. The same as Fig. 3.
Crossed nicols, × 48.

Plate XLIX (XIV)

Fig. 1. Aggregate of pink rhodonite crystals.
Parallel nicols, × 54.

Fig. 2. The same as Fig. 1, illustrating twinnings.
Crossed nicols, × 48.

Fig. 3. Recrystallized rhodonite heavily contaminated with black substance. The pink belted zone is frequently mistaken for a pink rhodonite veinlet traversing the black rhodonite.
Parallel nicols, × 42.

Fig. 4. Intimately interwoven fibrous crystals of pink rhodonite.
Parallel nicols, × 31.

Fig. 5. The same as Fig. 4.
Crossed nicols, × 29.

Plate L (XV)

Fig. 1. Dannemorite crystals in a metamorphosed saccharoidal carbonate ore (first carbonate ore). Opaque spots are crystals of marmatite.
Parallel nicols, × 42.

Fig. 2. A polished specimen showing the contact-zone between *Azuki*-ore (A) and a pegmatitic quartz vein (Q).
T; tephroite, R; carmine-red rhodonite.
Nat. size.

Fig. 3. Polysynthetic twinning of carmine-red rhodonite.
Crossed nicols, × 82.

Fig. 4. A green hornblende vein traversing *Kuroboku*.
Parallel nicols, × 20.

Fig. 5. Crystals of green ironhornblende in a biotite-hornfels. Their remarkable pleochroism is illustrated.
Parallel nicols, × 42.

Plate LI (XVI)

Fig. 1. Crystals of mangantremolite.
× 8.

Fig. 2. Fragments of an ironrhodonite vein strongly altered into mangantremolite.
Parallel nicols, × 24.

Fig. 3. Quartz biotite spots in hornfels, with a later-formed cordierite spot (right, lower).
Parallel nicols, × 16.

Fig. 4. Crystals of actinolitic hornblende in a contact-metamorphosed metadiabase.
Parallel nicols, × 42.

Fig. 5. Crystals of black garnet in a manganactinolite vein.
Parallel nicols, × 12.

Plate LII (XVII)

Fig. 1. Pleochroic haloes around allanite crystals which were produced in hornfels-biotite.
Parallel nicols, × 114.

Fig. 2. Contact-metamorphosed *Tetuban* with biotite actinolite spots (grey) and andalusite spots (black). A peculiar-shaped fragment of an actinolite veinlet is seen in the center.
Parallel nicols, × 13.

Fig. 3. Peculiar spots in a contact-metamorphosed *Azukiban*. Right half shows portion which has been replaced by a hornstone vein.
Parallel nicols, × 13.

Fig. 4. The same as Fig. 3.
Crossed nicols, × 12.

Fig. 5. Brown penwithite pseudomorphous after tephroite.
Parallel nicols, × 42.

Fig. 6. Allanite crystals in a manganactinolite vein. Note the strong pleochroism and deep-coloured haloes.
Parallel nicols, × 42.

Plate LIII (XVIII)

Fig. 1. A cordierite porphyroblast.
Note the isotropic rim around it.
Crossed nicols, × 24.

Fig. 2. A polished surface of pink *Azuki*-ore proper, brecciated and cemented with black *Azuki*-ore.
Nat. size.

Fig. 3. A crystal of scapolite, cut nearly perpendicular to its c-axis, in a scapolite salite aplite.
Parallel nicols, × 42.

Fig. 4. Allanite crystals enclosed in a quartz crystal.
Parallel nicols, × 84.

Fig. 5. A pleochroic halo around an allanite crystal found embedded in a chlorite crystal.
Parallel nicols, × 160.

Fig. 6. The same as Fig. 5.
Note the remarkable birefringence of the halo.
Crossed nicols, × 150.

Plate LIV (XIX)

Fig. 1. Black *Tetuban* with a few fragments of an albite quartz veinlet. Note the segregation of black substances near the end of such a xenolith.
Parallel nicols, × 18.

Fig. 2. Orbicular surface-markings of black penwithite.
× 11.

Fig. 3. Titanite crystals surrounded by a rim of Fe-Ti-ore in a rhodonite vein.
Parallel nicols, × 115.

Fig. 4. Two minute crystals of andalusite. Note the contamination of black substances.
Parallel nicols, × 250.

Fig. 5. Crystals of alleghanyite.
Parallel nicols, × 150.

Fig. 6. The same as Fig. 5.
Note the polysynthetic twinning of alleghanyite.
Crossed nicols, × 130.

1a

1b

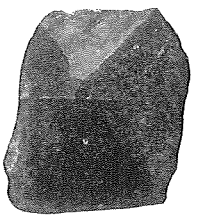

1c

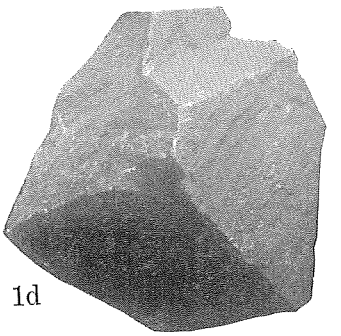

1d

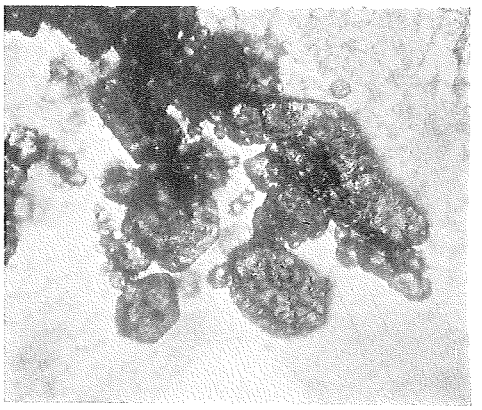

2

3

4

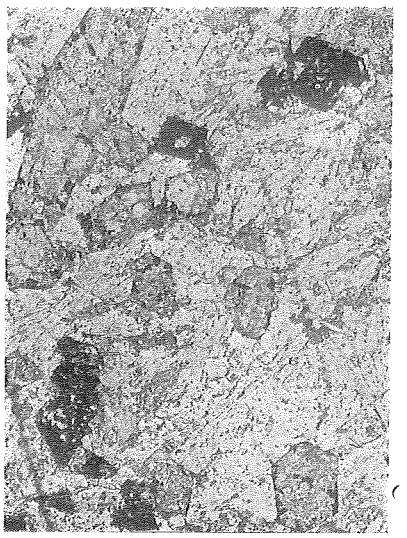

5

T. Yosimura: Minerals from the Kaso Mine.

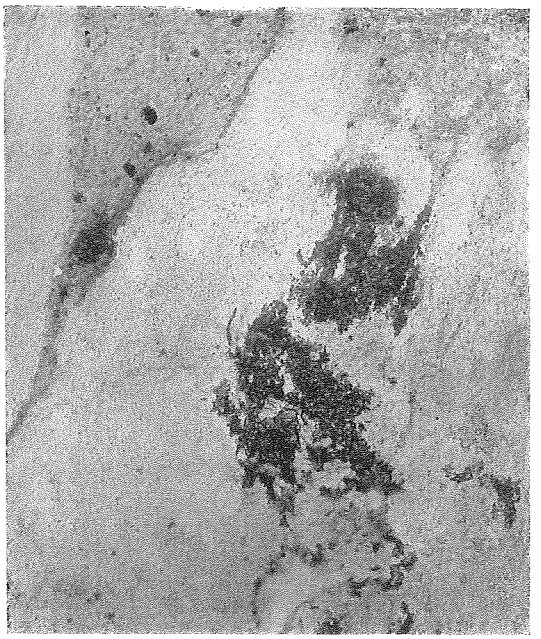

1

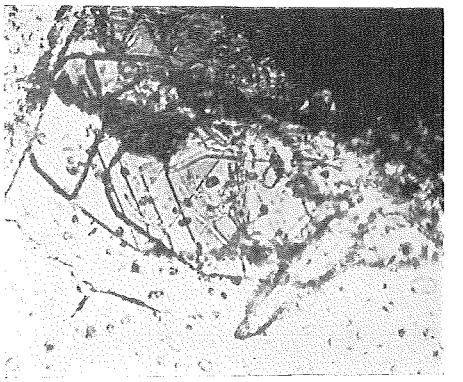

2

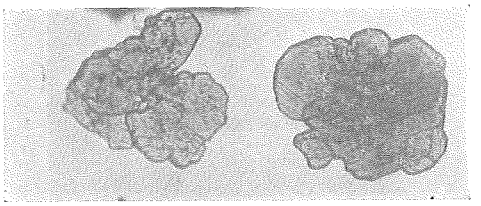

3

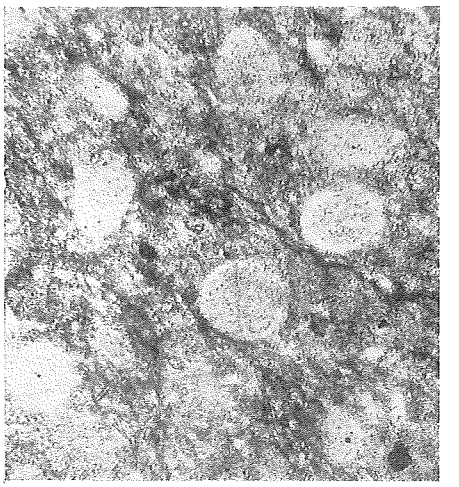

4

5

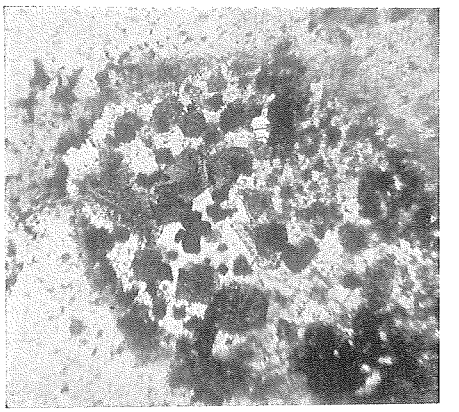

6

T. Yosimura : Minerals from the Kaso Mine.

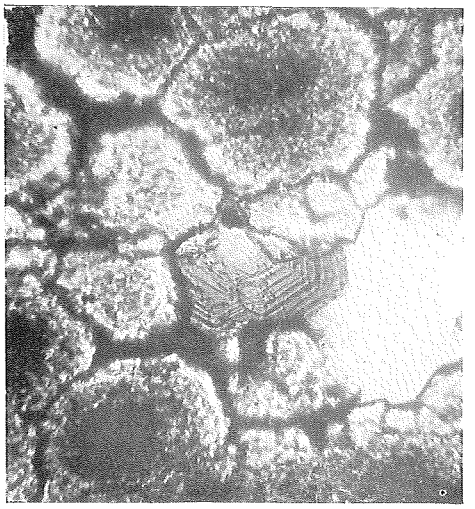

1

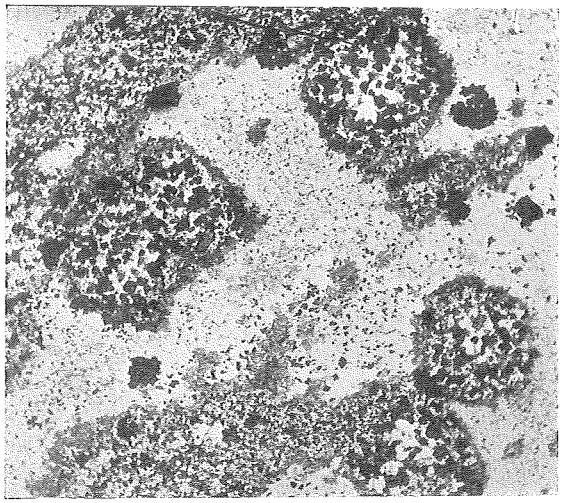

2

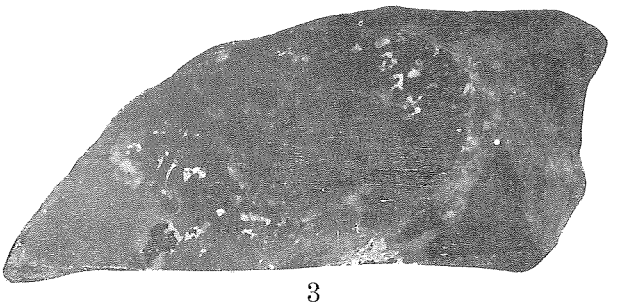

3

4

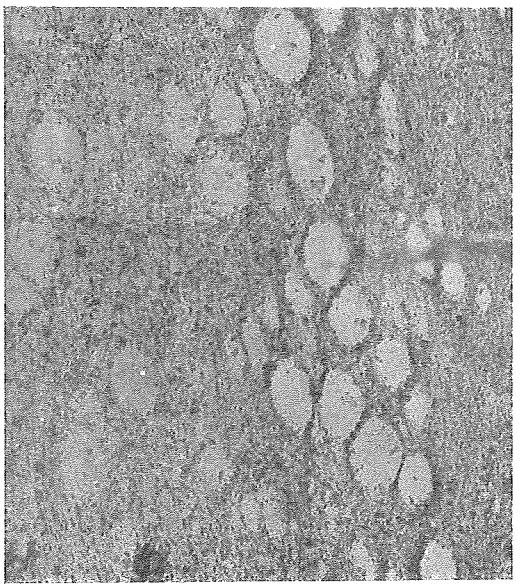

5

T. Yosimura : Minerals from the Kaso Mine.

1

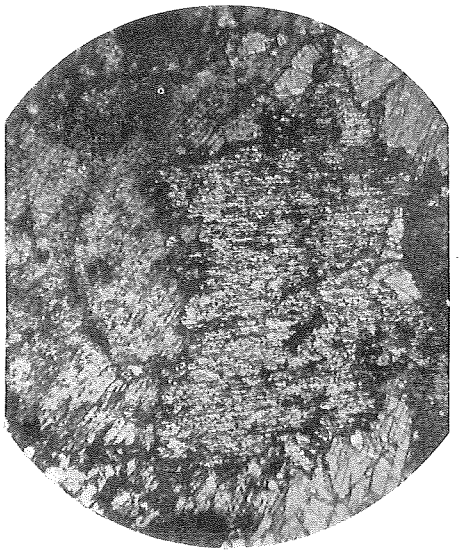

2

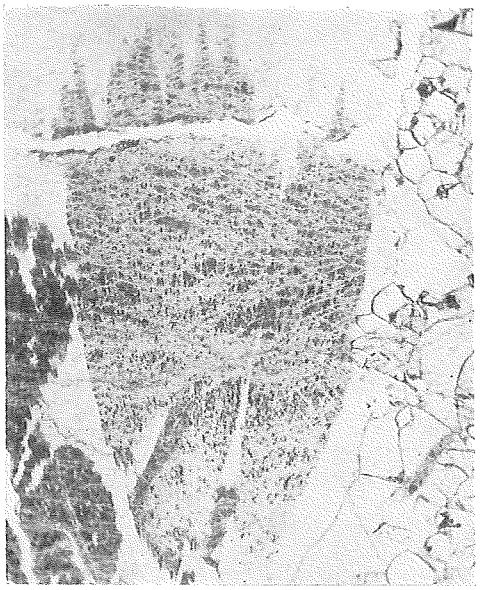

3

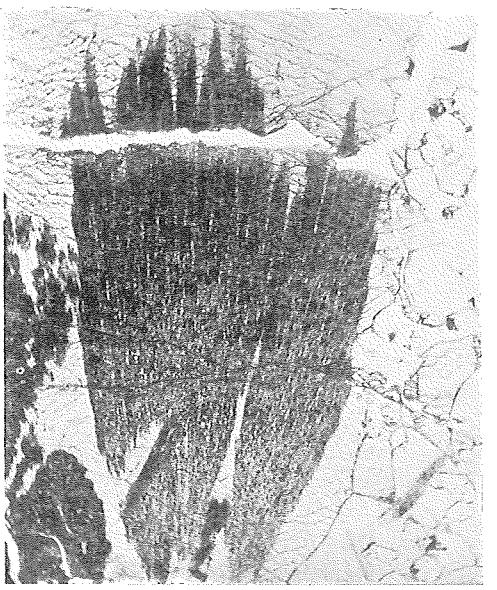

4

T. Yosimura : Minerals from the Kaso Mine.

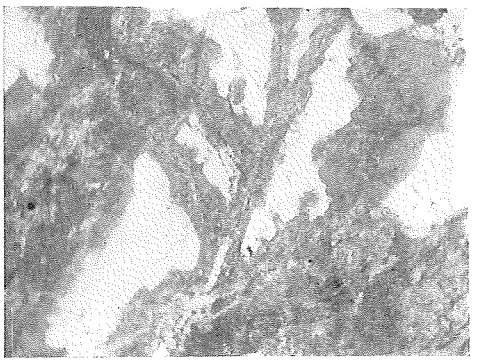

1

2

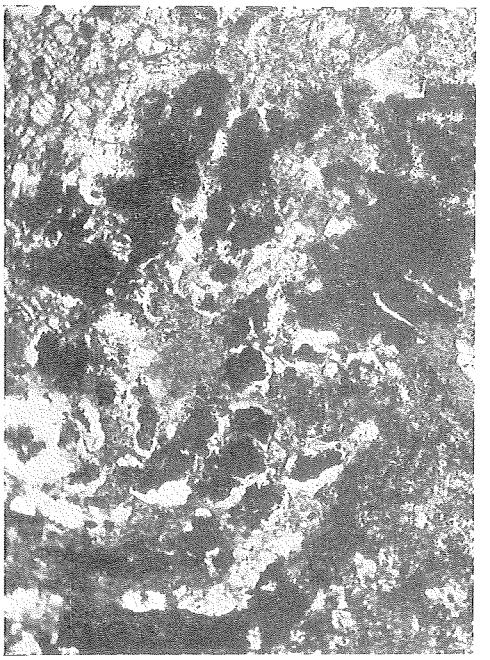

3

4

5

T. Yosimura : Minerals from the Kaso Mine.

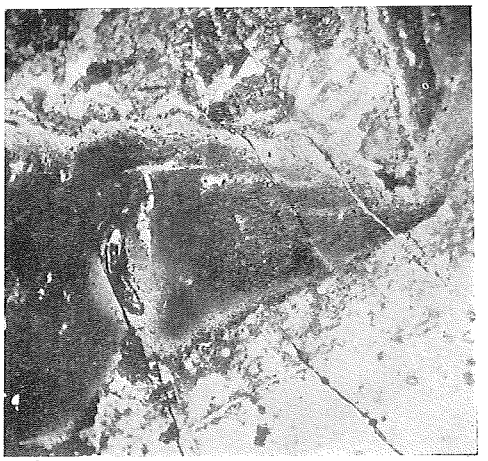

1

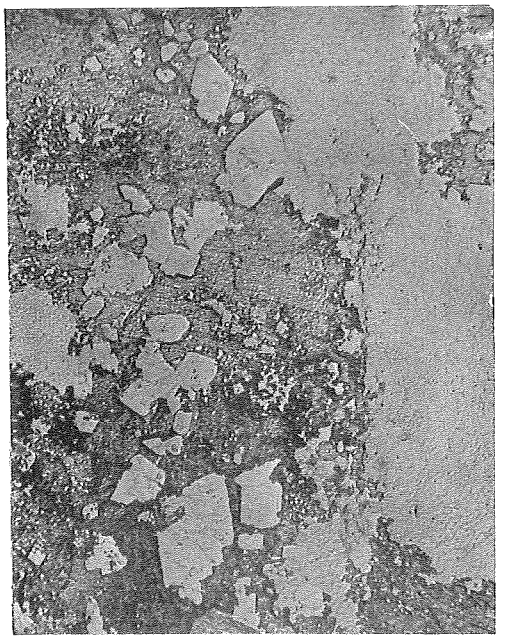

2

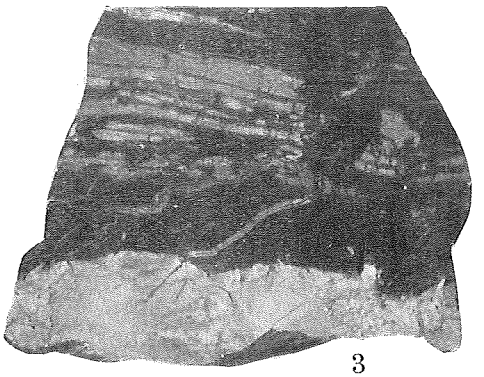

3

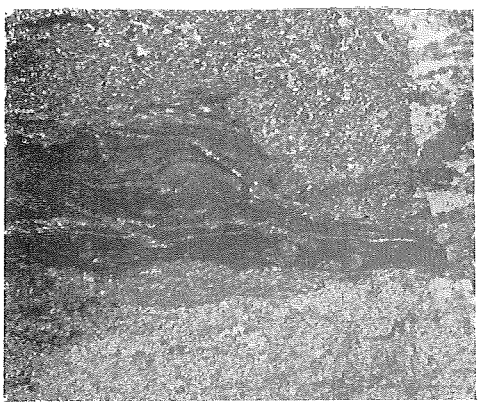

4

5

T. Yosimura : Minerals from the Kaso Mine.

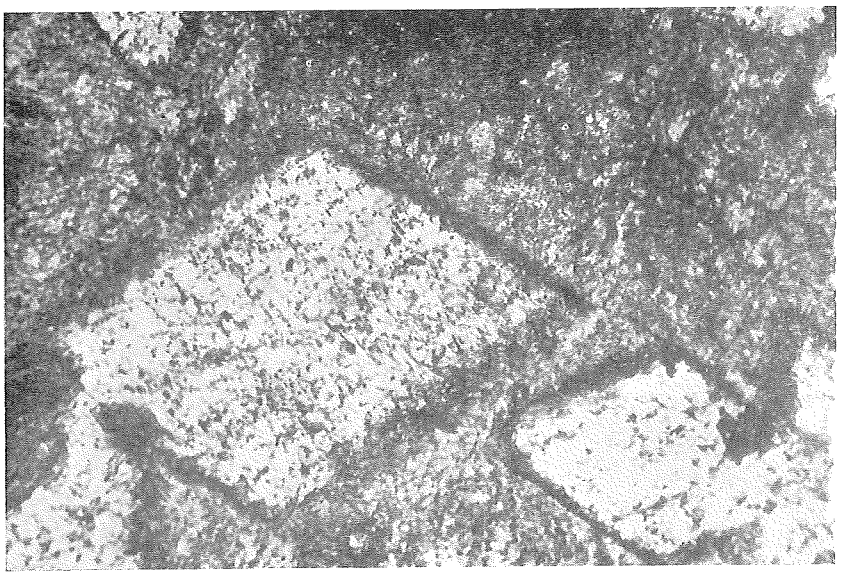

1

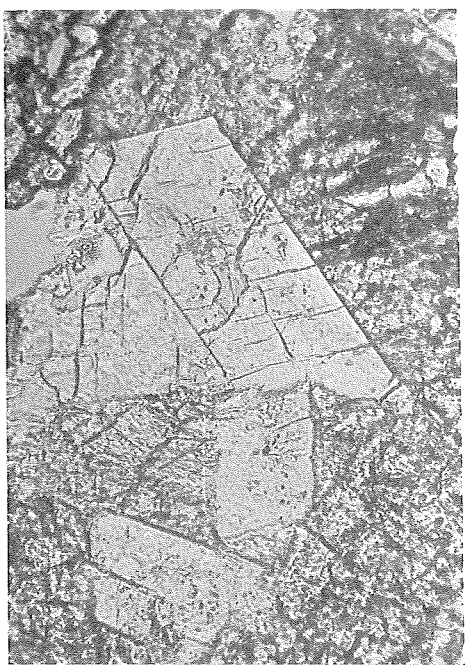

2

3

T. Yosimura : Minerals from the Kaso Mine.

1

2

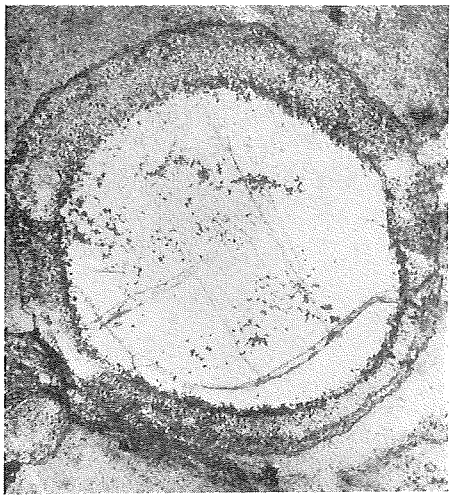

3

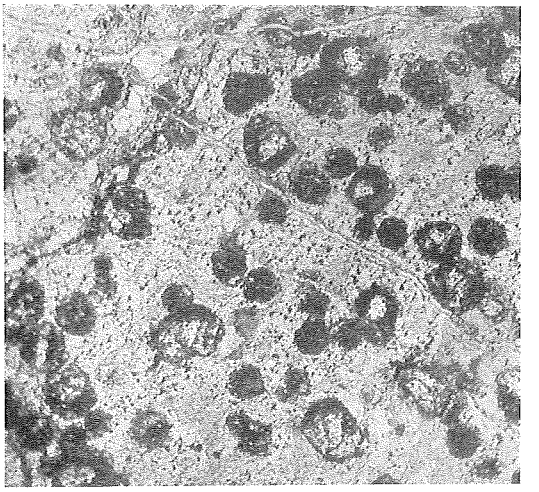

4

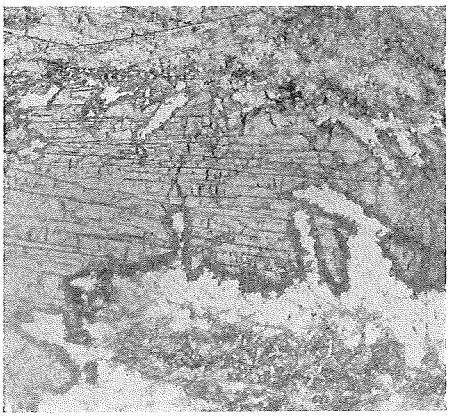

5

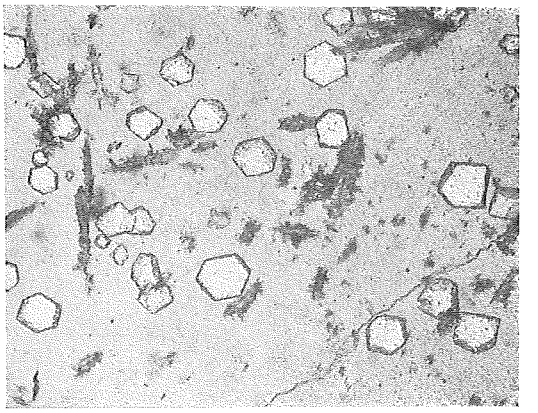

6

T. Yosimura : Minerals from the Kaso Mine.

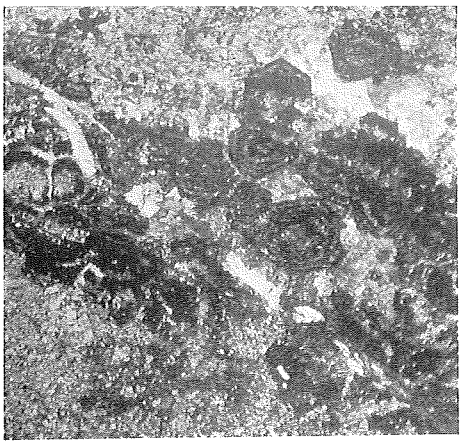

1

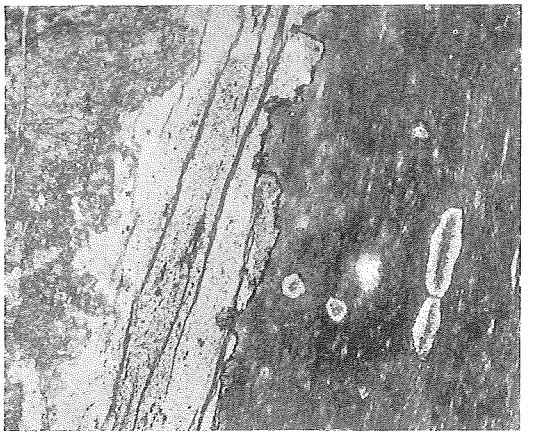

2

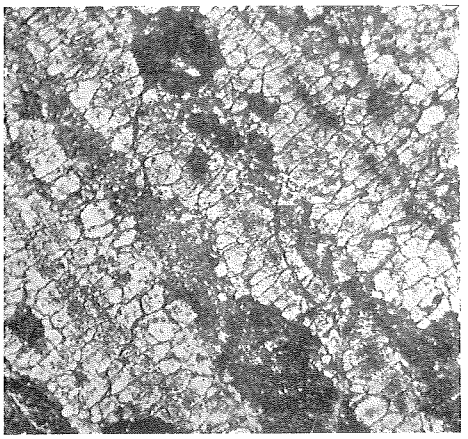

3

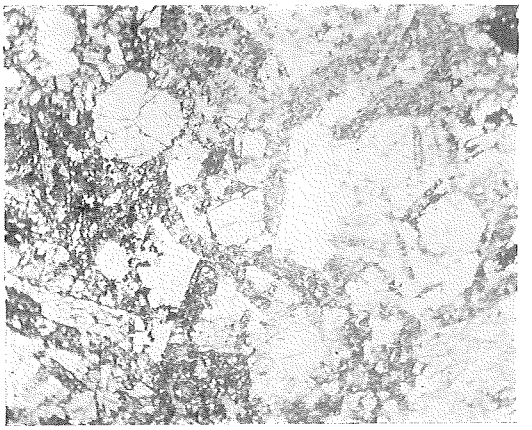

4

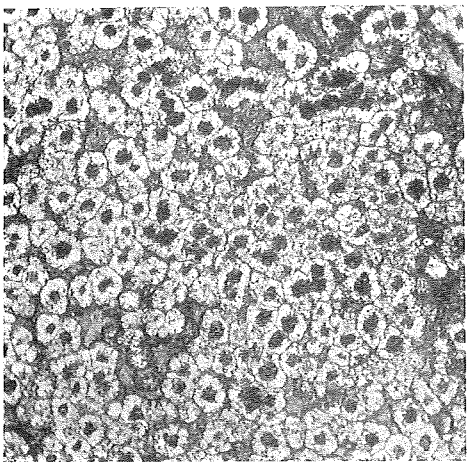

5

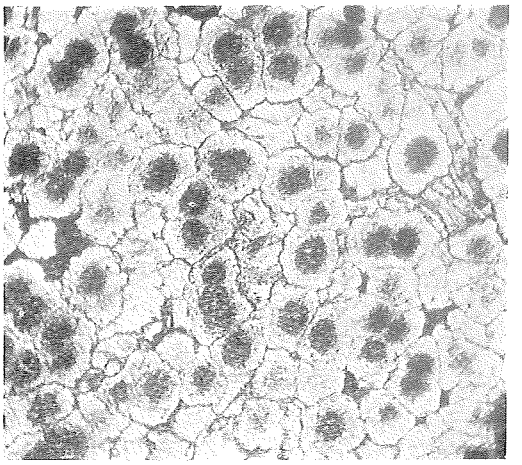

6

T. Yosimura : Minerals from the Kaso Mine.

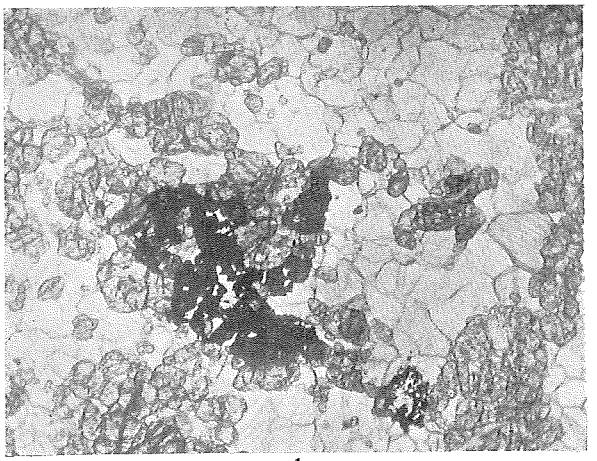

1

2

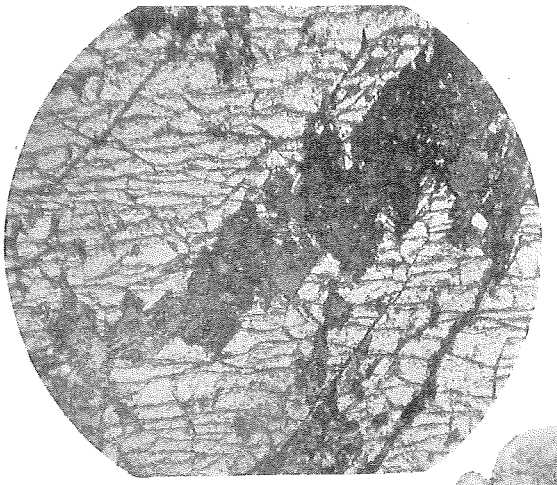

4

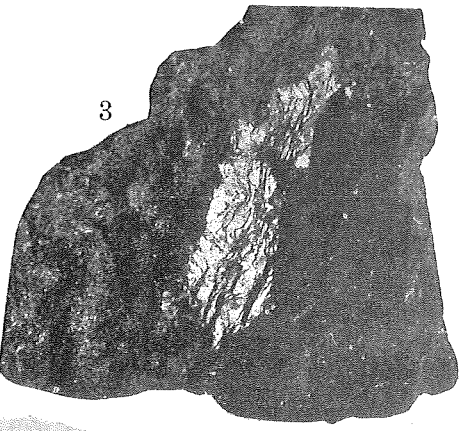

3

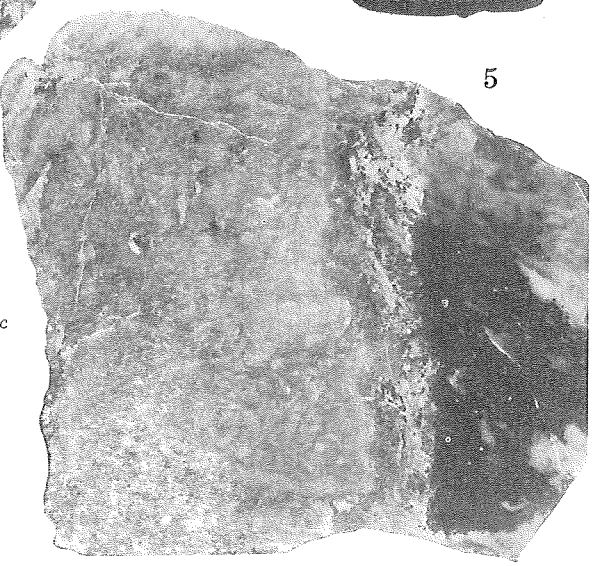

5

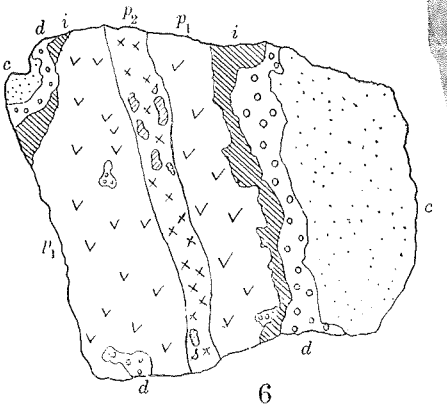

6

T. Yosimura : Minerals from the Kaso Mine.

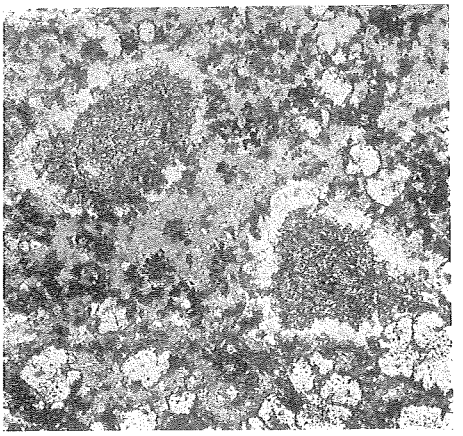

1

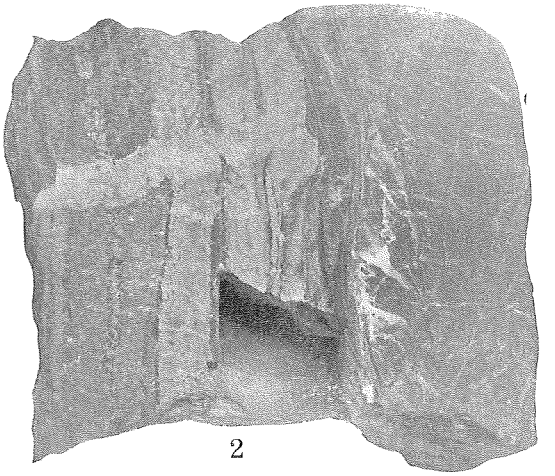

2

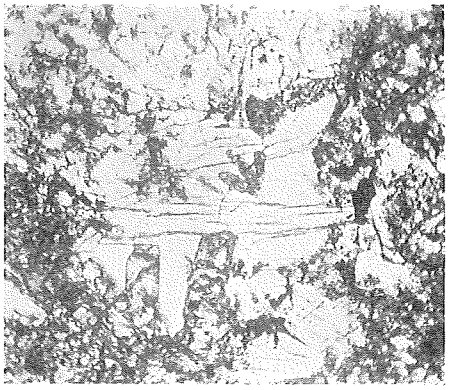

3

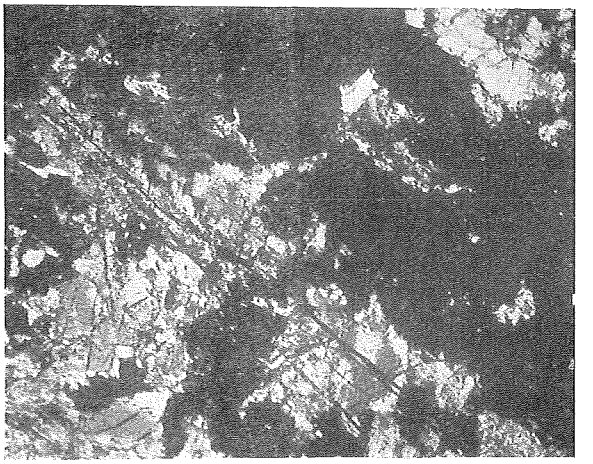

4

5

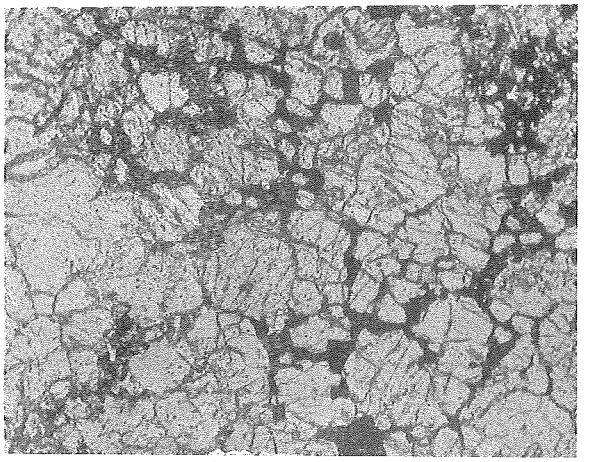

6

T. Yosimura: Minerals from the Kaso Mine.

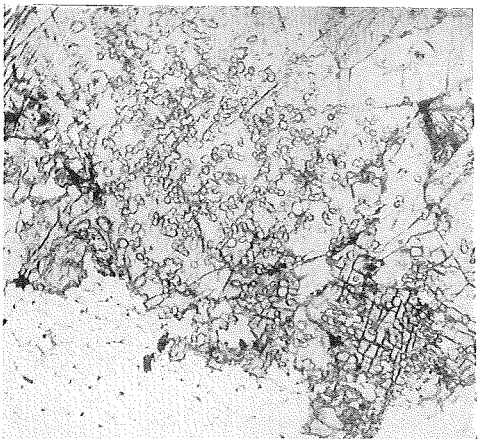

1

2

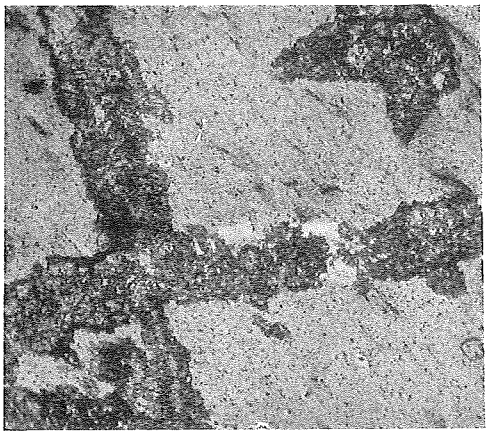

3

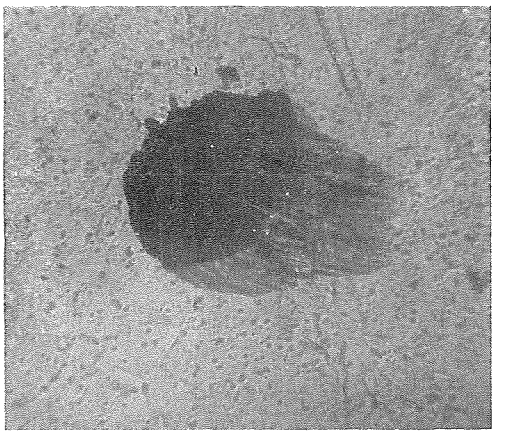

4

5

6

T. Yosimura : Minerals from the Kaso Mine.

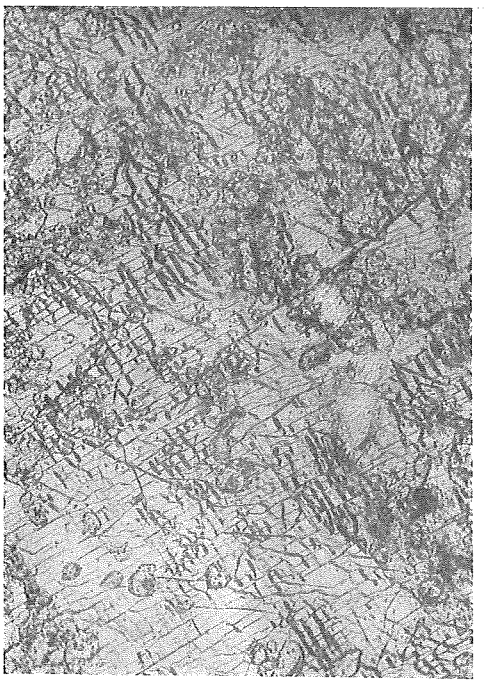

1

2

3

4

T. Yosimura : Minerals from the Kaso Mine.

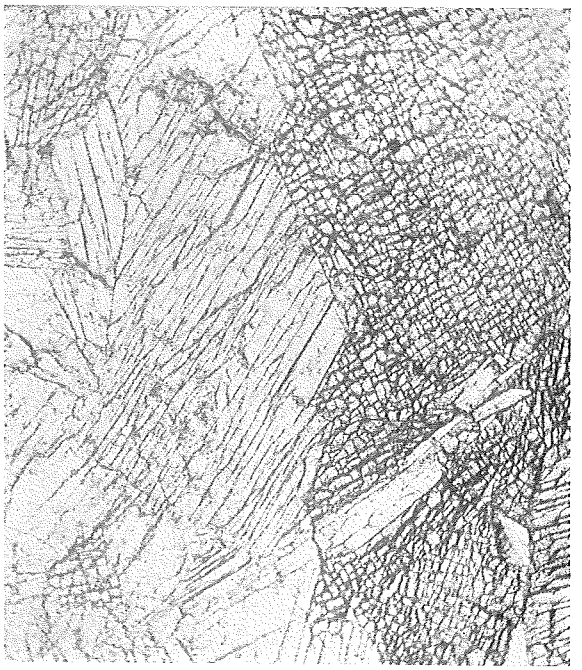

1

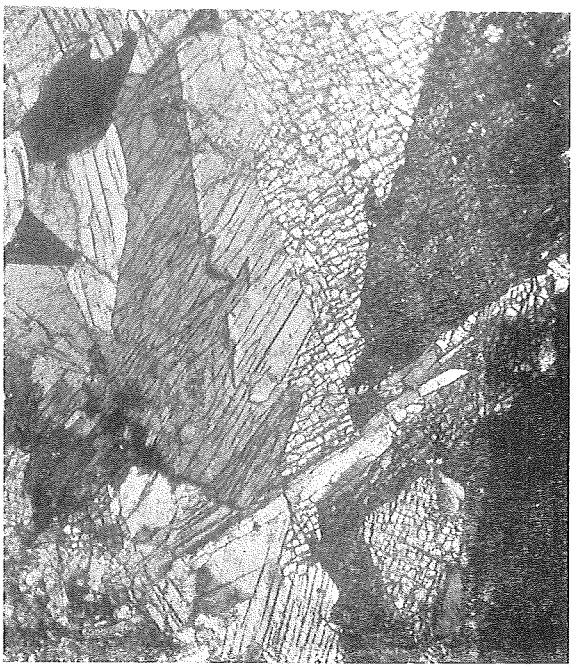

2

3

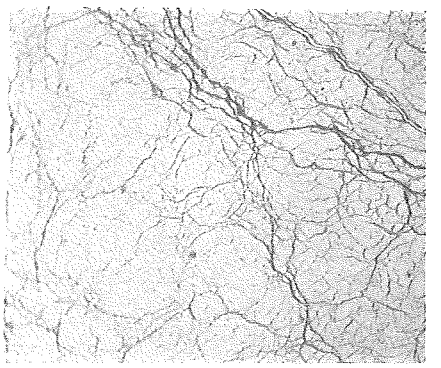

4

5

T. Yosimura : Minerals from the Kaso Mine.

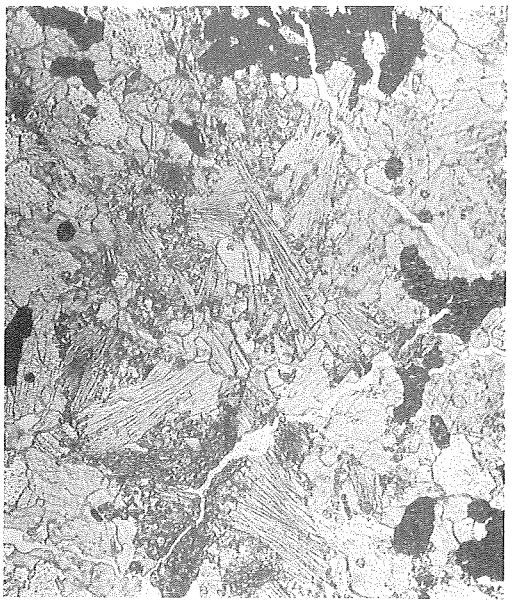

1

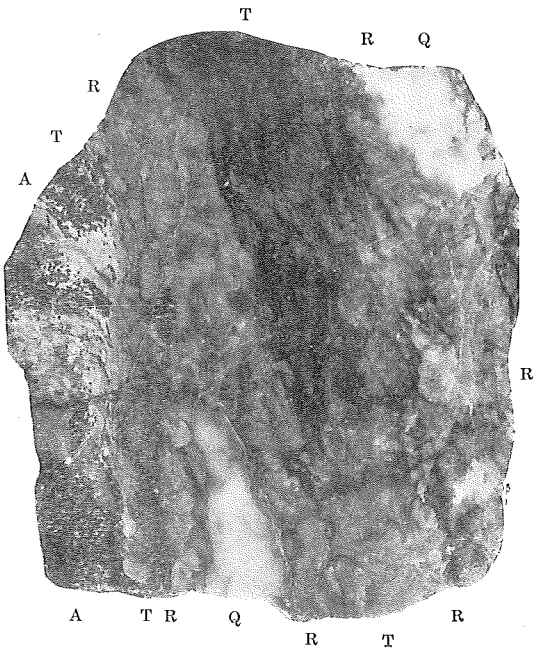

2

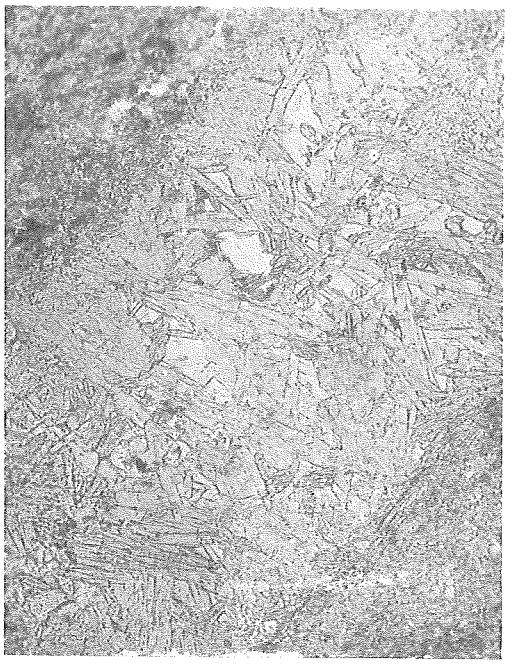

4

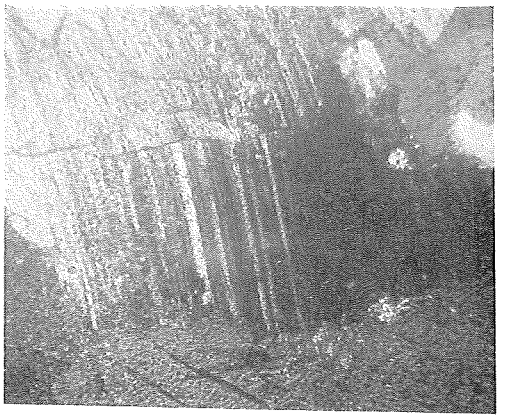

3

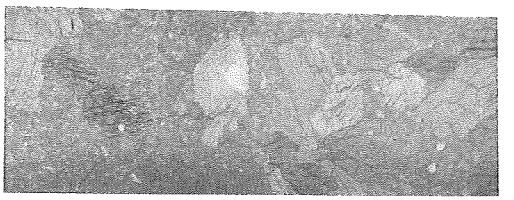

5

T. Yosimura : Minerals from the Kaso Mine.

1

2

3

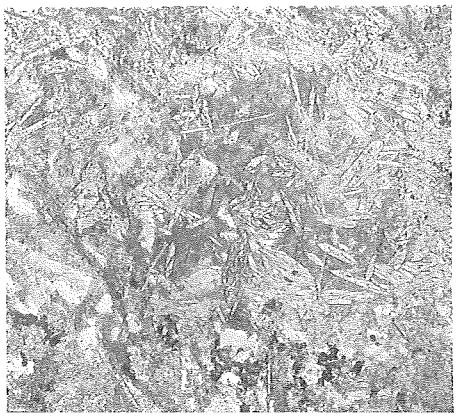

4

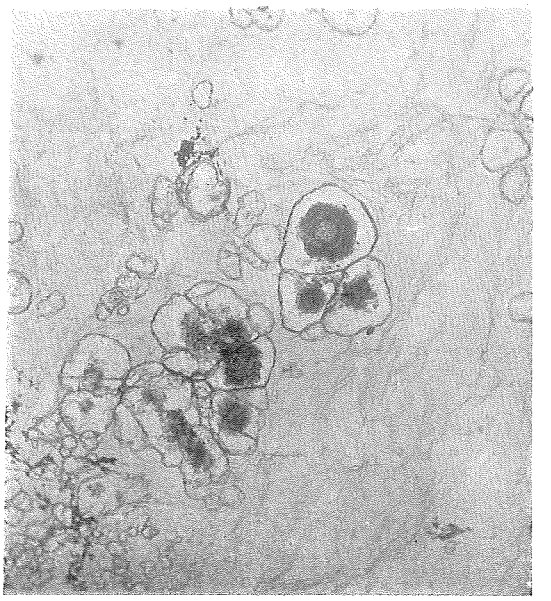

5

T. Yosimura : Minerals from the Kaso Mine.

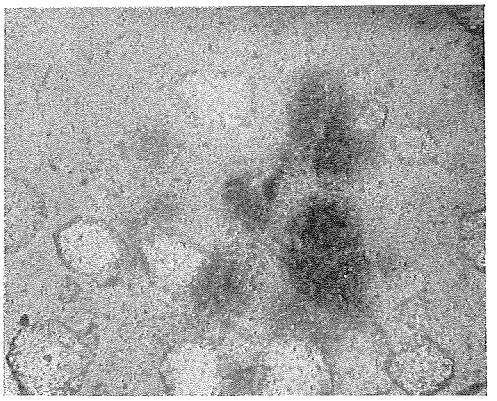

1

2

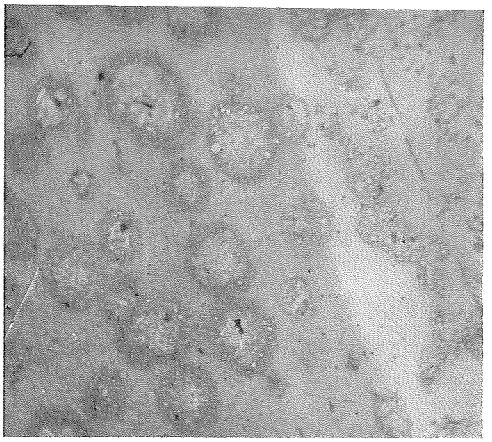

3

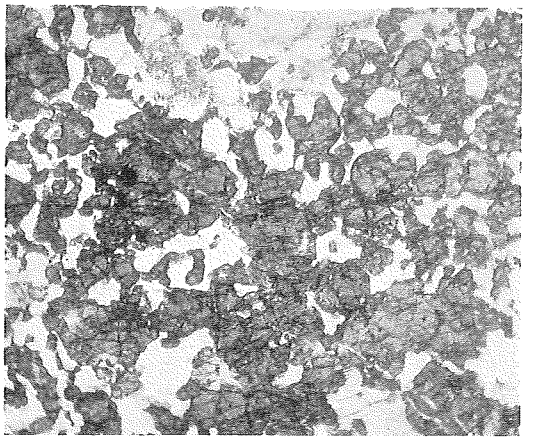

5

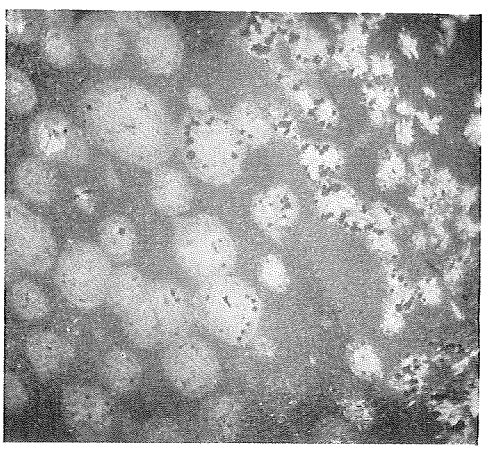

4

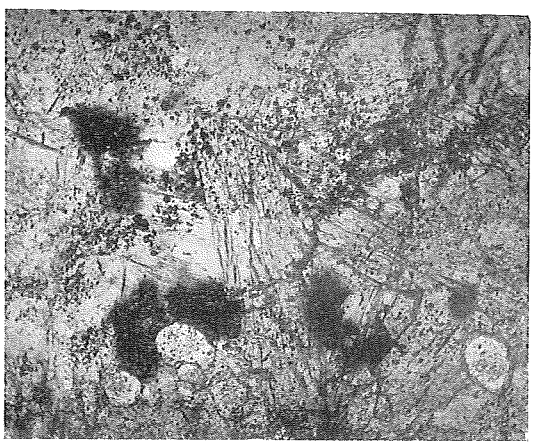

6

T. Yosimura : Minerals from the Kaso Mine.

1

2

3

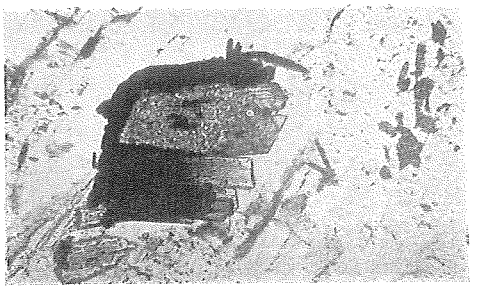

4

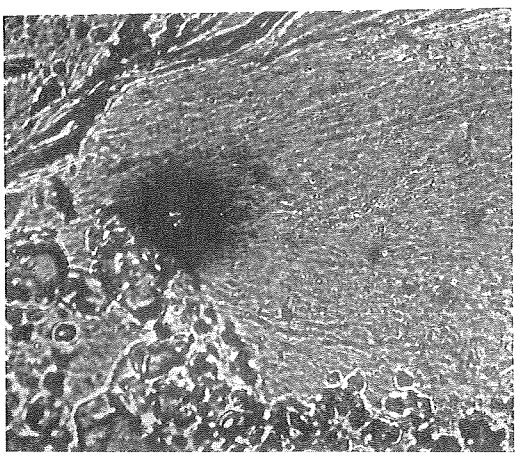

5

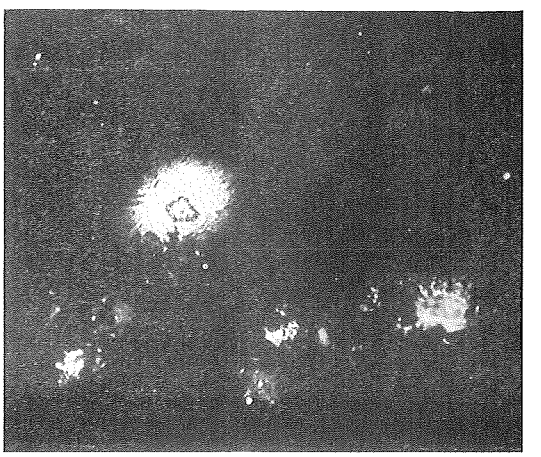

6

T. Yosimura : Minerals from the Kaso Mine

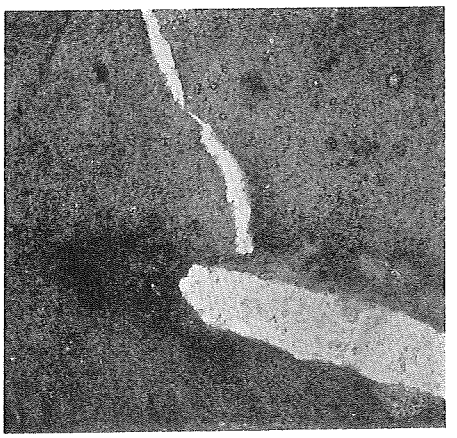

1

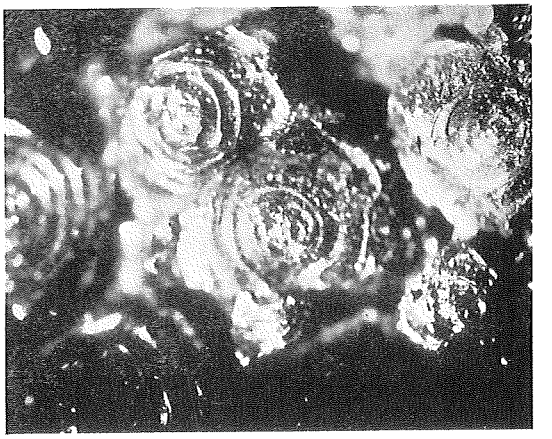

2

3

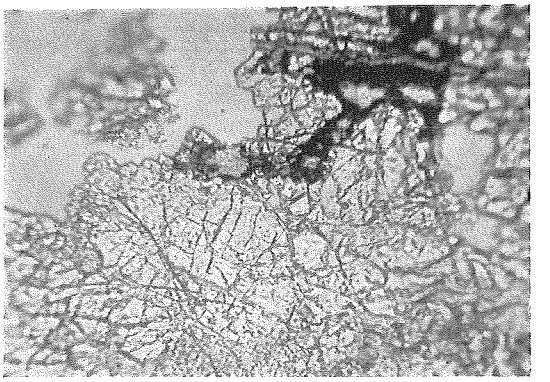

5

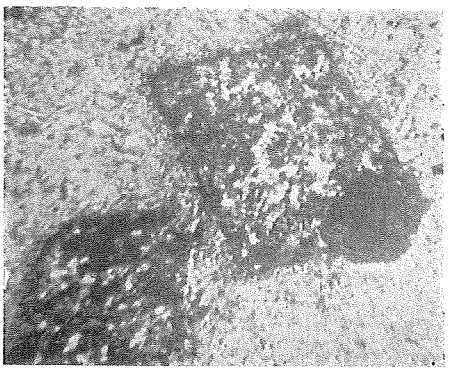

4

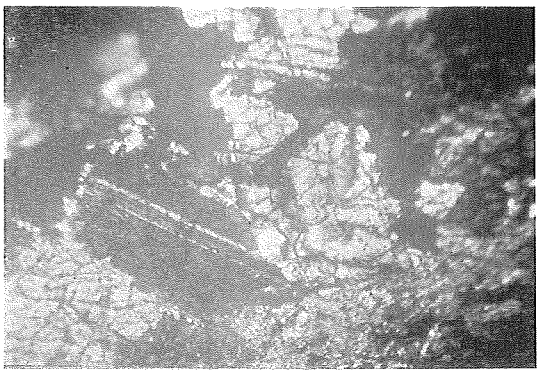

6

T. Yosimura : Minerals from the Kasoi Mine.